MODELLING CLIMATE CHANGE IMPACTS ON MOUNTAIN SNOW HYDROLOGY, MONTANA-ALBERTA

Robert Larson
Bachelor of Science, McGill University, 2004

A Thesis
Submitted to the School of Graduate Studies
of the University of Lethbridge
in Partial Fulfillment of the
Requirements for the Degree

MASTER OF SCIENCE

Department of Geography
University of Lethbridge
LETHBRIDGE, ALBERTA, CANADA

ABSTRACT

A modelling approach focused on snow hydrology was developed and applied to project future changes in spring streamflow volumes in the St. Mary River headwaters basin, Montana. A spatially distributed, physically-based, hydrometeorological and snow mass balance model was refined and used to produce snow water equivalent (SWE) and rainfall surfaces for the study watershed. Snowmelt runoff (S_R) and effective rainfall runoff (R_R) volumes were compiled for the 1961-2004 historical period. A statistical regression model was developed linking spring streamflow volume (Q_S) at Babb, Montana to the S_R and R_R modelled data. The modelling results indicated that S_R explained 70% of the variability in Q_S while R_R explained another 9%.

The model was applied to climate change scenarios representing the expected range of future change to produce annual Q_S for the period 2010-2099. Compared to the base period (1961-1990), average Q_S change ranged from -3% to -12% for the 2020s period. Percent changes increased to between -25% and -32% for the 2050s, and -38% and -55% for the 2080s. Decreases in Q_S also accompanied substantial advances in the onset of spring snowmelt. Whereas the spring pulse onset on average occurred on April 8 for the base period, it occurred 36 to 50 days earlier during the 2080s. The findings suggest that increasing precipitation will not compensate for the effects of increasing temperature in watershed SWE and associated spring runoff generation. There are implications for stakeholder interests related to ecosystems, the irrigation industry, and recreation.

ACKNOWLEDGEMENTS

Fulfilling this project and living in Lethbridge has been a great learning and cultural experience. I thank my supervisor, Dr. James Byrne, who has been a good friend, colleague, and mentor. Jim: your open-mindedness is commendable and you have an uncanny ability to instill confidence in a student. Sometimes I wish, however, that ideas pertaining to research directions were *not* a renewable resource! I am also thankful to my committee members, Dr. Dan Johnson, Dr. Stefan Kienzle, Dr. Matthew Letts, and Dr. Alice Hontela, for their feedback and sincerity. Dr. Craig Coburn and Dr. Dave Sauchyn (University of Regina) were also helpful at various stages of my progress. We live in exciting but daunting times. I hold my deepest respect for the commitment you all have to education and scientific progress, much needed for the challenges that lie ahead.

I extend my gratitude to the Geography Department and the School of Graduate Studies for their support, as well as the project's main funding source: the Alberta Ingenuity Centre for Water Research. I am also indebted to Dr. Dan Fagre and the United States Geological Survey (USGS) West Glacier Field Station, who provided key project data. I owe thanks to other agencies, such as Alberta Environment and Environment Canada, whose staff I liaised with along the way.

I thank the many friends I made here, who provided excellent sources of distraction and/or learning of different kinds. My office mates helped blur the lines between work and fun, and they included Kate, Ryan, Franco, Kean, and Geoff. My roommate, Stan, made life very easy at home. Finally, I am grateful for the love and encouragement from

my family. My parents passed on their joy of mountains to me when I was a boy. This thesis was completed sitting in front of a computer; however, I hope some of those hours will help to enrich the moments I spend in the alpine winter wonderland in the future (at least, as long as this lasts).

TABLE OF CONTENTS

ABSTRACT iii
ACKNOWLEDGEMENTS iv
TABLE OF CONTENTS vi
KEY EXPRESSIONS viii
LIST OF FIGURES ix
LIST OF TABLES xi

CHAPTER 1: Introduction 1
1.1 Problem Statement 1
1.2 Thesis Rationale 2
1.2.1 Objective and Milestones 3
1.2.2 Format 4

CHAPTER 2: Literature Review 5
2.1 Overview 5
2.2 Global Climate Change 5
2.2.2 Climate Variability 6
2.2.3 Impacts on the Hydrologic Cycle 7
2.3 Water Supply Hydrology in Western North America 9
2.3.1 Hydroclimate System 9
2.3.2 Trends 12
2.3.2.1 Historical Hydroclimate 12
2.3.2.2 Future Projections 17
2.4 Snow Hydrology Modelling 18
2.4.1 Accumulation and Ablation Factors 19
2.4.2 Snowmelt Simulation 22
2.4.3 Spring Streamflow Prediction 24
2.5 Snow Water Equivalent Model 27
2.5.1 SIMGRID 28
2.5.1.1 MTCLIM 28
2.5.2 SNOPAC 31
2.6 Climate Change Scenarios 34
2.6.1 Global Circulation Models 34
2.6.2 Emissions Forcings 35
2.6.3 Impact Assessments Modelling 37

CHAPTER 3: Refining a Watershed Snow Water Equivalent Model for the Montana-Alberta Rockies 39
3.1 Introduction 39
3.2 Study Area 41
3.3 Model Description 44
3.4 Methods and Data 47
3.4.1 SIMGRID: Spatial Climate Distribution 47

3.4.1.1 Temperature Routine Verification 47
3.4.1.2 Proxy Precipitation-Elevation Formulation 48
3.4.1.3 Climate Time Series Construction 53
3.4.2 SNOPAC: SWE and Rain Estimation 54
3.4.2.1 Rain-on-Snow Consideration 54
3.4.3 Summary of SWE Model Inputs and Outputs 56
3.5 Analysis 58
3.5.1 Lakeview Ridge Temperature Simulations 58
3.5.2 Precipitation-Elevation Relationship 62
3.5.3 Climate Station Regressions 64
3.5.4 Snow Water Equivalent Surfaces 69
3.6 Summary 71

CHAPTER 4: Developing a Statistical Spring Streamflow Prediction Model 72
4.1 Introduction 72
4.2 Mass Balance Data 73
4.3 Methods and Analysis 74
4.3.2 Spring Streamflow and Rainfall Runoff Variable Definition 81
4.3.2.1 Critical Snowpack Julian Dates 81
4.3.3 Multiple Linear Regression Model Selection 82
4.4 Results 85
4.5 Summary 87

CHAPTER 5: Climate Change Assessment of St. Mary Headwaters Snow Hydrology 88
5.1 Introduction 88
5.2 Methods 88
5.2.1 Climate Change Scenarios Construction 89
5.2.1.1 Global Circulation Model Data 89
5.2.1.2 Scenarios Selection 91
5.2.1.3 Downscaling 95
5.2.2 Snow Hydrology Model Runs 98
5.3 Analysis 99
5.4 Results and Discussion 103

CHAPTER 6: Conclusions 112
6.1 Thesis Summary 112
6.2 Recommendations 114

REFERENCES 118

KEY EXPRESSIONS

Abbreviations

GCM	Global Circulation Model
MTLCLIM	Mountain Microclimate simulator
SIMGRID	Grid Simulating program
SNOPAC	Snow accumulation and ablation program
SNOPAC-ROS	Snow accumulation and ablation, with rain-on-snow, program
SWE	Snow Water Equivalent
WNA	Western North America

Variables

A	Area
E	Elevation (relative to St. Mary base station)
$Jdep$	Julian date of snowpack depletion
$Jmax$	Julian date of maximum snow accumulation
$MELT$	Snowmelt
P	Precipitation
Q_S (Q_{S114})	Spring runoff volume (occurring 114 days after $Jmax$)
$RAIN$	Rainfall
R_R (R_{R40})	Rainfall runoff volume (occurring 40 days after $Jdep$)
$SNOW$	Snowfall
S_R (S_{R3})	Snowmelt runoff volume (determined using SNOPAC-ROS)
StM	St. Mary climate station
SWE	Snow water equivalent
t	Time
$Tmax$	Maximum temperature
$Tmean$	Mean temperature
$Tmin$	Minimum temperature
$TREQ$	Temperature required for melt
V	Variable
Δ	Change
ΔP_{diff}	Precipitation increment with elevation, relative to StM

Terms

Historical Period	1961-2004
Base Period	1961-1990
2020s	2010-2039
2050s	2040-2069
2080s	2070-2099

LIST OF FIGURES

Figure 2.1. (a) Fraction [%] of annual discharge occurring during the primary snowmelt runoff season April through July (AMJJ) for snowmelt dominated streams. (b) Average temporal center of mass streamflow (CT) [month] for snowmelt dominated gauges from the 1951-1980 climatological period. Source: Stewart et al. (2004). 12

Figure 3.1. The area shown encompasses Waterton-Glacier International Peace Park, where the British Columbia (BC), Alberta (AB) and Montana (MT) borders meet (inset). The Preston Snow course begins at the west end of Upper St. Mary Lake, and curves clockwise as it gains elevation. 43

Figure 3.2. Study watershed elevation band areas, classified according to Table 3.1. The elevation bands encompassing the Preston snow course are in black. 49

Figure 3.3. The primary data sources input to the SWE Model are shown. SIMGRID distributes the climate variables for the watershed. The outputs are then input into SNOPAC and SNOPAC-ROS to obtain SWE (and in the case of SNOPAC-ROS, rainfall) outputs for the 1961-2004 water years. 58

Figure 3.4. Daily *Tmax* and *Tmin* observed vs. simulated scatter plots for three aspects at Lakeview Ridge field site (November 26, 2005 – March 23, 2006). 61

Figure 3.5. The variability of predicted ΔP_{diff} values, based on elevation, is shown by the scatter plot. The forced-origin trend line is shown. 62

Figure 3.6. Standardized residuals plot of the ΔP_{diff} variable. Highest frequencies occur around the zero value, and the distribution resembles that of a normal distribution. Mean = 0.06, Std. Dev. = 0.998, n = 536. 63

Figure 3.7. Example daily *Tmax* and *Tmin* regressions between St. Mary and Babb stations, grouped for the month of April (1981-2006). 64

Figure 3.8. Spatial snowpack distribution on 8 dates during the 1980 water year (November 1979 - June 1980). 70

Figure 4.1. Study watershed average monthly naturalized streamflow volumes, 1961-2004 78

Figure 4.2. Prediction model results are shown by the observed versus modelled spring streamflow scatter plot, for the years 1961-2004. The 1:1 line is shown. 86

Figure 5.1. The four grid cells of the CGMC2 used to average the regional climate scenarios are shown, along with the area of Waterton-Glacier International Peace Park (within which lies the study watershed) 90

Figure 5.2. GCM climate change scenarios are shown through changes in precipitation and mean temperature relative to the base period. See Table 5.1 for GCM abbreviations. In addition to model acronym abbreviations, the emissions scenario identifier, along with the number of the model experiment appears as labels. For example, CB23 denotes the 3rd experiment of the CGCM2 forced by the B2 emissions scenario. 94

Figure 5.3. Changes in actual seasonal mean temperature (averaged from minima and maxima) and precipitation for the St. Mary station from one time slice to the next. 101

Figure 5.4. Weibull frequency distribution plot of the 1961-1990 modelled spring streamflow volumes. The high, median, and low Q_S years appear larger, for easy recognition. 103

Figure 5.5. Modelled annual Q_S for the period 1961-2099. The variability of the three future periods (i.e. 2010-2039, 2040-2069, and 2070-2099) reflects that of the base period (1961-1990). The annual timeseries for the three future periods serve as examples of typical spring streamflow years in order to illustrate possible future ranges. 108

Figure 5.6. Changes in critical snowpack Julian dates indicating maximum snow accumulation (*Jmax*), and snowpack depletion (*Jdep*) for both scenarios. The difference between *Jdep* and *Jmax* is the length of the snowmelt season. The variability of the three future periods (i.e. 2010-2039, 2040-2069, and 2070-2099) reflects that of the base period (1961-1990). The annual timeseries for the three future periods serve as examples of typical spring streamflow years in order to illustrate possible future ranges 110

LIST OF TABLES

Table 2.1 GCMs whose output is publicly available through the Pacific Climate Impacts Consortium. 35

Table 2.2. Matrix of development levels represented by the six main SRES scenarios. Source: Canadian Climate Change Scenarios Network (CCCSN 2007) 36

Table 3.1. Study watershed terrain classes used to lump the 5,549,283 pixels into 566 Terrain Categories 45

Table 3.2. Descriptive statistics of the observed vs. simulated *Tmax* and *Tmin* at Lakeview Ridge. In the equation y = ax + c, y is the simulated and x is the observed temperature.. 60

Table 3.3. Comparison of model and coefficient statistics for the Figure 3.5 regressions, both with and without constant (y = ax + c).. 63

Table 3.4. Monthly *Tmax* and *Tmin* regressions for the period 1981-2006. The regression equation yields y = ax + c, where y = St. Mary temperature, x = Babb temperature, and c is a constant. 65

Table 3.5. Monthly average precipitation (*P*, mm) and forced-origin regression results, 1981-2006. The equations are in the form y = ax, where y = St. Mary P and x = nearby station *P*. 68

Table 4.1. Linear regression results evaluating the three SWE volume measures (or S_R). Units are in million m^3. 79

Table 4.2. Best model results from multiple linear regressions using S_{R3}, along with the various R_R and Q_S variables are shown. Results for the selected model are bolded. 84

Table 5.1. The centre point coordinates of the upper left and lower right cells surrounding the St. Mary study area are shown to illustrate the extent of each model's spatial coverage, along with its resolution (defined as the average length of one of the grid cell sides). (The bolded first letter(s) of the model acronym are those used for labeling model runs in Figure 5.2). 91

Table 5.2. Seasonal temperature and precipitation changes for each scenario, relative to the 1961-1990 base period. *Tmax* and *Tmin* changes are in °C, and precipitation changes are in %. 100

Table 5.3. High, median, and low flow years used as representative years for snow hydrology comparisons. Percentage probabilities are those designated by the Weibull frequency distribution. 103

Table 5.4. Hydrologic variables under the two scenarios and three future periods, for the three flow type years. All units are in million m^3. 106

Table 5.5. Julian dates of maximum snow accumulation (*Jmax*) and maximum snow depletion (*Jdep*) for the three flow type years. 109

CHAPTER 1: Introduction

1.1 Problem Statement

Mountain snow-dominant regions are a source of freshwater supply for 1/6 of the world's population (Arnell 1999). Data from the last half-century over western North America (WNA) indicate hydroclimates have undergone significant change (Barnett et al. 2005). Surface air temperatures have risen at a rate of 1-2°C per century over WNA since 1950. The rise has been more pronounced during the winter and spring seasons (Karl et al. 1993, Lettenmaier et al. 1994, Vincent et al. 1999, Mote et al. 2005a). Concurrently, widespread snowpack decline has been observed (Brown and Braaten 1998, Selkowitz et al. 2002, Mote 2003, Hamlet et al. 2005, Mote et al. 2005a, Schindler and Donahue 2006), and peak snowmelt has advanced approximately 1-4 weeks (Groisman et al. 1994, Stewart et al. 2005), despite a small increase in annual precipitation (Groisman and Easterling 1993). The above trends are due to increasing rain-to-snow ratios (Knowles et al. 2006), shorter snow accumulation seasons, and the increased incidence of winter melt periods (Nash and Gleick 1991, Shabbar and Bonsal 2003, Hamlet et al. 2005).

Due to anticipated climate warming, the above trends are generally expected to continue in the future (Leung et al. 2004). Peak snowpack accumulation will likely decrease, resulting in reduced amounts of water stored in snowpacks (snow water equivalent, or SWE) (Hamlet and Lettenmaier 1999b, McCabe and Wolock 1999, Cayan et al. 2001, Payne et al. 2004, Lapp et al. 2005). Increasing rain-to-snow ratios are expected to increase winter runoff and advance peak snowmelt periods, resulting in reduced spring runoff (Leith and Whitfield 1998, Hamlet and Lettenmaier 1999a, Merritt et al. 2006).

These changes threaten water supply, with considerable consequences for downstream regions, and particularly those with heavy summer water demand such as irrigation-intensive lands (Barnett et al. 2005, Sauchyn et al. 2006).

1.2 Thesis Rationale

The St. Mary headwaters study basin is located on the eastern slopes of the Rocky Mountains in Glacier National Park, MT. It is the principal water source for almost 200,000 ha of downstream irrigation in southern Alberta (Canada) and 56,600 ha in Montana (United States) (AAFRD 2000). The river's water supply in these semi-arid regions is nearly fully allocated in most years. Effective water storage and diversion system design has aided water management. However, this has not been without concerns for ecosystem impacts (Rood et al. 1995, Rood et al. 2005a), transboundary water allocation (Halliday and Faveri 2007), and water quality (Byrne et al. 2006).

The St. Mary River's water users have suffered through shortfalls, such as in 1988 and in more recent years. For example in 2001, a series of conditions (e.g., lowered reservoir levels due to maintenance, depleted soil moisture, small winter snowpack, and little spring and summer precipitation) forced the St. Mary River Irrigation District (SMRID) to undergo water rationing (R. Renwick, SMRID, June 15, 2007, personal communication). The combination of such circumstances is not likely to be reproduced in the near-future. However, with continued irrigation development and population growth, this region is clearly vulnerable to climate warming and water shortage (Barnett et al. 2004, Kundzewicz et al. 2007).

For the study region, Global Climate Models (GCMs) project temperature increases of +3°C to +5°C (relative to the 1961-1990 normal), with marginal and more uncertain increases in precipitation (Barrow and Yu 2005). Increasing precipitation is a source of potential SWE increase, while increasing temperature is a source of potential SWE decline. Detailed assessments are needed to model the net effect of these influences on SWE in mountain watersheds, and to predict the associated changes in water supply.

1.2.1 Objective and Milestones

A snow hydrology modelling approach was adopted to assess the impacts of climate change on the St. Mary River headwaters basin water supply. To address this objective, the following milestones were reached:

1. A spatially distributed and physically-based SWE Model was refined for the St. Mary headwaters, and used to produce daily SWE surfaces, along with rainfall depths for the historical (1960-2006) period;
2. SWE Model output was used to compile snowmelt runoff (S_R) and rainfall runoff (R_R) volumes, which were evaluated and used to develop a statistical regression model predicting spring streamflow volume (Q_S).
3. GCM outputs were used to alter the base period climate in three future time periods, spanning 2010-2199, and the snow hydrology approach was applied under two climate change scenarios to quantitatively assess future changes in Q_S.

1.2.2 Format

This thesis is organized according to six chapters. Chapter 1 provides an introduction to the thesis, including the problem statement and rationale for the work undertaken. Chapter 2 links the concepts that relate the thesis to the broader knowledge base, covering global climate change, water supply hydrology in western North America, snow hydrology modelling, the snow water equivalent model (SWE Model), and impacts assessment modelling. Chapter 3 is the first of three analytical chapters. In it, the SWE Model is refined and applied in the study area. Chapter 4 is the second analytical chapter, and builds on the output generated from the SWE Model in Chapter 3. A statistical regression model is developed to predict spring streamflow volumes over the historical period, rounding out the snow hydrology modelling approach. Chapter 5 applies this approach under climate change conditions. Scenarios are selected and future climates are constructed using the baseline climate record. Finally, Chapter 6 summarizes the research, and includes recommendations for future work.

CHAPTER 2: Literature Review

2.1 Overview

This chapter contains information underpinning the objectives of the thesis, beginning with an overview of global climate change. Following this, climate warming impacts on hydroclimates and threats to water supply hydrology in western North America are discussed. Background on snow hydrology modelling and the SWE Model used in this thesis is then discussed. Finally, key concepts in applying climate change scenarios are elaborated.

2.2 Global Climate Change

Climate change is defined as a statistically significant variation in either the mean state of the climate, or in its variability, persisting for an extended period of time, typically decades or longer (Houghton et al. 2001). Global temperatures increased 0.76 [90% certainty range of +0.57 to +0.95]°C from 1850–1899 to 2001–2005 (IPCC 2007). This temperature increase is the result of a perturbation in the global climate system's energy balance, which also causes Earth's climate to change. Climate change may be due to natural internal processes (e.g., volcanic emission of atmospheric gases affecting the radiation balance at the Earth's surface), external forcings (e.g., Earth's orbiting distance from the Sun and fluctuations in solar output), or to anthropogenic effects (e.g., deforestation or greenhouse gas emissions) (Houghton et al. 2001). Each of these processes may be expressed in terms of radiative forcing, which is used to compare the relative influence of each perturbation on the climate system (IPCC 2007).

2.2.1 Anthropogenic Warming

There is very high confidence that the globally averaged net effect of human activities since 1750 has been one of warming, with a total net radiative forcing of +1.6 [+0.6 to +2.4] Wm^{-2} (IPCC 2007). In contrast, radiative forcing from the sun over the same time period has been +0.12 [+0.06 to +0.30] Wm^{-2}. Human activities have enhanced the greenhouse effect via the emission of long-wave-trapping gases such as carbon dioxide, methane, nitrous oxide, and fluorocarbons (Manabe and Wetherald 1967, Dickinson and Cicerone 1986, Crowley 2000, Hengeveld 2000, IPCC 2007). The observed increases in such greenhouse gases (GHGs) is very likely the cause of increases in globally averaged temperatures since 1850 (IPCC 2007). Atmospheric concentrations of the most important GHG, carbon dioxide, have risen steadily from 280 ppm in 1850, to 385 ppm in 2006 (NOAA 2006), and are now far higher than anytime in the last 650,000 years (IPCC 2007). Quantifying anthropogenic warming is crucial in future climate projections, which are determined in large part by future GHG emissions scenarios.

2.2.2 Climate Variability

The Earth's climate system is dynamic and subject to natural variability, which is defined by the IPCC as the departure in mean state of the climate, including the occurrence of extremes, on all temporal and spatial scales beyond individual weather events (Houghton et al. 2001). Larger-scale trends in natural variability are more easily explained, but understanding the low-frequency variations in climate is helpful in predicting regional impacts extending from natural and/or anthropogenic warming on natural resources, such as snowmelt (Karl et al. 1995, Pederson 2004, Romolo et al. 2006). For example, in any

given year, the spring SWE within a snow course over the US may deviate by 25-60% of its long-term average (Cayan 1996). This variability results in a range of water supply scenarios, some of which include flood or drought conditions (Redmond and Koch 1991, Cohen and Miller 2001).

In the future, it is likely that new patterns of climate variability will emerge. Global warming is likely to lead to increased extreme climate conditions (Katz and Brown 1992, Zwiers and Kharin 1998, Katz 1999, Kharin and Zwiers 2000, Hansen et al. 2007). Clear examples of such changes have been observed for surface temperature extremes. Changes in the annual number of frost days, warm and cold days, and warm and cold nights have been linked to global warming (Hegerl et al. 2007, Trenberth et al. 2007).

2.2.3 Impacts on the Hydrologic Cycle

Climate warming will notably change the hydrologic cycle, as sensible and latent heat exchanges affect the state and movement of water around the globe. Following are three key changes among the many impacts that will occur as the atmosphere interacts with the hydrosphere and the cryosphere.

Increased Atmospheric Water

A warmer atmosphere will lead to increased evaporative demand (Del Genfo et al. 1991, Loaiciga et al. 1996). The atmosphere's water-holding capacity is estimated to rise by 7% per °C (Trenberth et al. 2007). This will result in a "higher energy" atmosphere, due to its increase in latent heat content (Ahrens 2007). Increases in atmospheric water content

over land and oceans, as well as in the troposphere, have already been observed (IPCC 2007). An increase in global precipitation (Allen and Ingram 2002, Dore 2005, Huntington 2006) corroborates these findings. Over WNA for example, a slight increase of about 0.7%/decade has been observed (Groisman et al. 1994, Zhang et al. 2000). Changes in the intensity, frequency, and type of precipitation have also been observed for the globe (Trenberth et al. 2007). The above concepts form part of the theory of the intensification (or magnification) of the hydrologic cycle (Douville et al. 2002).

Change in Atmospheric Circulation

A warmer atmosphere and increased atmospheric water will affect circulation patterns. Circulation is largely the atmospheric response to uneven heating of the Earth, which on average is largest at the tropics and least at the poles. As the north pole continues to be heated faster relative to the rest of the latitudes (ACIA 2004), the positioning of the jet streams, and resultant precipitation patterns, could be altered (Rind 1996). For example, a poleward shift in storm track location and a possible increase in storm intensity have been noted over the northern hemisphere (Trenberth et al. 2007). Some studies project warmer and wetter winters for WNA in future (Leung et al. 2004, McKechnie 2005, Mote et al. 2005b).

Snow Cover Decline

The extent of snow cover reaches up to 49% of land coverage in January in the Northern Hemisphere (Lemke et al. 2007), and a strong correlation between increasing temperatures and recent snow cover decline has been observed (Karl et al. 1993, Frei et

al. 1999). Lemke et al. (2007) reported that in the latitude band of greatest variability in snow covered area (SCA), SCA is correlated with temperature, in almost every month, owing to the snow-albedo feedback. The correlation was strongest in spring ($r = -0.68$) (updated from Brown 2000). Furthermore, the albedo of snow may be decreasing even more due to anthropogenic soot (Hansen and Nazarenko 2004), likely leading to enhanced snow cover decline. A shorter winter snow cover period (Robinson and Frei 2000, Dye 2002) will result in strong changes to the snow hydrology of mountain regions. Additionally, climate warming is projected to be more pronounced at higher elevations (Giorgi and Hurrell 1997, Fyfe and Flato 1999, Kim and Kim 2002).

2.3 Water Supply Hydrology in Western North America

WNA is one of the regions in the world where climate warming impacts on water resources have been most intensely studied. Similar weather and landscape factors drive the hydroclimatic system throughout the region. The majority of the region's water supply regime will be explained through snow hydrology processes. Observed large-scale hydroclimatic trends can provide insight into the changes happening on smaller scales within the region, such as the study area of this thesis.

2.3.1 Hydroclimate System

The first factor to consider in the hydroclimate system driving WNA snow hydrology is precipitation, which is the input to basin water balance. Precipitation is a discrete variable that can fluctuate widely through time and space. Thus a key component of snow hydrology involves understanding the factors controlling winter precipitation. Over

WNA, two important factors are the variability of the predominantly westerly synoptic flow and the interactions of these processes with regional landscapes. In this section, the hydroclimate system refers to the integrated links between climatologic and hydrologic components of precipitation, temperature, snowpack, and runoff. The focus is on the winter water balance; evaporation issues are largely ignored because evaporation rates remain low during the cold season.

Precipitation

In WNA, global scale circulation causes air mass convergence in the latitudes between 30° and 60° North (Ahrens 2007). During winter, when energy gradients between the poles and the equator are strongest, the mid-latitude jet stream intensifies. Westerly geostrophic winds (resulting from the above-mentioned energy gradients as well as the Coriolis force) dominate the winter season continental climatology. Moisture-laden air masses, originating over the Pacific Ocean develop into storms and bring the bulk of the region's annual precipitation, generally falling as winter snowfall (Shafer et al. 2005).

Mountains exert a strong and clear regional effect on precipitation volumes. These physical barriers force the Pacific air masses to rise, causing orographic uplift (Barry 1981). The rising air masses reach the lifting condensation level (LCL), where air temperature and dew point converge. Above this level, the saturated air releases precipitation (Ahrens 2007). Temperature gradients in mountains affect the precipitation type (e.g., rain, snow, sleet, graupel, hail), with larger proportions falling as snowfall due to cooler temperatures at higher elevations (Serreze et al. 1999). Mountains also create

rain shadows in the larger lee areas. This is an important consideration on the eastern slopes of the Rockies (where the thesis study area lies), and is discussed further in Chapter 3.

Snowpack and Runoff

Snowpack acts as a hydrologic reservoir, storing snow water equivalent (SWE) over the winter months. Snow cover insulates underlying surfaces, and restricts latent heat exchanges and associated evaporation losses to the atmosphere (Gray and Male 1981, Clark et al. 1999). During the spring melt period, the shallow alpine soils quickly become saturated. High runoff coefficients result in much of the melt water reaching channels, increasing streamflow (Gray and Male 1981, Byrne 1989, Xiuqing et al. 2001, Dingman 2002, Bayard et al. 2005). Similarly, precipitation occurring during the snowmelt season, or shortly thereafter, likely results in overland flow (Dingman 2002). The result is that a high proportion of annual flow (i.e., water supply) in such watersheds occurs during spring and early summer snowmelt (Barnett et al. 2005).

The water supply regime of mountain watersheds of WNA is depicted in Figure 2.1 (a). In many regions, about 70% of annual runoff occurs during the period April through July, suggesting strong contributions from snowmelt. Figure 2.1 (b) shows that interior regions show slightly later center of mass timing of spring streamflow. This is due to both cooler temperatures (meaning snowmelt occurs later in the year), and a precipitation regime that is less winter-dominant, and shifted more toward spring (Shafer et al. 2005).

Thus, water supply in many regions of WNA is clearly dependent on mountain snowpack.

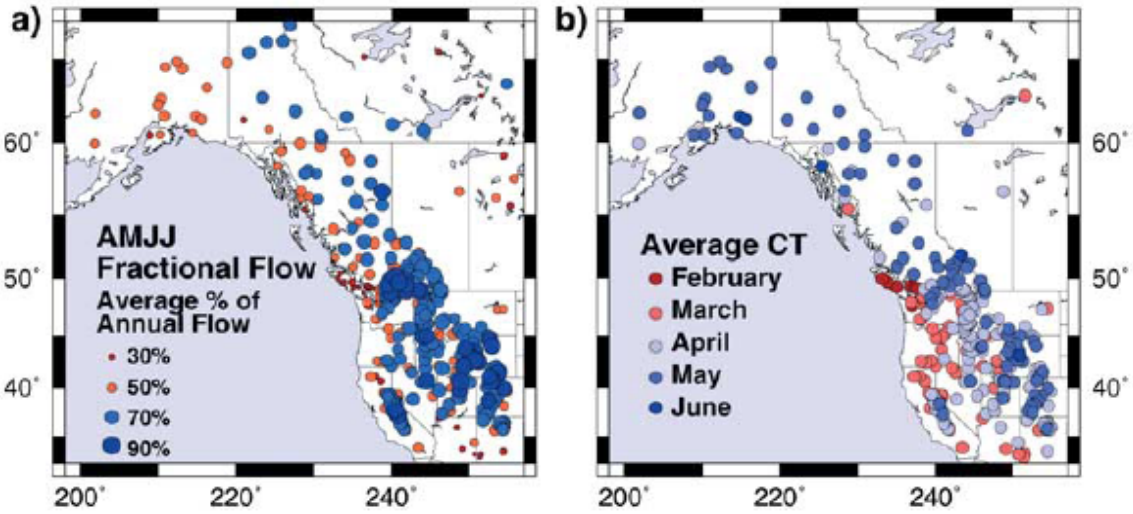

Figure 2.1. (a) Fraction [%] of annual discharge occurring during the primary snowmelt runoff season April through July (AMJJ) for snowmelt dominated streams. (b) Average temporal center of mass streamflow (CT) [month] for snowmelt dominated gauges from the 1951-1980 climatological period. Source: Stewart et al. (2004).

2.3.2 Trends

2.3.2.1 Historical Hydroclimate

Within the last century, snow cover has fluctuated over the northern hemisphere. For example, from 1915 to 2004, snow cover increased in the months of November, December and January, owing to increases in precipitation (Groisman et al. 2004), with the most apparent snow cover decreases occurring during the spring period since 1950 over WNA. Historical hydroclimatic trends will be shown here, with a focus since 1950, given the increased monitoring that began around that time.

Snowpack

In Southern Canada, Brown and Bratten (1998) used trend analysis for the period 1946-1995, to identify the trend of snowpack decline. Canadian snow depth decreased in nearly all months, with the most significant local decreases occurring in February and March. Greatest reduction amounts ranged from 1.0 to 1.5 cm per year. The largest decreases in snow cover duration were observed over western Canada during spring (i.e., March, April, and May). Of interest to the present thesis study, Selkowitz et al. (2002) reported a decline of 0.38 cm per year since 1952 in the Glacier National Park area, using Snowpack Telemetry (SNOTEL) and snow course data. This decline is modest compared to those reported by Brown and Bratten (1998).

Mote et al. (2005a) conducted a WNA-wide study using linear trends of April 1 SWE from 824 snow course and SNOTEL locations for the period 1950-1997. Many sites exhibited relative SWE losses in excess of 50%, and 75% of the locations showed negative SWE trends over the period. Smaller decreases, between 15-30%, were observed for the cooler and interior Alberta-Montana Rockies region (corroborating the more modest reductions found by Selkowitz et al. (2002) for this region).

To explain the hydroclimatic causes of snowpack decline, Mote et al. (2005a) also investigated the relative influences of temperature and precipitation, separately. These were determined by applying the Variable Infiltration Capacity (VIC) Model over the observed time period, while isolating the rates of change of each variable in separate runs. They found that the snowpack decline is more strongly linked to increasing

temperatures than to changes in precipitation for most regions. However, in cooler interior regions such as the Montana-Alberta Rockies, temperatures have influenced snowpack decline, but not overwhelmingly compared to available precipitation. This is likely because most of the region's snowpack has remained above the freeze line during winter over the historical period.

Temperature

Warming in the south and west of Canada has been greatest in winter and spring, and has reduced the diurnal temperature range of these seasons (Zhang et al. 2000). Groisman et al. (2003) indicated that the annual severity of the cold season (i.e., the sum of daily negative temperatures) for the 1950-2000 period has substantially decreased in southern Canada. This has lead to increased duration and frequency of winter warm spells in southern Canada (Shabbar and Bonsal 2003).

Precipitation

Precipitation changes have been variable both temporally and spatially across WNA. Despite the slight increase in annual precipitation (noted previously) over WNA, some regions have experienced a decline during winter. For example, in southwestern Canada, Zhang et al. (2000) found that winter precipitation decreased about 25% from 1950-1998. Vincent and Mekis (2006) reported decreases in snowfall over the last century for the same region. Warmer temperatures have caused the rain-to-snow ratio to increase by as much as +6% for regions of southwestern Canada (Zhang et al. 2000). In a similar study, Knowles et al. (2006) observed an average 9% increase in the rain-to-snow ratio over

WNA and parts of southwestern Canada from 1949-2004. Furthermore, the trend was widespread, as increases were observed at 75% of the study's snowy climate stations.

Streamflow

Summarizing the above sections, snowpack decline has logically resulted from increasing temperatures and decreasing winter precipitation. Compared to snowpack, however, changes in runoff, and especially annual streamflow volume, have been less clear. This is because land-based effects such as soils, landcover, and topography result in varied hydrologic responses at the watershed scale (Bales et al. 2006). Having noted this, one hydrologic trend has been ubiquitous over WNA: earlier onset of spring snowmelt.

The timing of snowmelt was investigated by Burn et al. (1994), who applied a trend test to a database of snowmelt runoff peak dates across west-central Canada (with median record length of 37 years). While no rivers displayed positive trends, 30% of the gauges displayed decreasing trends, significant at the 95% confidence level. In a similar study using a network of 302 gauges within WNA over the period 1948-2002, Stewart et al. (2005) found that increasing fractions of annual flow now occur 1-4 weeks earlier in the spring season. The study suggests this is directly linked to maximum mountain SWE having shifted to earlier in the season by about two weeks (Lemke et al. 2007).

Some general seasonal streamflow trends are found in the literature. For example, Lettenmaier et al. (1994) noted increases in November-April streamflow for the period 1948-88 over the USA. This coincided with areas where winter precipitation had

increased (along with warmer temperatures inducing winter snowmelt). Leith and Whitfield (1998) found evidence of spring streamflow decline associated with warming, in British Columbia. They found that during warmer periods, the hydrograph was shifted with an earlier peak and longer recession, resulting in lower summer volumes.

Some basins have experienced decreases in annual streamflow. Walter et al. (2004) showed that annual streamflow decreased in the Colorado and Columbia river basins since 1950 (Walter et al. 2004). Century-scale trends show that annual streamflow has decreased by 2% per decade in the central Rocky Mountains (Rood et al. 2005b), and Schindler and Donahue (2006) report runoff declines in rivers draining into the Western Prairie Provinces of Canada over the same time period.

Summary

Snow-dominant mountain regions have responded to warming in similar ways (i.e., more rain and less snow; shorter winter season and more winter melting resulting in snowpack decline; and reduced streamflow volumes related to the earlier onset of spring melt). From a physical processes point-of-view, spring streamflow decline is likely due to higher snowmelt-runoff coefficients compared to rainfall-runoff coefficients. This explains why increases in annual precipitation do not translate to increased streamflow. Because of this physical difference, spring streamflow decline is expected to continue in the future (with variations according to the modelling method used).

2.3.2.2 Future Projections

Temperature over WNA is projected to increase from +2 to +6°C over the next century (Field et al. 2007). Comparatively, changes in annual mean precipitation may be modest, and more uncertain (but generally consist of an increase in winter, and a decrease in summer) (Christensen et al. 2007). There is greater certainty in future snowpack decline where declines have been strongest in recent history. For example, studies show snowpack declines of 60-100% for coastal regions (e.g. Cascades) and in the US southwest (e.g. Sierra Nevada) by the end of the century (Leung and Wigmosta 1999, McCabe and Wolock 1999, Leung et al. 2004).

In interior, cooler regions, where snowpack decline has been more modest, contradictions occur in the magnitude, and even direction, of changes. Differences between studies arise due to the varied modelling approaches used. For example, McCabe and Wolock (1999) reported +9% and +3% changes in snowpack for the 2025-2034 and 2090-2099 periods, respectively, for the Montana-Alberta Rockies region. They directly analyzed coarse-resolution Global Climate Model (GCM) outputs. Leung and Wigmosta (1999), on the other hand, used GCM output to drive a Regional Climate Model (RCM), which captured orographic effects. They reported snowpack changes of -18% in a representative watershed of the Montana-Alberta Rockies within the next century.

Similar to Leung and Wigmosta (1999), Lapp et al. (2002, 2005) downscaled GCM data for use in an even more detailed mountain snow accumulation and ablation model and projected a 38% reduction in snowpack for a mountain watershed in the southern Alberta

Rockies. Therefore, differences in future estimates are linked to the scale of the modelling approach and how the opposing factors of precipitation and temperature changes in mountain regions are simulated.

Where snowpack declines, the decrease in snow storage is likely to lead to earlier onset of spring melt and reduced spring streamflow volume. Peak flows are estimated to advance 30-40 days earlier in the future, relative to the observed 1948-2000 trends (Stewart et al. 2004, Stewart et al. 2005). A wetter and warmer climate is expected to shift watershed streamflow to a more rainfall-dominated regime (Whitfield et al. 2002), especially in areas west of the continental divide such as in BC (Loukas et al. 2002a, Morrison et al. 2002, Loukas et al. 2004, Merritt et al. 2006). Changes to annual streamflow are less certain, due to the strong dependency on changes in precipitation. Related to this, Thompson et al. (2005) found that interannual variability in streamflow would be greatest (±50%) for semi-arid areas.

2.4 Snow Hydrology Modelling

The previous section has shown that models are used to make hydroclimatic projections, and can be useful in quantifying hydrologic change in WNA. Efforts to model changes in future water supply are most likely to be effective if there is a focus on the snow hydrology system. Modelling spatial and temporal snowpack variability is a crucial step in predicting spring streamflow volumes. During the cold season, many factors must be considered to simulate the mass balance of snowpack. Once snowmelt begins, energy fluxes are crucial in simulating snow mass state changes from solid to liquid (or gas). As

snowmelt becomes runoff and is channeled into streams and rivers, volumes are reflected in the watershed's streamflow measurements. Models incorporate routines designed to simulate key processes, and examples of modelling approaches used to simulate them are discussed next.

2.4.1 Accumulation and Ablation Factors

Precipitation Partitioning

Precipitation gauges do not discriminate between solid and liquid precipitation, or they do so with little accuracy (Larson and Peck 1974, Bales and Cline 2003). To circumvent this, models use algorithms to partition precipitation into rain and snow. Using more reliable climate stations, studies show that precipitation will fall as snow when air temperatures are near or below freezing, and rain will fall above a threshold precipitation somewhere between +4°C and +6°C, with a mix of the two between these temperatures (Auer 1974, Rohrer 1989, USACE 1998). Examples of studies that use variations of these temperature thresholds include Anderson (1976), Coughlan and Running (1997), Marks et al. (1999), and Wyman (1995).

Wind

Wind redistributes snow by scouring zones of high wind speeds and creating drifts in areas of low wind speeds caused by topographic features or vegetation. Wind can also contribute to in-transit snow loss through sublimation. The percentage of annual snowfall lost to wind-induced sublimation has been found to range from 15% in the Colorado Front Range (Hood et al. 1998) to as much as 41% in the Canadian Prairies (Pomeroy

and Li 2000), the latter having a measured maximum sublimation rate of 1.2 to 1.8 mm/day (Pomeroy and Essery 1999).

A few attempts have been made to model wind-driven sublimation (Déry and Yau 1999, Winstral and Marks 2002, Bowling et al. 2004). Such endeavours are complicated by the lack of distributed wind data and by the non-linear control wind has on sublimation rates (Essery et al. 1999, Pomeroy and Essery 1999). Lapp et al. (2005) incorporated a physically-based sublimation routine into a snow accumulation-melt model. They compared overwinter SWE simulations with snow pillow observations for mountain snow pillow sites. Inclusion of the sublimation routine did not statistically improve results, which was likely due to temperature effects; the snow pillows were at relatively high (and cold) elevation (with high vapour pressure deficit), having modest sublimation rates.

Canopy

Landcover has a dampening effect on wind, and can prevent snow from reaching the ground. Canopies can intercept over 50% of cumulative snowfall by mid-winter in alpine environments (Pomeroy et al. 1998); and 25-45% of the intercepted snow can sublimate rather than unload to the ground, due to the relatively warm and dry atmosphere within and above the canopy (Pomeroy and Gray 1995, Harding and Pomeroy 1996, Montesi et al. 2004). Snow interception decreases with both snow canopy load and snowfall amount, and increases with canopy density (Pomeroy and Gray 1995, Hedstrom and

Pomeroy 1998, Lundberg and Koivusalo 2003). These canopy abstractions, however, are hard to predict beyond the experimental plot scale.

Canopies also control latent heat fluxes to the snow cover, affecting snowpack energy balance. In dense forests, longwave radiation from forests to snowpacks represent the dominant energy source, and may become increasingly relevant in energy balance models (Link and Marks 1999). Examples of snow canopy interception routines are found in Gelfan et al. (2004) and Coughlan and Running (1997).

Topography

Elevation may be the most important topographic factor controlling snow accumulation patterns in mountainous areas (Aguado 1990, Reece and Aguado 1992). Steep elevation gradients cause different precipitation and temperature effects on snowpack within small areas. For example, higher elevations escape the freeze line, and may be subject to enhanced orographic lifting of warmer, saturated air, bringing more precipitation (Howat and Tulaczyk 2005, Jin et al. 2006). Negative temperature lapse rates with elevation result in more precipitation falling as snow, and more importantly, the snow is subject to less melt and sublimation losses (Gray and Prowse 1993).

Strong linear relations are often found at a single transect between snow water equivalent and elevation (USACE 1956), although there may be high variability in year-to-year rates of SWE increase (Meiman 1970). This suggests that SWE databases are a good source to explore precipitation-elevation relationships (which is undertaken in this thesis).

Thornton et al. (1997) used a precipitation factor which rises exponentially with elevation, to extrapolate observed precipitation at a base station. Little high-elevation data exists to validate hypotheses about precipitation-elevation relationships (Diaz 2005).

The combination of aspect and slope also affects accumulation rates, due to their effect on precipitation, temperature, and wind exposure (Luce et al. 1998). Higher precipitation volumes occur on windward aspects, with rain shadows at lower elevation lee slopes. South-facing aspects (in the northern hemisphere) receive more solar radiation, increasing the chance of snow sublimation and melt. Windward aspects experience scour and deposition occurs on lee slopes, often with patterns reoccurring on an annual basis (Elder and Dozier 1991). Slope and aspect also affect snow redistribution through avalanching (Zalikhanov 1975, Schweizer et al. 2006).

2.4.2 Snowmelt Simulation

Snow models consider the above factors in simulating snow accumulation surfaces during the cold season. With the spring onset of snowmelt, many sources of heat energy must be considered, the most important of which is shortwave radiation (Elder and Dozier 1991, USACE 1998, Hock 2003). A snowmelt modelling review by Ferguson et al. (1999) suggests there are two general approaches to simulating snowpack heat absorption: energy balance (EB) and temperature index (TI). EB models attempt to quantify melt as a residual of the surface energy balance, while TI models assume an empirical relationship between air temperatures and melt.

EB models are more accurate than the considerably more simplified TI models. They can better account for the energy exchanges contributing to snowmelt, including shortwave radiation change due to snow cover and canopy albedo, canopy attenuation, ground heat flux, and heat transfer due to rainfall. As a result, EB models can simulate internal snowpack processes such as metamorphism and ripening, which are crucial factors controlling snowmelt timing and runoff routing. Examples of more recently developed snow energy balance models include Alpine 3D (Lehning et al. 2006), SnowModel (Liston and Elder 2006a), and ISNOBAL (Marks et al. 1999). In many applications, however, the benefits of using EB models such as these are often outweighed by their prohibitive data requirements (Rango and Martinec 1995, Brubaker et al. 1996). The advent of geographic information systems (GIS), multi-parameter spatial data products, and increased computer capacity is rendering EB models evermore attractive.

TI snowmelt models are less data-intensive than EB models, and are based on calculations of heat accumulation units (e.g., degree-days). TI models have been widely used in applied research such as in hydrological runoff modelling, with reliable results (Ohmura 2001). Examples of hydrologic models utilizing the TI approach include the Streamflow Simulation and Reservoir Regulation (SSARR) model (USACE 1991), the Precipitation-Runoff-Evapotranspiration-HRU model (PREVAH) (Gurtz et al. 1999), and the Snowmelt Runoff Model (SRM) (Martinec 1975, Brubaker et al. 1996). Temperature index snowmelt models adjust the daily air temperature and the critical melt temperature (usually 0°C) according to a melt factor. The melt factor may reflect a combination of net solar radiation, elevation, albedo, topography and vegetation (Gray and Prowse 1993,

Hock 2003). A disadvantage to TI models is that they cannot simulate unusual climatic conditions. Large rain-on-snow events (and associated heat transfers to snowpack), for example, can create flood conditions, with important water management implications (Garen and Marks 2005).

Ferguson et al. (1999) characterize some TI models as partial, or parametric, energy balance (partial EB) models. Instead of deriving melt from a single melt factor, these models estimate various energy exchanges (e.g., sensible, latent, and net radiation) from temperature measurements (i.e., mean temperature, minimum temperature, and daily temperature range). Examples are the snow accumulation and ablation model within the US NWS River Forecasting System (Anderson 1973) and the snowmelt routine nested within the UBC Watershed Model (Quick and Pipes 1977). The latter of these two models is incorporated into this study's SWE Model.

2.4.3 Spring Streamflow Prediction

As deduced from Figure 2.1, the snowmelt-runoff relationship is strong in the Mountain West. The snowmelt-runoff transition may be described in three parts (USACE 1998). First, lower elevation snowpack melts, and warmer temperatures push the snow-line to higher elevations. Second, receding snowpack leads to an increase in snow-free area, and a decrease in snow-covered area. The soil moisture in the snow-free area decreases, leaving the watershed with two regions of different runoff characteristics. Third, spring precipitation falling during the melt season occurs differently depending on elevation. It

can fall as fresh snow at higher elevations, as rain-on-snow at lower elevations, and as rain on bare ground (with reduced soil moisture) at low elevations.

To estimate time-sensitive runoff volumes, snowmelt models employ different methods, including empirically-derived snow cover depletion curves (Donald et al. 1995, Rango and Martinec 1999), snow bands (Quick 1995), and grid-cell based runoff-routing (Pietroniro et al. 2006). Remote sensing techniques are increasingly used to derive snow covered area estimates, validated with interpolated ground-based snow course and snow pillow observations (Bleha 2004, Dozier 2004). Increasingly, snow models are being coupled with fully distributed hydrologic models, to obtain simulated streamflow on daily or sub-daily time steps (Garen and Marks 2005). However, such approaches are currently limited to the research setting, due to the time and resource needs required for such models.

Statistical Regression Method

In the Mountain West, spring streamflow forecasts are made during mid-season to obtain spring water supply information (e.g., flood or drought conditions). Compared to the research setting, time is critical in the operational streamflow forecasting setting; therefore, less data and resource-intensive methods are used. For example, a statistical method is used that incorporates snowmelt runoff and rainfall runoff variables as surrogates for spring runoff. The method works largely because variability of winter snow water equivalent (SWE), which represents snowmelt runoff, is highly linked to variability in spring streamflow (Doesken et al. 1989).

Forecasters use point-scale SWE, precipitation, and temperature observations (each derived from snow surveys), SNOTEL or snow pillow instruments, and climate stations (USACE 1998, Pagano et al. 2005). They also use stream gauge information. Z-scores or principal components analyses are used to weight the above input data. This improves the horizontal spatial representation of the data, relative to the watershed whose streamflow is being forecasted (Garen 1992). The data are converted to indices, and used in multiple linear regressions (MLRs). Following is an example equation used in water supply forecasting (USACE, 1998):

$$Y = a + b_1BF + b_2FP + b_3WP + b_4SWE + b_5SP \quad (2.1)$$

Where:

Y is the seasonal streamflow volume (e.g., April-July)
a is the intercept coefficient
b_1, b_2, etc. are the regression coefficients
BF is the base-flow volume (e.g., October-December)
FP is the fall-precipitation index
WP is the winter-precipitation index

SWE is the snow-water-equivalent index
SP is the spring-precipitation index

The MLR is calculated for a minimum of 15 years, and error evaluation can include analyzing the following criteria: rationality of the coefficients; relative importance of the predictor variables; characteristics of the residuals; coefficient of multiple determination; and standard error of the estimate (McCuen 1985).

Despite the straight-forward application of the MLR method, relative to fully distributed hydrologic snowmelt modelling, it does present limitations. For example, the complex terrain of mountain basins has a strong influence on temperature and precipitation. In turn, this can substantially affect SWE variations from year to year on a watershed scale (Braun 1991, Reuna 1994). Therefore, an obvious improvement to this method would be to use regression variables that have been derived from a spatially distributed, physically-based, SWE model. This thesis adopts such a model to derive spatially distributed, mass balance-based snowmelt runoff and rainfall runoff variables to predict spring streamflow volume (using a statistical regression similar to Equation 2.1).

2.5 Snow Water Equivalent Model

The physically-based SWE Model used in this study does not consider some of the snow accumulation and ablation processes discussed in the previous section. Rather, it uses available data to spatially distribute daily hydrometeorological variables throughout the study watershed, and simulate key snow mass balance processes. This is achieved using the SIMGRID and SNOPAC programs. The following provides background to these

programs, which combined are referred to as the SWE Model. All programs are written in the Fortran-77 programming language.

2.5.1 SIMGRID

The SIMGRID model (Shepperd 1996) was developed to create distributed hydrometeorologic output to cover an entire watershed, considering its complex topography. This is achieved by repeating (looping) the calculations for weather estimates according to sites having different combinations of elevation, slope, and aspect classes. Terrain Categories (TCs) are the unique combinations of the aforementioned classes. For example, Sheppard (1996) used 10 elevation, 3 slope, and 4 aspect classes, yielding a combination of 120 TCs, to characterize a watershed covering 144,558 pixels, each 100 m by 100 m. The Mountain Microclimate Simulation Model (MTCLIM) is used to determine weather estimates at the sites.

2.5.1.1 MTCLIM

The MTCLIM model was developed by the Intermountain Research Station (Ogden, Utah), as a means of generating climate data for a variety of ecosystem-based modelling purposes (Hungerford et al. 1989). MTCLIM logic has been used in a number of studies throughout western North America (Glassy and Running 1994, Coughlan and Running 1997, Kimball et al. 1997, Thornton et al. 2000). It predicts hydrometeorologic variables for mountainous sites by extrapolating data measured at base weather stations (BASE). In MTCLIM terminology, weather data from the BASE drives the simulation of weather

recorded at the SITE. Data are corrected for the differences in elevation, slope, and aspect between BASE and SITE.

Key data for the BASE weather stations include latitude, daily air temperature extremes, and precipitation. Input requirements for the SITE include terrain features, vegetation characteristics, and precipitation. The SITE's terrain features include elevation, aspect, slope, and east-west horizon angles. Vegetation characteristics are Leaf Area Index (the leaf area per square metre of ground surface; LAI) and the associated albedo (the percentage of solar radiation reflected by a surface). Hungerford et al. (1989) use an LAI of 1.0 and suggest it as being appropriate for a Northern Rocky Mountain coniferous forest. With respect to albedo, forest canopies reflect approximately 10-20% of incoming solar radiation, while grasses and rock reflect 20-25% and 10-30%, respectively. Given the landcover in the study area (described in section 3.1), albedo was left constant at 20% for this study. The model outputs four meteorological variables for the site, as discussed below.

Solar Radiation

Incoming solar radiation is calculated using an algorithm relating diurnal air temperature amplitude to atmospheric conditions. First, clear sky transmissivity is computed for the elevation of the site of interest, assuming clear sky transmittance at mean sea level is 0.65, and increasing by 0.008/m elevation. Final atmospheric transmissivity is then calculated as an exponential function of diurnal temperature amplitude of the BASE station. This accounts for clouds, water vapour, pollutants, and other atmospheric factors

reducing clear sky transmissivity. Solar radiation was not explicitly used in this study. Rather, its use was in simulating maximum temperatures on varying slopes and aspects. South-facing aspects, for example, receive greater amounts of solar radiation relative to north-facing aspects, and thus experience greater maximum daily temperatures.

Precipitation

Given the highly variable nature of mountainous precipitation, accurate simulation is very difficult, especially for short (i.e., daily) timescales. MTCLIM uses a simplistic algorithm that applies the ratio between BASE and SITE annual average precipitation (isohyets) to the daily BASE station values. SITE annual precipitation is estimated from annual isohyetal maps while BASE station annual precipitation is obtained from long-term averages for the BASE stations used. More recent studies using MTCLIM to derive SWE improved this precipitation derivation method for the alpine headwaters of the Oldman River Basin (Shepperd 1996, Lapp et al. 2005). The precipitation formulation was adjusted in this study, and discussed in Chapter 3.

Temperature

Daily ground surface maximum, minimum, and daylight average temperatures are computed for each SITE. The extreme temperatures are corrected for elevation using minimum and maximum temperature lapse rates of 3.8 and 8.2°C, respectively. These lapse rates were verified in Chapter 3. Maximum and daylight average temperatures are affected by slope and aspect. Leaf Area Index (LAI) also influences maximum and

daylight average temperatures, as canopy absorption decreases the amount of radiation reaching the ground surface.

Relative Humidity

SITE humidity is derived from BASE station dew point or minimum temperature and simulated SITE daylight average temperature, and is given as a percent relative to saturated air conditions. SITE dew point is either measured or estimated from the BASE minimum temperature, and then corrected using a lapse rate of 2.7°C/1000 m, modified to account for radiation. The relative humidity output was not used in this study.

2.5.2 SNOPAC

The SNOPAC model derives daily SWE for each Terrain Category (TC), based on the daily maximum and minimum temperatures and precipitation output from SIMGRID. The program's two main routines include temperature-based precipitation partitioning and snowmelt using a three-way parametric energy balance. Both of these routines are addressed below, while the main program is discussed in Chapter 3, where changes made for purposes of this study are explained.

Precipitation Partitioning

The precipitation partitioning algorithm was taken from Wyman (1995). On each day, for each TC, snowfall is calculated using:

$$SNOW = P - RAIN \tag{2.2}$$

Where:

SNOW is the snowfall (mm)
RAIN is the precipitation that falls as rain (mm)
P is the total daily precipitation (mm)

And where:

RAIN is 0 if $Tmean < 0.6°C$
RAIN is $P \times [(Tmean/3) - 0.2]$ if $0.6°C < Tmean < 3.6°C$,
(*Tmean* is mean daily temperature)

Snowmelt

Snowmelt is computed using a technique from the UBC Watershed Model (Quick and Pipes 1977), which takes into consideration three primary sources of snow melting energy. First, convective heat transfer from warm air is estimated as being equal to the mean daily temperature above freezing. Second, the net radiant energy gain from shortwave and long-wave radiation exchange is considered, and is represented as the daily temperature range. Finally, the latent heat gain from condensation or loss through evaporation at the surface is derived as a function of the minimum temperature (approximating the dew point temperature).

Snow melt is related to the rate at which the snowpack absorbs heat. Pipes and Quick (1977) use a negative melt decay (degree-day) function to deplete snowpack cold storage. The snowpack's heat balance is determined for each day, and potential melt conditions are thus delayed even if daily temperature conditions would appear warm enough for

melt. When the snowpack's temperature required for melt (TREQ, see section 3.3) becomes positive, open area melt occurs according to the following formula:

$$MELT_i = \text{PTM}*(Tmax_i + \text{TCEADJ} * Tmin_i) \quad (2.3)$$

Where:

i is the day of snowmelt simulation
MELT is the melt depth (mm)
PTM is the point melt factor (a value of 1.8 mm/day/°C was used in this study, as in Lapp et al. (2005))
Tmax is the daily maximum temperature (°C)
Tmin is the daily minimum temperature (°C)
TCEADJ is the energy partition multiplier

And where:

$$\text{TCEADJ} = \frac{Tmin_i + Tr/2}{\text{XTDEWP} + Tr/2} \quad (2.4)$$

Where:

Tr is the range of temperature over the particular day (°C)
XTDEWP is the reference dew point that controls energy partitioning between melt and sublimation (a value of 18°C was used in this study, as in Lapp et al. (2005)

Mass Balance

Once daily snowfall and snowmelt are determined, the day's snow water equivalent is added to the snowpack:

$$SWE_i = SWE_{i-1} + SNOW_i - MELT_i \quad (2.5)$$

Where:

i is the simulated day of snow accumulation
SWE is the accumulated snow water equivalent in the snowpack
SNOW is the daily snowfall
MELT is the daily snowmelt

2.6 Climate Change Scenarios

Climate change impact assessments use regional-scale models, such as the ones described previously, to make future projections for a study area. Predicting the impacts of climate change on regional climate is paramount for adapting to future water supply regimes (Barnett et al. 2004). Generally, Global Circulation Model (GCM) output is used to "downscale" changes in temperature and precipitation (climate change scenarios) for a given region. The uncertainty of these inputs compounds the uncertainty and limitations of the regional-scale models used (Mitchell et al. 1999).

2.6.1 Global Circulation Models

Among their many uses, GCMs provide useful information about the rate and magnitude of climate change (Barrow et al. 2004). Many GCMs have been developed around the world, each with their own variations of numerically portraying the Earth's climate system through algorithms. The model equations are based on physical laws such as the conservation of energy, mass, and momentum, as well as the ideal gas law (McGuffie and Henderson-Sellers 2001). Many GCMs now include atmosphere-ocean coupling (also referred to as AOGCMs). These GCMs link three-dimensional models of the atmosphere with a three-dimensional model of the ocean. With simulated ocean circulation, the models account for heat and moisture exchange from ocean to atmosphere, which means they are able to simulate the climate response to changes in atmospheric composition. Most GCMs have a horizontal resolution of between 250 and 600 km, with 10 to 20 vertical layers in the atmosphere and as many as 30 layers in the ocean (McGuffie and Henderson-Sellers 2001, Barrow et al. 2004). A selection of the coupled GCMs found in

the literature, and whose data is publicly available through the Pacific Climate Consortium website (from which data was downloaded for this study), appear in Table 2.1.

Table 2.1. GCMs whose output is publicly available through the Pacific Climate Impacts Consortium.

Model Description	Modelling Centre/Agency	Reference
Second generation coupled global climate model (CGCM2)	Climate Centre for Modelling and Analysis (CCCMA), Canada	(Flato and Boer 2001)
(CCSRNIES)	Center for climate Research Studies (CCSR) and National Institute for Environmental Studies (NIES), Japan	(Emori et al. 1999)
CSIRO Mark 2 (CSIROMk2b)	Commonwealth Scientific and Industrial Research Organization (CSIRO), Australia	(Gordon and O'Farrell 1997, Hirst et al. 1997)
Third generation coupled model (HadCM3)	Hadley Centre for climate prediction and Research, England	(Gordon et al. 2000)
Parallel climate model (NCARPCM)	National Center for Atmospheric Research (NCAR), United States	(Manabe and Stouffer 1994)
Fourth generation model (ECHAM4)	Max Planck Institute for Meteorology, Germany	(Roeckner and co-authors 1996)
(GFDL_R30)	Geophysical Fluid Dynamics Laboratory	(Dixon et al. 2003)

2.6.2 Emissions Forcings

CGMs are driven by changes in radiative forcing, which correspond to future GHG emissions scenarios. On average, they simulate increases in carbon dioxide equivalent concentrations of about 1% per year from 1990 to 2100 (IPCC 2001). Storylines were established to characterize 40 plausible future emission paths related to different combinations of economic, technical, environmental, and social development (Nakićenović et al. 2000). The six main storylines from the Special Report on Emissions Scenarios (SRES) are summarized in Table 2.2.

Table 2.2. Matrix of development levels represented by the six main SRES scenarios. Source: Canadian Climate Change Scenarios Network (CCCSN 2007).

Scenario Group	A1FI	A1B	A1T	A2	B1	B2
Population Growth	Low	Low	Low	High	Low	Medium
GDP Growth	Very High	Very High	Very High	Medium	High	Medium
Energy Use	Very High	Very High	High	High	Low	Medium
Land Use Change	Low-Medium	Low	Low	Medium-High	High	Medium
Oil/Gas Resource Availability	High	Medium	Medium	Low	Low	Medium
Technological Change	Rapid	Rapid	Rapid	Slow	Medium	Medium
Change Favouring	Coal, Oil and Gas	Balanced	Non-Fossil Fuel	Regional	Efficiency and Dematerialization	"dynamics as usual"

The output from GCMs forced by a particular emissions scenario is called a model experiment. GCMs are transient, and different model experiments yield differing results, due to the simulation of non-linear physical processes. Therefore, many GCMs are run several times with the same forcing. Typical nomenclature used to describe a specific model experiment indicates the acronym for the model, followed by the emissions scenario used and the number of the model experiment. For example, output from the CSIROMk2b A21 was produced by the Commonwealth Scientific and Industrial Research Organization's model, using the A2 scenario for the first model experiment.

2.6.3 Impact Assessments Modelling

GCM outputs are used to alter observed climate records to run regional-scale models to obtain future impacts assessments. Historical 30-year normals are recommended, since they are likely to reflect extreme conditions for a particular area (Smith and Hulme 1998, IPCC-TGCIA 1999). GCM output for the grid cell(s) overlying the impact assessment area are downscaled to the study area's climate station network. This provides a quantifiable projection of climate changes to expect, which are rooted in global-scale climate science. Among methods used to achieve climate downscaling is the delta technique (Wood et al. 1997, Hay et al. 2000). This simple method applies the hydroclimatic changes (e.g., on daily, monthly, or seasonal scales) to the baseline climate record. For example, the future climate change scenario for the period 2040-2059 is obtained by adding the projected changes in temperature and precipitation for the said period onto those observed for the period 1961-1990.

Numerous sources of uncertainty exist in climate change impacts assessment modelling (Döll et al. 2003, Prudhommes et al. 2003, Arnell 2004), including:

- Natural climatic variability
- Emissions scenarios and associated GHG concentrations
- GHG concentrations and associated radiative forcings
- Radiative forcings and associated climate sensitivities
- GCM structure and precipitation outputs
- Grid-cell resolutions, particularly over complex terrain such as mountains
- Regional model simulation (in this thesis, the SWE Model)

2.7 Summary

The literature shows that modest snowpack decline has been observed for the St. Mary River headwaters region in the last half-century. Acknowledging differences in model projections, this could be expected to continue with warmed climate, as widely observed and projected over greater WNA. This is likely to have consequences for the River's water supply and its users. A model that can distribute daily climate data through complex terrain is essential to simulate snow accumulation and melt. Such data may then be used to estimate associated changes in spring streamflow. The first step in adopting such a modelling approach is undertaken in Chapter 3.

CHAPTER 3: Refining a Watershed Snow Water Equivalent Model for the Montana-Alberta Rockies

3.1 Introduction

Snowpack acts as an effective water reservoir, storing a large percentage of winter precipitation, and releasing this water during spring snowmelt (Bales et al. 2006). A substantial set of climate stations, snow courses and snow pillows, and stream gauges are in operation in the Mountain West. Such data are very useful for the observation of large-scale (e.g., western North America) spatial trends in snow hydrology (Mote et al. 2005a, Stewart et al. 2005). In contrast, watershed-scale studies are usually deficient in data sources, especially at high elevations (Diaz 2005). This inhibits the consideration of topographic influences. Models can simulate such influences, and can thus help fill gaps in mountain watershed hydrology research.

Complex terrain plays an important role in watershed SWE patterns. High elevations experience greater precipitation (due to orographic effects) and lower temperatures, but represent small proportions of total watershed area. Lower elevations, representing greater proportional area, tend to be closer to the freezing line in winter. Snowpack at these elevations is greatly influenced by small temperature changes, because of the sensitivity of rain-to-snow ratios and melt incidence in this critical temperature range (Regonda et al. 2005).

Spatially explicit temperature and precipitation simulations are thus necessary components of mountain SWE modelling in complex terrain. However, challenges

remain with microclimate estimation (particularly precipitation) using spatial interpolation models at a watershed scale (e.g., Daly et al. 1994, Huntchinson 1995, Thornton et al. 1997, Hay et al. 1998, Liston and Elder 2006b). Therefore, high-elevation and site-specific precipitation data is valuable in SWE modelling research.

Objective

This work refines a spatially distributed and physically-based watershed SWE Model (see Shepperd 1996, Lapp et al. 2005). The key objective is to produce daily watershed SWE and rainfall volumes, for use in Chapter 4. To achieve this objective, regionally specific input data was used in the following steps:

- Verify the model's temperature routine using field data for the Lakeview Ridge research site near Waterton, AB;
- Formulate a site-specific proxy precipitation-elevation (P-E) relationship based on snow course SWE data, and link into the model using the St. Mary, MT, climate data as the model input;
- Develop a daily historical record for the St. Mary climate station for the period 1960-2006, through the investigation of regional climate station relationships;
- Refine the model's main snow accumulation algorithm to account for rain-on-snow conditions, and run the SWE Model.

3.2 Study Area

Hydroclimate

The general study area lies on the eastern slopes of the Alberta-Montana Rockies, in the area of Waterton-Glacier International Peace Park (Figure 3.1). The modelled watershed comprises the headwaters of the St. Mary River basin. The St. Mary is a transboundary river whose headwaters stem from 3000 m high mountains. Waters from the Upper and Lower St. Mary lakes flow northward to the drier prairies of southern Alberta, Canada (Figure 3.1). The watershed's westernmost peaks are part of the Continental Divide. The area is unlikely to be directly affected by human landuse change in future. It is thus an excellent site for studying global environmental change impacts on natural ecosystems (Fagre et al. 2003).

Broadly, the area is sharply transitional between a northern Pacific coastal and continental climate. Superimposed are mountain climate characteristics. In winter (November-March), the Pacific influence is noted by increased cloudiness and precipitation over the park. The orographic effect is strong, especially on the western side of the Continental Divide, and also affects upper elevations east of the divide due to precipitation "blow-over" (Finklin 1986). The effect is also noted on the eastern slopes in spring, when Arctic low pressure systems traveling westward encounter the Front Ranges of the Rockies (Reinelt 1970). Most of the precipitation in the area occurs during winter and snowfall contributes about 70% of the total precipitation at high elevations (Selkowitz et al. 2002).

Chinooks are a dominant climatic factor for the eastern slopes of the study region. This warm, dry wind can induce rapid snowmelt. It originates due to the prevailing westerlies, which carry modified Pacific air masses eastward, resulting in orographic precipitation on the windward side of the Rockies and a rain shadow effect on the lee side (Ahrens 2007). As saturated air rises on the windward side of the continental divide, the air temperature falls at the moist adiabatic lapse rate. As the air descends on the lee side, the air temperature rises at the dry adiabatic lapse rate, resulting in an increase in sensible heat and a larger decrease in latent heat content. The result is a warmer but much drier air mass in the eastern slopes and prairie regions. Also, changes in wind direction result in large temperature variations over short time periods, especially in the fall and winter seasons (Grace 1987).

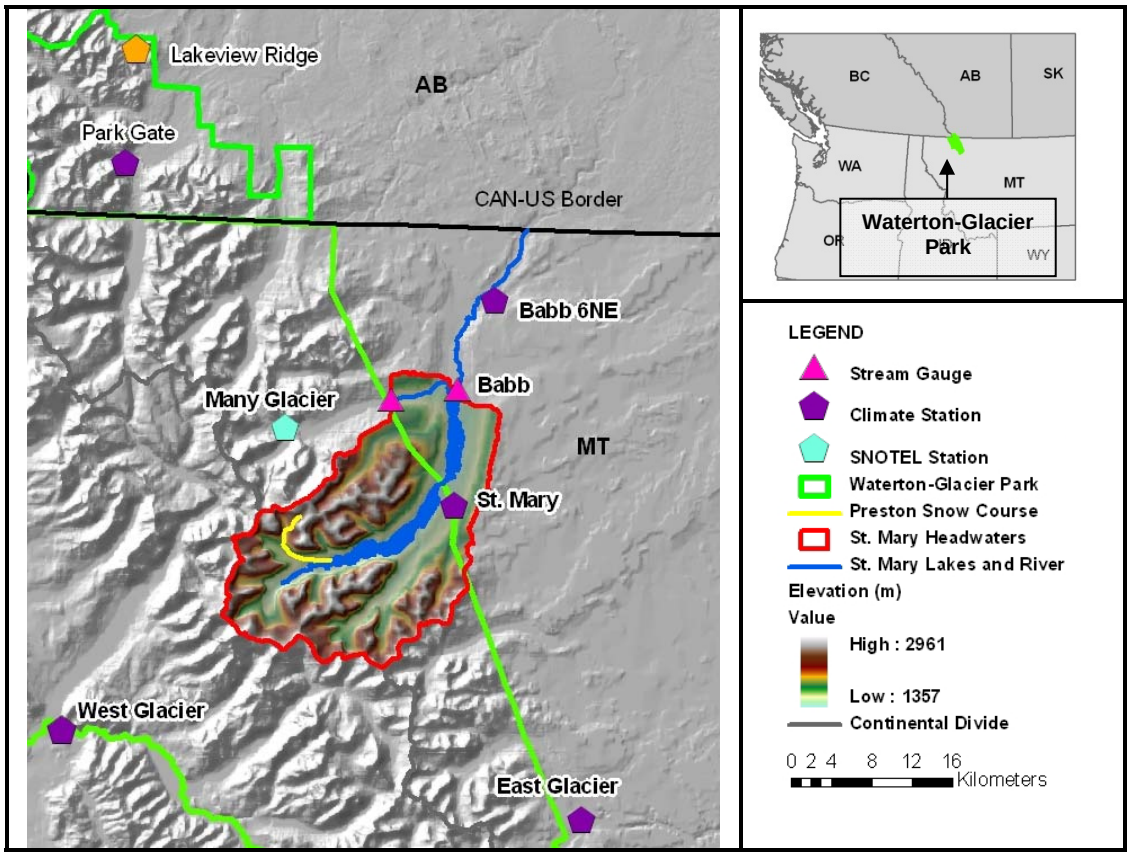

Figure 3.1. The area shown encompasses Waterton-Glacier International Peace Park, where the British Columbia (BC), Alberta (AB) and Montana (MT) borders meet (inset). The study watershed surrounds the St. Mary Lakes. The Preston Snow course begins at the west end of Upper St. Mary Lake, and curves clockwise as it gains elevation. The Lakeview Ridge and Park Gate climate stations are located to the north. Located within the watershed, the St. Mary climate station was used as the base station for the SWE Model. Nearby climate stations analyzed were West Glacier (west side of the continental divide), Many Glacier (mountain location), East Glacier (in the mountain-to-prairie transition zone, like St. Mary) and Babb 6NE (on the prairie).

Physiography

The study watershed's outlet is at Babb (1363 m elevation). Babb is located just downstream of St. Mary Lakes, and these natural reservoirs have an attenuating effect on streamflow. For naturalized streamflow analysis purposes (Chapter 4), the delineated area of the watershed comprises the upstream contributing portion from the Babb gauging

station, minus the portion located upstream of the Lake Sherburne Dam outlet gauge station.

Coniferous species (e.g., lodgepole pine, white spruce, Douglas-fir) cover 35% of the area, while another 25% is covered by deciduous and herbaceous plants. Approximately 20% of the land is characterized as rock or soil, and water accounts for just over 4% of the area (USGS 2000). The average slope is 20° in this rugged terrain (according to a 10 m × 10 m digital elevation model). The watershed area is 554 km^2, and the mean elevation is 1840 m. While the elevation range is 1363-2961 m, 98% of the elevation lies below 2600 m.

3.3 Model Description

The SWE Model used in this study is a combination of SIMGRID and SNOPAC programs. The SIMGRID program (Shepperd 1996) distributes simulated climate variables across a watershed, based on aspect, slope, and elevation terrain classes derived from a digital elevation model (DEM). It incorporates the Mountain Microclimate (MTCLIM) Model (Hungerford et al. 1989), which uses basic atmospheric physics and terrain characteristics to estimate solar radiation, air temperature, precipitation, and relative humidity on a daily time step. Daily maximum and minimum air temperatures, as well as precipitation are the key MTCLIM routines used in this study. The base climate station data is used to extrapolate data to watershed locations. These locations are SIMGRID terrain categories (TCs).

The St. Mary headwaters DEM (provided by D. Menicke, USGS, February 2006) comprises 5,544,283 pixels of 10 m × 10 m. Extrapolating to all pixels at such a scale would be time-consuming with no benefits to accuracy. To address this, each pixel in the watershed was reclassified according to 100 m × 100 m block means, using the elevation, slope, and aspect classes in Table 3.1. The resampled pixels were then lumped into Terrain Categories (TCs) of equivalent terrain features using a SIMGRID Preprocessor program (provided by S. Kienzle, U of L Geography Dept.). This was the input, having originated from high-resolution data, through which SIMGRID looped to cover the watershed for daily calculations. Out of the 816 possible TCs resulting from the class combinations, 566 actually occurred in the watershed. This was a considerable reduction compared to the 5.5 million original pixels.

Table 3.1. Study watershed terrain classes used to group the 5,544,283 pixels into 566 Terrain Categories (TCs).

Elevation (m)	% Area
1351-1450	14.43
1451-1550	11.58
1551-1650	9.32
1651-1750	9.70
1751-1850	9.69
1851-1950	8.18
1951-2050	8.35
2051-2150	7.60
2151-2250	6.43
2251-2350	5.38
2351-2450	4.45
2451-2550	2.72
2551-2650	1.37
2651-2750	0.54
2751-2850	0.17
2851-2950	0.06
2951-3050	0.02

Aspect	% Area
N	2.62
NE	9.07
E	14.57
SE	18.31
SE	16.53
SW	9.30
W	15.80
NW	13.80

Slope (°)	% Area
0-15	49.50
15-30	26.19
30-45	18.90
45-60	5.07
60-75	0.35

The SNOPAC program estimates daily snow accumulation and ablation for each TC output from SIMGRID. The main program encompasses precipitation partitioning and snowmelt routines. The former algorithm is that of Wyman (1995), which partitions precipitation as snow if the mean daily temperature is below 0.6°C. Rain occurs when mean daily temperatures exceed 3.6°C, with a mix of rain and snow occurring on days when mean daily temperatures are within the above thresholds.

The snowmelt algorithm is based on the UBC Watershed Model (Quick and Pipes 1977). Snowmelt occurs by using daily temperatures as proxies for three primary sources of melt energy. First, convective heat transfer from warm air is estimated with the mean daily temperature above freezing. Second, the net radiant energy gains from shortwave and longwave radiation exchange is considered, and is represented as the daily temperature range. Third, the latent heat gain from condensation or loss through evaporation at the surface is derived as a function of the minimum temperature (approximating the dew point temperature).

3.4 Methods and Data

Several steps were needed to complete the SWE Model runs covering the period 1960-2004; these are described below. Program routines were verified and modified where appropriate. A continuous climate data set was also created for model input.

3.4.1 SIMGRID: Spatial Climate Distribution

3.4.1.1 Temperature Routine Verification

The MTCLIM temperature routine is an important component of the SWE Model, for temperature controls rain/snow partitioning, snow accumulation and melt. The routine adjusts maximum temperature (*Tmax*), according to a lapse rate of 8.2°C/km (Shepperd 1996). *Tmax* is also adjusted according to slope and aspect, based on ratios of daily solar radiation received on such complex surfaces compared to flat surfaces. Minimum temperature (*Tmin*) is simply adjusted by a lapse rate of 3.8°C/km, since nighttime longwave radiation dampens the effects of complex terrain on daytime solar heating (Thornton et al. 1997, Blennow 1998).

To verify the routine, simulated maximum and minimum temperatures were compared to those observed at 1 m height at Lakeview Ridge site (49.16°N, 113.91°W), an isolated 1938 m peak alongside the NE boundary of Waterton Lakes National Park (Figure 3.1). Observations were made from November 26, 2005 to March 23, 2006 using HOBO (H21-001) weather loggers (unpublished data was provided by M. Letts, U of L Geography Dept. The site is located approximately 50 km from the St. Mary watershed, and exhibits near-perfect NW, SW, SE, and NE aspects. Each station is located at 1902

m. The base station used for the simulations was the Park Gate climate station (1296 m), located 12 km from the Lakeview Ridge site (Figure 3.1).

3.4.1.2 Proxy Precipitation-Elevation Formulation

A relationship explaining how precipitation increases with elevation within the watershed was defined. The precipitation-elevation (P-E) formulation approximated the orographic effect. To do this, SWE data from the Preston snow course was used, and observations were used as proxies for precipitation observations.

Survey SWE

Snow water equivalent (SWE) is the depth of liquid water stored in a snowpack. It is calculated from snow depth measurements using a Federal snow sampler (a calibrated tube with known weight and volume) (ASCE 1996). The Preston snow survey began in 1994, and is ongoing by the United States Geological Survey (USGS). Data were acquired from the inception of the Preston survey to the end of the 2006 snow year, totaling 73 dates (Fagre 2006). The 10 km-long survey is located near the centre of the study watershed (Figure 3.1), and consists of 32 sampling points, mainly on south and southwest aspects. Sampling locations span from 1438 m to 2290 m elevation. Considering the proportional areas of the 100 m elevation bands used for SIMGRID modelling (Table 3.1), the snow survey transects 85% of the total watershed area (Figure 3.2).

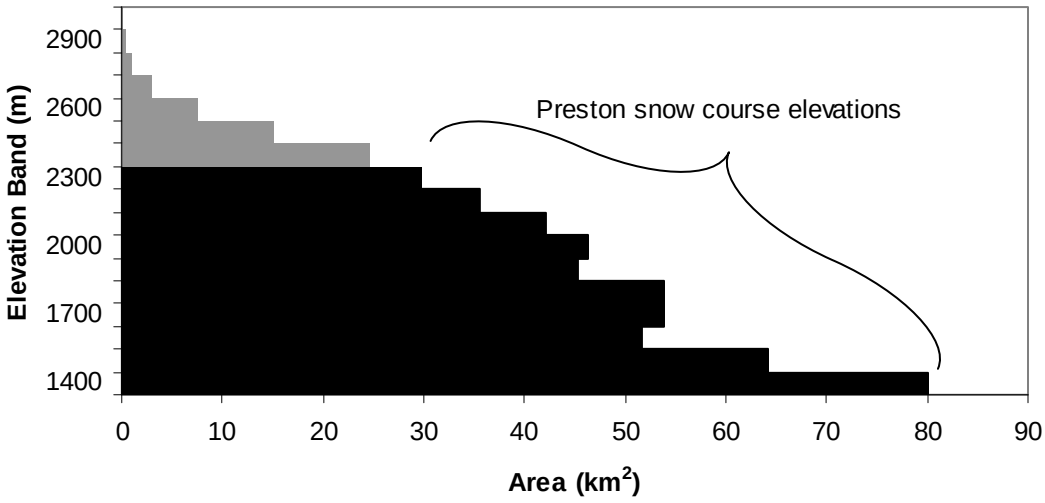

Figure 3.2. Study watershed elevation band areas, classified according to Table 3.1. The elevations bands encompassing the Preston snow course are in black.

Throughout this study, SWE and precipitation data from the Many Glacier automated snow pillow (SNOTEL) were used for verification (NRCS 2007). The SNOTEL site is located in a basin adjacent to the St. Mary headwaters basin, to the north (Figure 3.1), at an elevation of 1494 m. A check was made to verify the consistency of the Preston survey. Measurements of SWE (mm) recorded at the SNOTEL site (SWE_S) were compared with those taken manually from the corresponding survey point elevation (SWE_M) on the same day. Close SWE measurement matches were found, as $SWE_M = (1.01 \times SWE_S) - 19.30$ ($r^2 = 0.76$; n = 46).

The snow survey data were linked to the St. Mary climate station (48.73°N, 113.42°W; 1391 m elevation), and selected as the SIMGRID BASE station, to develop a proxy precipitation-elevation relationship. For this climate station, daily minimum and maximum temperatures are recorded manually, while precipitation is measured using a standard rain gauge (D. Divoky, US National Park Service, personal communication,

June 2006). The procedure used to link the St. Mary and snow survey datasets is described below.

ΔSWE Calculations

Snow surveys were conducted at approximately monthly intervals, and snow accumulation at a specific sampling point elevation was determined by subtracting one monthly measurement from the previous one. For example, ΔSWE values for 1-Feb-99 correspond to those measured on that date, minus those measured on the previous snow survey date, 7-Jan-99:

$$\Delta SWE_E^{\Delta t} = SWE_E^{t_2} - SWE_E^{t_1} \tag{3.1}$$

Where:

t is the snow survey date sequence
E is the sampling point local elevation (m above St. Mary climate station)
ΔSWE is the snow water equivalent accumulation from one survey date to the next (mm)
SWE is the recorded snow water equivalent (mm)

Two assumptions were made in obtaining ΔSWE values. The first is that ΔSWE is a proxy for cold-season precipitation (i.e., $\Delta SWE^{\Delta t} = \Delta P^{\Delta t}$), meaning that all the precipitation falling at the survey point is stored in the snowpack. This is reasonable since most ΔSWE measurements were taken between the months of January and March, and the Preston survey points lie at a high-enough elevation to assume solid precipitation during these months. (A check was made to verify this assumption by comparing ΔSWE and ΔP values recorded at the Many Glacier SNOTEL site corresponding to the Δt dates chosen for the Preston survey. The ΔSWE values at the SNOTEL site explained 73% of the variability in ΔP values. This shows that, as expected, snow water equivalent varies

closely with precipitation during the cold season. Furthermore, most of the Preston snow course lies above the Many Glacier SNOTEL station elevation. Colder temperatures along it likely lead to an even greater percentage of ΔSWE explaining ΔP variability).

The second assumption considers that melting during warm periods will result in lower SWE values recorded on one survey date compared to the previous date. Negative ΔSWE calculations were automatically rejected, as they do not accurately represent total accumulation during the time period. Furthermore, melt periods at a sampling point were defined a) based on the average temperatures recorded at the St. Mary climate station for the same time period and b) using a lapse rate of 6.5°C/km (Barry and Chorley 1987). An average temperature was thus calculated for each ΔSWE value. If the average temperature for a Δt period was above freezing, the ΔSWE value was rejected, on the assumption that melt had occurred.

P-E Formula

Following the assumptions for rejecting ΔSWE values due to melt, 31 snow survey periods were retained (from the period 1994-2006), resulting in 536 ΔSWE values spanning the 32 survey point elevations. Precipitation accumulations observed at the St. Mary climate station were matched with ΔSWE values according to time period. Given that $\Delta SWE^{\Delta t} = P^{\Delta t}$, a relationship expressing P_E as a function of St. Mary climate station precipitation and for a precipitation-elevation increment was established:

$$P_E^{\Delta t} = P_{StM}^{\Delta t} + C \times E \tag{3.2}$$

Where:

$P_E^{\Delta t}$ is the precipitation for a given elevation and time period (mm)
$P_{StM}^{\Delta t}$ is the St. Mary precipitation for a given time period (mm)
C is a constant
E is the sampling point local elevation (m above St. Mary climate station)

Equation 3.2 was rearranged in order to derive C, using a simple linear regression. The variable ΔP_{diff} replaces the term $(P_E^{\Delta t} - P_{StM}^{\Delta t})$ for clarity.

$$(P_E^{\Delta t} - P_{StM}^{\Delta t}) = C \times E$$

$$\Delta P_{diff} = C \times E \tag{3.3}$$

A scatter plot was created with ΔP_{diff} values as the independent variables, and E as the dependent variable, and a trend line was drawn (shown in section 3.5.2). Since the intercept of the fitted line was close to zero relative to the data spread (y-intercept = 26.50, Mean = 99.54, SD = 110.00) a forced-origin regression was used to further develop the relationship, and to reduce the number of terms in it. The forced-origin regression yielded a slope C = 0.232. This constant became the predictor of precipitation increment with elevation.

The relationship was derived based on approximately monthly snow accumulation data. To apportion the accumulation over a month on a daily time step, a P_{StM} ratio of daily to monthly precipitation was incorporated:

$$P_E(daily) = P_{StM}(daily) + 0.232 \times E \times \left(\frac{P_{StM}(daily)}{P_{StM}(monthly)} \right) \tag{3.4}$$

3.4.1.3 Climate Time Series Construction

A continuous climate time series was required to drive SIMGRID on a daily time step. In addition, a long-term time series, spanning 1960-2006, was sought. Such a period length is considered to capture extreme years, reflecting natural variability in the climate record (IPCC-TGCIA 1999). This was important given the future climate change assessment work in Chapter 5.

The St. Mary station climate record, however, contained some gaps, and recording began in May 1981. Therefore, temperature and precipitation regressions were conducted with nearby climate stations, for the overlapping period 1981-2006. The objective was to choose representative stations to both fill-in and extend the St. Mary station record back to 1960. Recent data (i.e., 2003 to 2006 data) were obtained on-line directly from the National Ocean and Atmospheric Administration and National Climatic Data Center joint on-line portal (NOAA/NCDC 2006). Historical climate data was obtained from NCDC's Global Daily Climatology Network (GDCN) via compact discs (NCDC 2005).

The Babb 6NE station (hereafter referred to simply as Babb) had the best combination of data completeness and representation, and was chosen to extend and fill-in the St. Mary temperature record. However, the Babb precipitation record was not suitable to represent conditions at St. Mary. There is considerable spatial variation in precipitation surrounding the study area; therefore, precipitation comparisons between climate stations surrounding the study area were required (section 3.5.4).

3.4.2 SNOPAC: SWE and Rain Estimation

The spatially distributed outputs of SIMGRID climate variables were used to determine snow mass balance using SNOPAC. In previous studies (e.g., Lapp et al. 2005) SNOPAC was used for snow accumulation to make crude estimates of watershed maximum potential snowmelt runoff. Key changes were made to SNOPAC herein to account for rain-on-snow (ROS) conditions, which would allow more accurate differentiation of inputs to snowmelt runoff versus rainfall runoff.

3.4.2.1 Rain-on-Snow Consideration

In the SNOPAC program, the onset of snowmelt begins when the snowpack's cold storage has been depleted. When the variable TREQ becomes positive, the temperature required for snowmelt has been reached. For each day, TREQ is calculated using a negative decay function:

$$TREQ_i = \text{ANMLTF} * TREQ_{i-1} + Tmean_i \quad (3.5)$$

Where:

i is the given day of simulation
TREQ is the temperature required for melt (°C)
ANMLTF is a constant (it was set to 0.85, as in Lapp et al. (2005))
Tmean is the mean temperature (°C)

SNOPAC's main algorithm was enhanced to include rain in snow mass balance, when the snowpack's cold content is not exhausted (i.e., $TREQ < 0$). Although such conditions are not frequent in the study watershed, rain-on-snow events do occur in the cool interior Rockies as early as September and as late as June, since thick snowpacks persist under warmer spring temperatures (McCabe et al. 2007). Rain-on-snow consideration improves model output (Marks et al. 1998). This is important, because the frequency of such conditions is likely to increase under climate warming (Loukas et al. 2002b, Leung et al. 2004).

The algorithms used in the refined SNOPAC program, named SNOPAC-ROS, to determine SWE added to the snowpack on each day were:

1. If $TREQ_i < 0$, then
   $SWE_i = SWE_{i-1} + SNOW_i + RAIN_i$ (3.6)
2. If $TREQ_i > 0$, then
   if $MELT_i < SWE_{i-1}$, then
   $SWE_i = SWE_{i-1} + SNOW_i - MELT$ (3.7a)
   if $MELT > SWE_{i-1}$, then
   $SWE_i = 0$ (3.7b)

Where:

i is the given day of simulation
SWE is the accumulated snow water equivalent in the snowpack (mm)
SNOW is the snowfall (mm)
RAIN is the rainfall (mm)
MELT is the amount of SWE melted (mm)

A large proportion of rain that falls on melting snowpack is not absorbed by the snowpack, but becomes runoff. This is consistent with what previous models have simulated when snowpack cold content is exhausted (D. Marks, Northwest Watershed Research Center, personal communication, June 30, 2007). Daily SWE surfaces were produced using SNOPAC. Using the refined SNOPAC-ROS, daily SWE surfaces along with rainfall depths were produced.

3.4.3 Summary of SWE Model Inputs and Outputs

The steps taken to run the SWE Model and manage data files are summarized in Figure 3.3, and described below:

- The SIMGRID precipitation routine was modified to incorporate Equation 3.4. A new monthly precipitation parameter was incorporated into the SIMGRID climate input file. Next, the complete daily historical temperature and precipitation data

for St. Mary base station, for the period 1960-2004, was formatted for SIMGRID input. (The climate data for 2005-2006 were not used, due to unavailable matching streamflow data, Chapter 4).

- Snow seasons span calendar years, and the SIMGRID program code limits runs spanning an excess of two years. Therefore, the 44-year climate file was reformatted into two-year files, which were run separately (e.g., 1960-61, 1961-62, 1962-63 and so on).
- A batch file was written to run the 44 two-year input files into the SIMGRID program. Daily outputs were produced for the four variables of interest (*Tmax*, *Tmin*, *Pdaily*, *Pmonthly*) for the 566 TCs over 44 years.
- The two-year SIMGRID output files were run separately through both SNOPAC and SNOPAC-ROS.
- For each of SNOPAC and SNOPAC-ROS output, the two-year files were reformatted to output one file containing daily values for each TC for each water year spanning 1961-2004. The water years began on October 1 of the previous year. For example, the first water year (WY1) spanned October 1, 1960 to September 30, 1961.

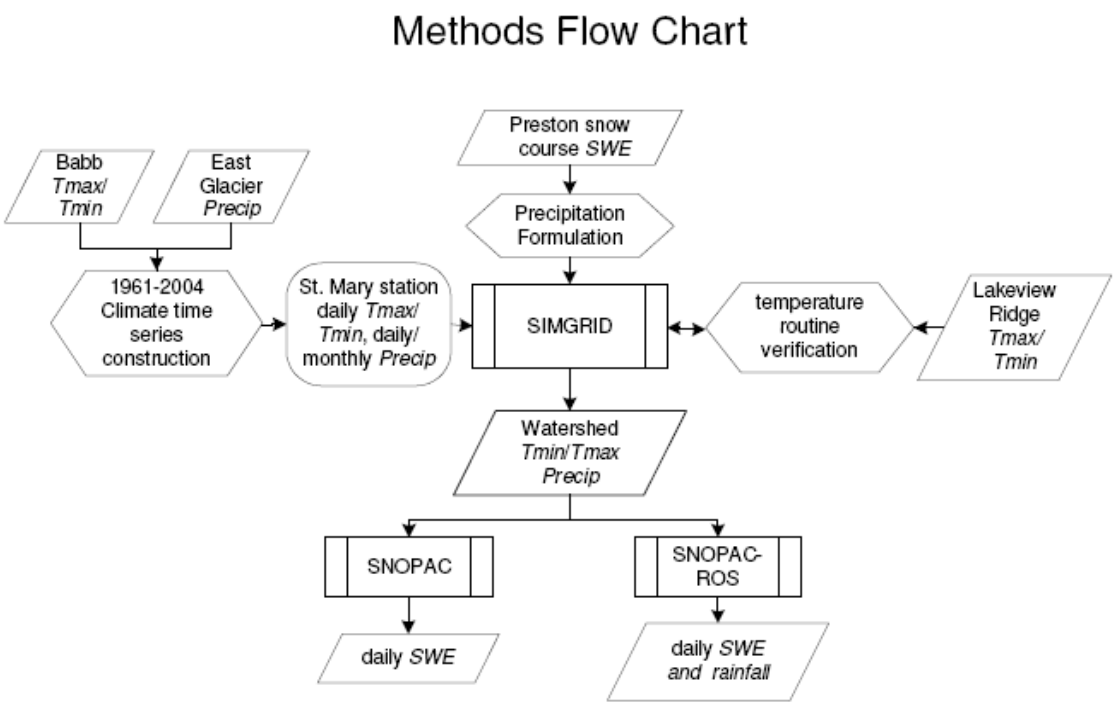

Figure 3.3. The primary data sources input to the SWE Model are shown. SIMGRID distributes the climate variables for the watershed. The outputs are then input into SNOPAC and SNOPAC-ROS to obtain *SWE* (and in the case of SNOPAC-ROS, rainfall) outputs for the 1961-2004 water years.

3.5 Analysis

3.5.1 Lakeview Ridge Temperature Simulations

The SIMGRID temperature routine was verified at a nearby mountain site, Lakeview Ridge, in Waterton Park, Alberta. Figure 3.4 shows the scatter plots of the daily observed and simulated values; patterns are similar for all aspects and both temperature extremes. Table 3.2 shows the observed versus simulated comparison statistics. The following inferences may be made about the model simulations:

- Generally the simulations result in small root mean square error values (RMSE ranges from 4.14°C to 4.68°C), which are below the standard deviations of the observed values (SD_{obs} = 5.49 °C).

- All the comparisons indicate that both *Tmin* and *Tmax* are under-simulated (more negative) compared to observed values.
- Under-simulations are slightly more obvious for *Tmax*. Lakeview Ridge is sparsely vegetated, lies on the edge of the prairies, and is subject to high winds. With little or no snowpack on sunny days, ground surface heating could be substantial on its slopes. This would result in higher-than-usual *Tmax* observations.
- Ground surface heating effects are likely strongest on SW aspects, where daily incident solar radiation peaks during the warmest part of the day (afternoon). This may explain the slightly lower coefficients of determination (r^2) for this aspect.
- Overall, simulation results reveal that the temperature routine performs well on differing aspects for the modelling purposes of this study.

Table 3.2. Descriptive statistics of the observed vs. simulated *Tmax* and *Tmin* at Lakeview Ridge. In the equation y = ax + c, y is the simulated and x is the observed temperature.

	Aspect	Slope (°)	r^2	a	p_a	c	p_c	SD_{obs}	SD_{sim}	RMSE
Tmax (°C)	SE	35	0.74	0.95	0.000	-3.305	0.000	5.49	6.08	4.49
	SW	40	0.67	0.91	0.000	-2.238	0.000	5.61	6.21	4.14
	NW	45	0.74	0.89	0.000	-2.894	0.000	5.84	6.08	4.15
Tmin (°C)	SE	35	0.79	1.19	0.000	-0.069	0.000	6.76	9.03	4.59
	SW	40	0.78	1.17	0.000	-0.239	0.000	6.81	9.03	4.68
	NW	45	0.79	1.17	0.000	-0.300	0.000	6.88	9.03	4.59

r^2 is the coefficient of determination; p is the significance value at the 95% confidence level; SD is the standard deviation; RMSE is the root mean square error between observed and simulated values.

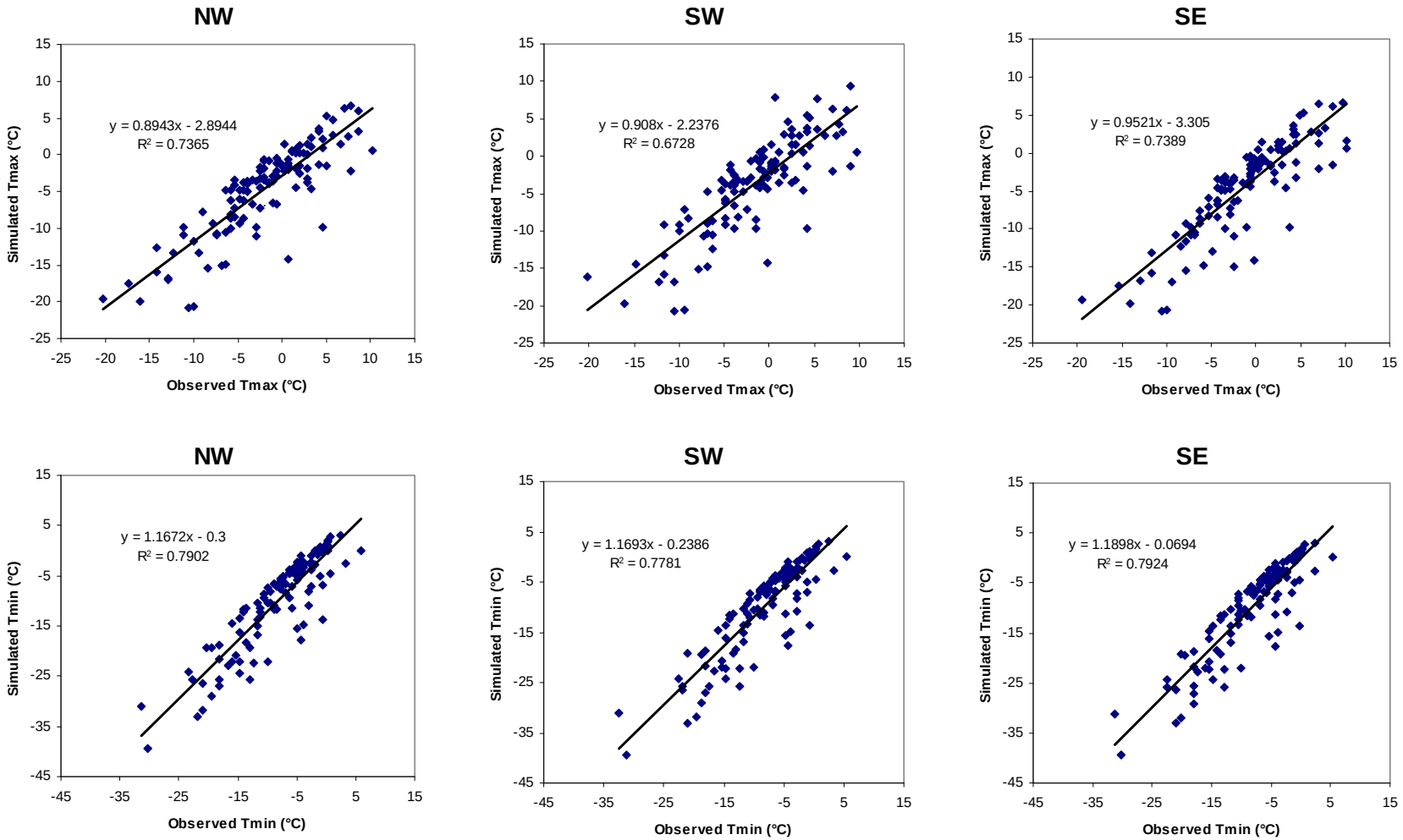

Figure 3.4. Daily *Tmax* and *Tmin* observed vs. simulated scatter plots for three aspects at Lakeview Ridge field site (November 26, 2005 – March 23, 2006).

3.5.2 Precipitation-Elevation Relationship

A site-specific proxy P-E formulation was developed from watershed SWE data and incorporated into SIMGRID. The relationship was obtained through a forced-origin regression of ΔP_{diff} vs. E, shown in Figure 3.5. A constant was not included in the relationship for the following reason: including a constant in such a relationship would have the effect of creating precipitation on days where no precipitation is recorded at the St. Mary (base) station. Furthermore, the shape of the forced-origin line does not differ substantially from the fitted line with constant, as shown in Table 3.3.

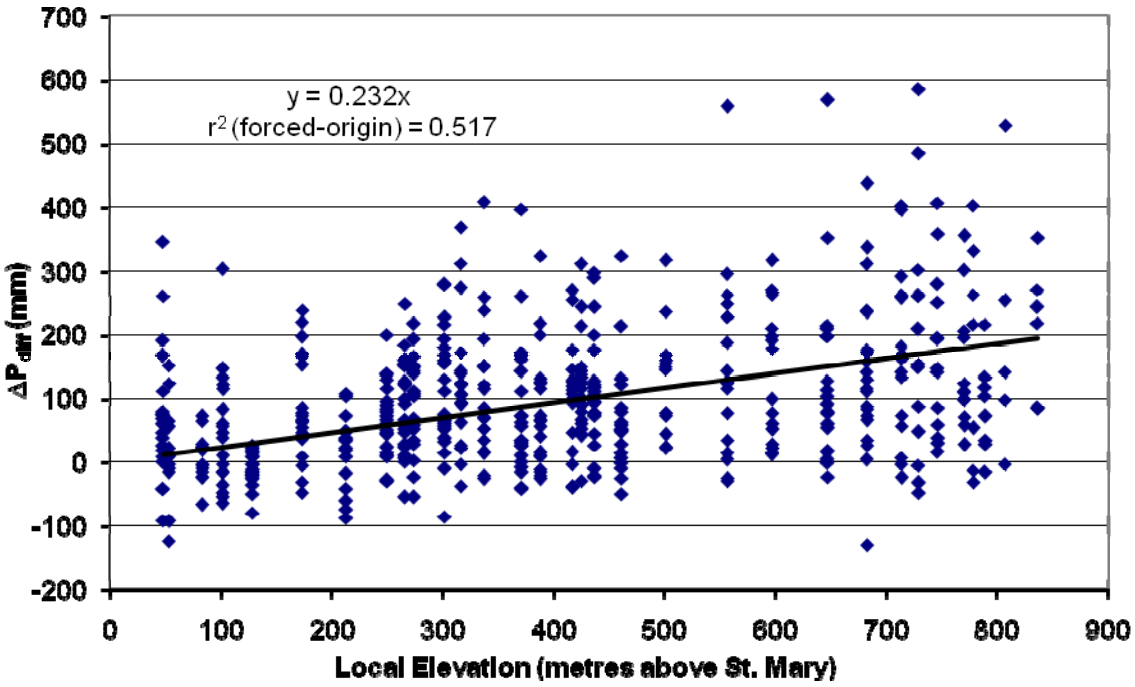

Figure 3.5. The variability of predicted ΔP_{diff} values, based on elevation, is shown by the scatter plot. The forced-origin trend line is shown.

Table 3.3. Comparison of model and coefficient statistics for the Figure 3.5 regressions, both with and without constant (y = ax + c).

	With constant	**Forced-origin**
SE_y	102.46	103.16
a	0.181	0.232
c	26.54	-
r^2	0.133	0.517
SE_a	0.020	0.010
SE_c	9.205	-

The residuals of the forced-origin line were tested for distribution. Figure 3.6 shows the distribution of the standardized residuals, which was near-normal. Log transformation did not help reduce the scatter in Figure 3.5, since the variability was distributed approximately evenly among all elevations. The ΔP_{diff} distribution was consistent with the overall trend in all months and years.

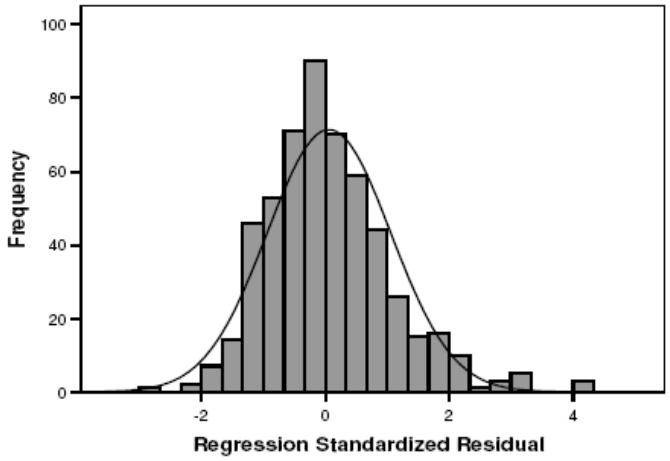

Figure 3.6. Standardized residuals plot of the ΔP_{diff} variable. Mean = 0.06, SD = 0.998, n = 536.

3.5.3 Climate Station Regressions

Temperature

The Babb station was chosen to reconstruct the St. Mary temperature record. To reconstruct the St. Mary record, daily temperature maxima (*Tmax*) and minima (*Tmin*) for the overlapping record were compiled and grouped by month. Scatter plots were created for each variable for each month, as shown in Figure 3.7. Table 3.4 shows monthly regression statistics, based on daily values. Goodness of fit, as indicated by r^2, was slightly smaller during summer months, and for *Tmin* compared to *Tmax*.

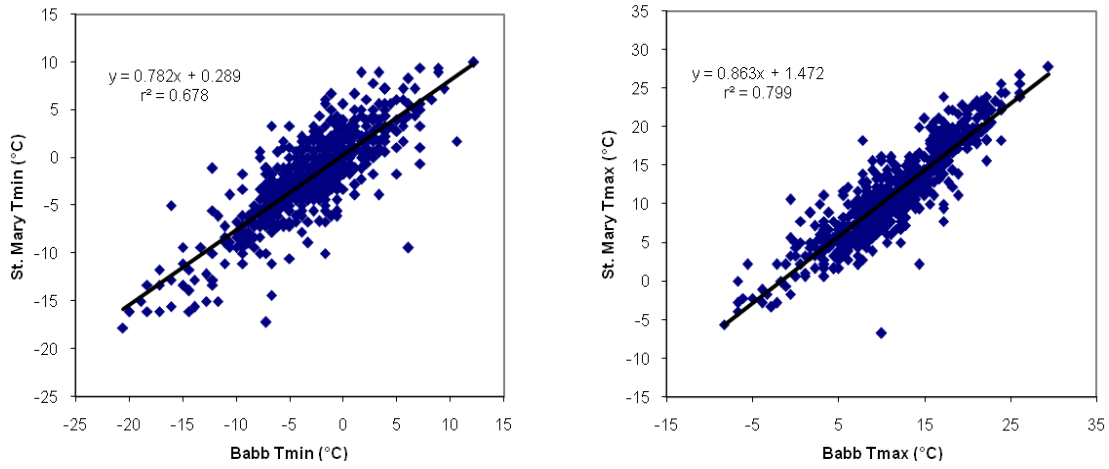

Figure 3.7. Example daily extreme temperature regressions between St. Mary and Babb stations, grouped for the month of April (1981-2006).

Table 3.4. Monthly *Tmax* and *Tmin* regressions for the period 1981-2006. The regression equation yields y = ax + c, where y = St. Mary temperature, x = Babb temperature, and c is a constant.

	Daily Tmax (°C)							Daily Tmin (°C)						
Month	**r^2**	**a**	**SE_a**	**p_a**	**c**	**SE_c**	**p_c**	**r^2**	**a**	**SE_a**	**p_a**	**c**	**SE_c**	**p_c**
Jan	0.86	0.775	0.12	0.000	-0.95	0.11	0.000	0.84	0.87	0.02	0.000	0.45	0.23	0.050
Feb	0.89	0.809	0.01	0.000	-0.19	0.1	0.060	0.84	0.88	0.02	0.000	0.58	0.22	0.000
Mar	0.83	0.793	0.01	0.000	0.86	0.13	0.000	0.84	0.91	0.02	0.000	0.56	0.15	0.000
Apr	0.78	0.852	0.02	0.000	1.56	0.22	0.000	0.67	0.78	0.02	0.000	0.26	0.12	0.030
May	0.84	0.981	0.02	0.000	0.37	0.29	0.200	0.53	0.69	0.03	0.000	1.21	0.10	0.000
Jun	0.8	0.999	0.02	0.000	0.55	0.41	0.180	0.51	0.72	0.03	0.000	1.97	0.18	0.000
Jul	0.74	0.952	0.02	0.000	2.02	0.54	0.000	0.36	0.65	0.03	0.000	3.57	0.26	0.000
Aug	0.74	0.931	0.02	0.000	2.95	0.55	0.000	0.39	0.64	0.03	0.000	3.28	0.23	0.000
Sep	0.83	0.987	0.02	0.000	0.57	0.37	0.120	0.54	0.84	0.03	0.000	1.88	0.13	0.000
Oct	0.93	1.013	0.00	0.000	-0.49	0.05	0.000	0.88	0.90	0.00	0.000	1.15	0.04	0.000
Nov	0.86	0.853	0.01	0.000	-0.84	0.12	0.000	0.81	0.86	0.02	0.000	1.08	0.17	0.000
Dec	0.87	0.836	0.01	0.000	-1.53	0.12	0.000	0.84	0.91	0.02	0.000	1.36	0.25	0.000

r^2 is the coefficient of determination; SE is the standard error; p is the significance value at the 95% confidence level.

Precipitation

Converse to temperatures, there is considerable spatial variation in precipitation surrounding the St. Mary area. This can be shown by comparing St. Mary precipitation with that of West Glacier, Many Glacier, East Glacier, and Babb (Figure 3.1). Average monthly precipitation depths for each station, along with their forced-origin regressions with St. Mary station are shown in Table 3.5. The regressions were forced through the origin, which assumes that precipitation at St. Mary station occurs exclusively when it occurs at the nearby climate station.

Precipitation in the study area is synoptically-driven in winter and more convectively-driven in summer. Western (more mountainous) locations of the study area receive more annual precipitation than do eastern locations. For example, the Many Glacier station receives nearly twice as much annual precipitation as does the St. Mary station (located just 100 m below), with strongest differences in winter (Table 3.5). This comparison suggests that proximity to mountains and/or the Continental Divide has a larger effect on precipitation regime than does elevation by itself. Precipitation "blow-over" is likely the main reason for such large differences in total accumulation between the two sites. Under stable atmospheric conditions, the westerly-moving moisture-laden air masses often release orographically-induced precipitation on areas in the immediate lee side of the Continental Divide (Finklin 1986, Milne and Wallmann 2007).

Unlike the Many Glacier station location, the St. Mary station is located in a mountain-to-prairie transition zone. It displays both high winter precipitation (mountain

characteristic), as well as a peak of summer precipitation (prairie characteristic). Similarly, precipitation patterns at East Glacier closely match those at St. Mary, particularly from October to February (Table 3.5). The consistency of this north-south pattern highlights the dominance of eastward-moving winter synoptic systems. Patterns recorded at these stations contrast to those located in the prairies a few kilometers to the east. For example, precipitation at the Babb station, located just 23 km from St. Mary, shows generally much smaller precipitation volumes, especially in winter (Table 3.5). Highest annual precipitation volumes at Babb occur due to stronger convection and higher precipitable water content. On the west side of the divide, West Glacier exhibits a strong winter wet cycle (i.e., $Precip_{Oct\text{-}Mar} > Precip_{Apr\text{-}Sep}$), a sign that the annual regime is dominated by synoptic patterns, common to the United States west of the Continental Divide (Shafer et al. 2005).

Overall, the strongest relationships were found between the St. Mary station and the East Glacier and Many Glacier stations. Monthly regressions for both these stations consistently exhibit high coefficients of determination and slopes close to 1. Finally, the East Glacier station was selected, since monthly volumes were closer to St. Mary, and its record extended back to 1960. Thus, daily precipitation gaps at St. Mary were synthetically reconstructed using the East Glacier station data. This was achieved by multiplying the East Glacier precipitation record for each day by the coefficient obtained for the month in which that day occurred.

Table 3.5. Monthly average precipitation (*P*, mm) and forced-origin regression results, 1981-2006. The equations are in the form y = ax, where y = St. Mary *P* and x = nearby station *P*.

Elevation / **Station**	**960 m West Glacier**			**1492 m Many Glacier**			**1391 m St. Mary**			**1466 m East Glacier**			**1390 m Babb 6NE**		
Month	**P**	**a**	**r^2**	**P**	**a**	**r^2**	**P**	**a**	**r^2**	**P**	**a**	**r^2**	**P**	**a**	**r^2**
Jan	82.3	0.61	0.10	140.0	0.40	0.74	55.1	-	-	64.2	0.81	0.79	11.2	4.70	0.48
Feb	49.4	0.84	0.17	100.0	0.47	0.76	45.4	-	-	51.6	0.89	0.75	13.7	2.71	0.41
Mar	51.7	0.90	0.26	104.7	0.48	0.80	50.9	-	-	55.5	0.84	0.67	23.2	2.06	0.40
Apr	48.6	0.96	-0.40	91.1	0.54	0.54	50.2	-	-	45.0	1.04	0.48	32.4	1.41	0.07
May	64.2	0.98	-0.01	95.8	0.72	0.31	71.5	-	-	63.3	1.08	0.80	71.1	0.89	0.78
Jun	88.4	0.98	0.14	117.2	0.80	0.72	92.5	-	-	81.3	0.97	0.57	92.1	0.93	0.81
Jul	45.6	0.93	0.33	56.0	0.88	0.78	44.9	-	-	41.3	1.10	0.89	45.3	0.89	0.75
Aug	32.8	1.12	0.36	47.7	0.83	0.72	42.9	-	-	38.7	1.06	0.89	46.5	0.89	0.77
Sep	53.5	0.97	0.56	78.4	0.64	0.52	54.2	-	-	45.3	1.00	0.44	44.7	1.08	0.66
Oct	63.4	0.81	0.35	120.3	0.46	0.84	56.0	-	-	54.6	0.97	0.88	25.2	1.89	0.32
Nov	82.8	0.82	0.54	159.5	0.43	0.87	64.3	-	-	75.6	0.90	0.91	21.7	2.88	0.57
Dec	72.2	0.70	0.52	123.9	0.42	0.81	49.1	-	-	60.2	0.79	0.87	16.3	2.06	-0.03
Annual	**734.9**	**-**	**-**	**1234.7**	**-**	**-**	**676.9**	**-**	**-**	**676.6**	**-**	**-**	**443.4**	**-**	**-**

r^2 is the coefficient of determination.

3.5.4 Snow Water Equivalent Surfaces

The SNOPAC program was enhanced with the consideration of rain-on-snow. The distributed SWE surfaces were displayed, using ArcGIS 9.2 software, to observe simulated snow accumulation and ablation patterns across the watershed. To highlight terrain variability, the SWE surfaces were overlaid on a hillshade surface of the watershed. Figure 3.8 shows the SWE pattern during the progression of the 1980 water year snow season, using SNOPAC-ROS output. As expected, lower elevations show less accumulation, and higher elevations have greater SWE values. On Nov 1, most of the area was clear of snowpack, except at higher elevations. SWE increased from December to April, and then decreased in May. On May 1, snowmelt began at lower elevations, while higher elevations were still accumulating snow. This trend continued into June.

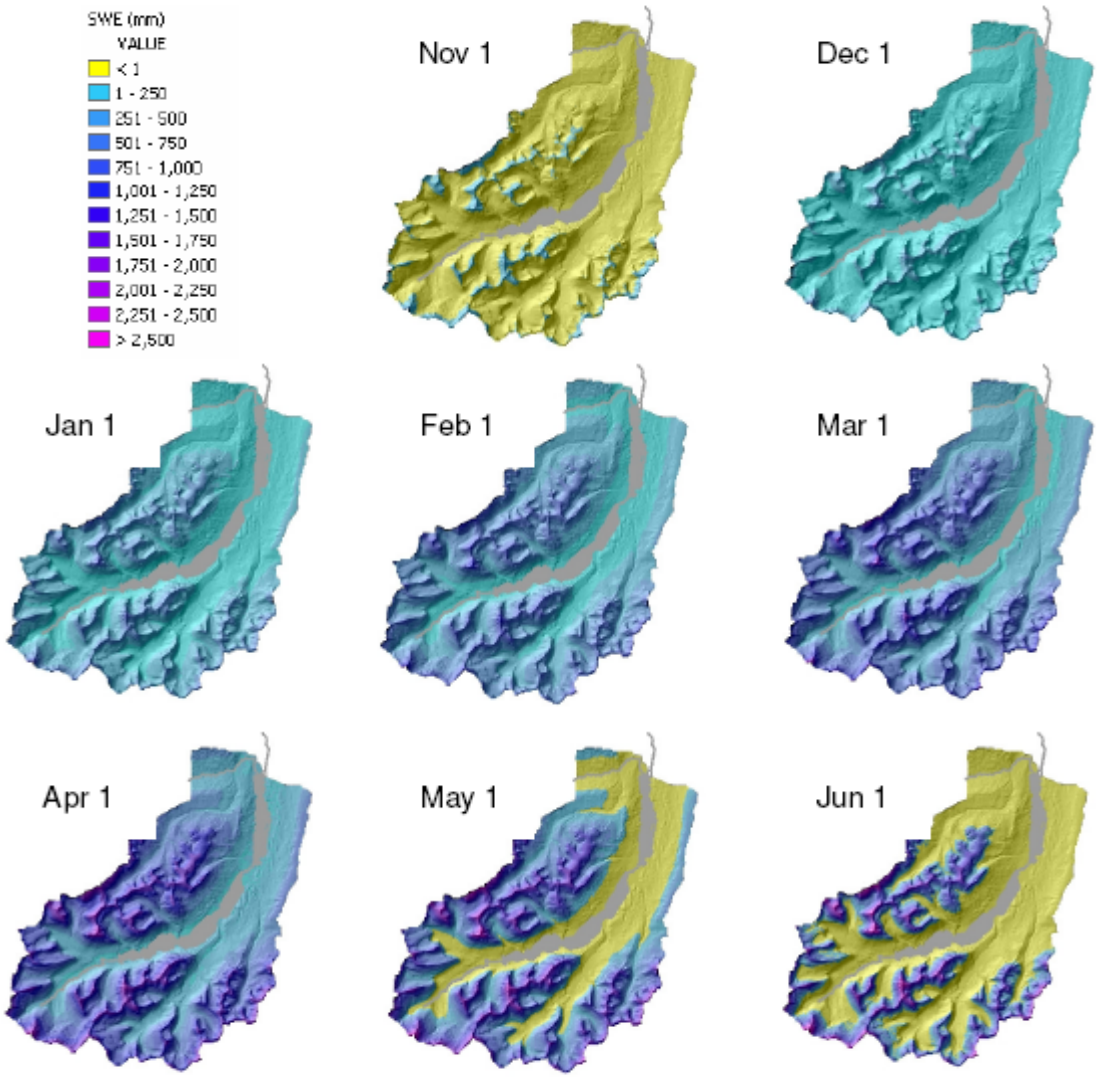

Figure 3.8. Spatial snowpack distribution on 8 dates during the 1980 water year (November 1979 - June 1980). The St. Mary lakes and river were overlaid onto the snow surfaces.

3.6 Summary

A distributed snow water equivalent (SWE) model was adopted for the St. Mary River headwaters study basin. The main innovation was the local proxy P-E relationship, developed with snow course SWE data. Using the site-specific SWE data was a likely improvement compared to using surface interpolation methods for the scale of study. As has been shown, precipitation patterns are highly variable in the area surrounding the study watershed. Work from this chapter produced spatially distributed SWE (and rainfall) surfaces for the 1961-2006 water years. The SWE Model is the first, and most important, step in the snow hydrology approach developed in this thesis. The SWE surfaces will be used as inputs in Chapter 4.

CHAPTER 4: Developing a Statistical Spring Streamflow Prediction Model

4.1 Introduction

Building on the refinements made to the SWE Model in Chapter 3, the initial objective of this chapter was to develop a physically-based, fully distributed, hydrologic model. With this model, daily watershed runoff was to be simulated to analyze spring water supply volumes. For this objective, preliminary work on soil moisture storage and evapotranspiration routines, as well as reservoir routing, was initiated; however, time constraints prevented full model development. Instead, a statistically-based approach was adopted.

Objective

A statistical regression model was developed to predict spring streamflow volumes. The mass balance-based variables used in the regressions were volumes output from the SWE Model, summed for each water year spanning 1961-2004. Hence, the objective of this chapter was to define the input volumes of snowmelt runoff (S_R) and rainfall runoff (R_R), as well as the spring streamflow volume (Q_S) these mass balance-based variables would be predicting on an annual basis.

The following steps were taken:

- Evaluate and select the best of three SWE volume measures;
- Determine the spring streamflow period and effective rainfall runoff period (and associated volumes). This required developing a time-sensitive means of predicting the onset of spring streamflow and the onset of effective rainfall.
- Establish the final statistical regression model, using S_R, R_R and Q_S in multiple linear regressions**.**

4.2 Mass Balance Data

Modelled Snowmelt Runoff

The accumulated snow water equivalent (SWE) over a watershed represents the maximum potential snowmelt water available for spring runoff. Under snowmelt conditions, soil water levels are high, and evapotranspiration rates are low, resulting in high proportions of SWE becoming runoff. Three distinct SWE volume measures, stemming from daily SWE Model output, were used to estimate snowmelt runoff volume (S_R).

Modelled Rainfall Runoff

In addition to snowmelt runoff, rainfall runoff contributes to watershed spring runoff. Once the snowpack is melted, soil water levels are high. During such conditions, a large proportion of rainfall becomes runoff. In the study watershed, the period following snowmelt (i.e., May and June) coincides with higher precipitation volumes (see Table 3.5), making this factor even more important to consider. As the season progresses, soil

water is evapotranspired and less rain becomes runoff. Thus, this variable defined the potential effective rainfall runoff volume (hereafter referred to as rainfall runoff volume, R_R). It was determined using daily spring rainfall output from the SWE Model.

Naturalized Streamflow

Watershed streamflow is a surrogate for watershed runoff. As such, streamflow measurements were used to validate the above simulated watershed runoff volumes. Daily Streamflow gauge recording began at Babb, MT, in 1901 and was accessed on-line via the United States Geological Survey web interface (USGS 2007). The Babb station is located at the outlet for both the St. Mary and Many Glacier valleys.

In 1921, Lake Sherburne Dam, located in the Many Glacier valley (just east of the Many Glacier SNOTEL site, Figure 3.1) came into operation. Managed water releases from the dam, especially in spring, alter the natural river flow recorded at Babb. Therefore, for the period 1961-2004, naturalized streamflow was calculated by subtracting the daily Sherburne Dam streamflow from that recorded at Babb. This naturalized streamflow dataset better represents the natural hydrologic responses of snowmelt runoff and rainfall runoff for the study watershed. The daily discharge data were converted to units of million m^3, from which spring streamflow volumes (Q_S) were determined.

4.3 Methods and Analysis

The first step in developing the statistical regression model involved selecting one of the three SWE volume measures. Once the appropriate snowmelt runoff variable was

determined, it was used, along with the rainfall runoff variable, in multiple linear regressions. Before this step, however, a time-sensitive means of determining the spring streamflow period (and associated volume) and the effective rainfall runoff period (and associated volume) was defined. This was achieved using watershed critical snowpack Julian dates output from the SWE model.

The distributed SWE Model (Chapter 3) produces output for the study watershed's 566 terrain categories (TCs). Throughout this section, watershed weighted sums (in the case of mass balance variables), or averages (in the case of critical snowpack Julian dates) were required, and computed using:

$$V_W = \frac{\sum_{i=1}^{566} V_i \times A_i}{\sum_{i=1}^{566} A_i} \tag{4.1}$$

Where:

V_W is the variable's weighted sum (or average) for the watershed
V_i is the variable's value for the i^{th} Terrain Category (TC)
A_i is the area for the i^{th} TC, in km^2

4.3.1 Snowmelt Runoff Variable Selection

SWE Volume Measures

In Chapter 3, the SWE Model's snow mass balance program (SNOPAC) was refined to account for rain-on-snow conditions (SNOPAC-ROS). Three SWE volume measures, created from these two programs, were evaluated. The three S_R variables were used as independent variables in linear regressions with general spring streamflow volumes.

Descriptions of how each SWE volume was derived follows, and they were:

S_{R1} = *SWEmax*(SNOPAC)

S_{R2} = *SWEmax*(SNOPAC-ROS)

S_{R3} = *SWEmax*(SNOPAC-ROS) + *SWEms*(SNOPAC-ROS)

S_{R1}: This volume was computed using output from the SNOPAC program. The maximum snow accumulation volume for each TC was calculated. A watershed sum was then determined for each water year by calculating *SWEmax*(SNOPAC) as V_W in Equation 4.1.

S_{R2}: Like S_{R1}, S_{R2} represented the watershed's maximum snow accumulation volume. This time, however, the output was taken from the SNOPAC-ROS program. A watershed sum was then determined for each water year by calculating *SWEmax*(SNOPAC-ROS) as V_W in Equation 4.1.

S_{R3}: This volume included the same watershed maximum snow accumulation value as did S_{R2}; however, precipitation during the snowmelt season was added to it in the following way:

- For each TC, any precipitation falling during the snowmelt season (i.e., starting on the day after maximum snow accumulation, and ending on the day of snowpack depletion) was summed. These inputs were represented as *SWEms*.
- A watershed sum was determined for each water year by calculating *SWEms* as V_W in Equation 4.1.

- Since *SWEms* occurs during snowmelt conditions, this mass variable was included as snowmelt runoff. Thus S_{R3} was the sum of both *SWEmax* and *SWEms*, both computed using SNOPAC-ROS output.

General Spring Streamflow Volumes

Different spring streamflow volumes (Q_S) were used as the dependent variable in the linear regressions to select the S_R variable. Figure 4.1 shows the watershed's average monthly streamflow for the historical period. Streamflow is at a minimum during the winter snow accumulation season (i.e., November to March). The spring snowmelt onset occurs in April, when streamflow increases. The primary snowmelt runoff (and annual streamflow) volume occurs between May and July, with a peak in June. As snowpack is depleted, snowmelt runoff declines, reflected in receding streamflow in July and August. These monthly streamflow volume patterns are consistent for many rivers across the snow dominant Mountain West, and especially for interior rivers at similar latitude (see Figure 2.1). Three general monthly streamflow volumes were used to represent Q_S. These were (inclusive) May to July (MJJ), April-July (AMJJ), and April to August (AMJJA).

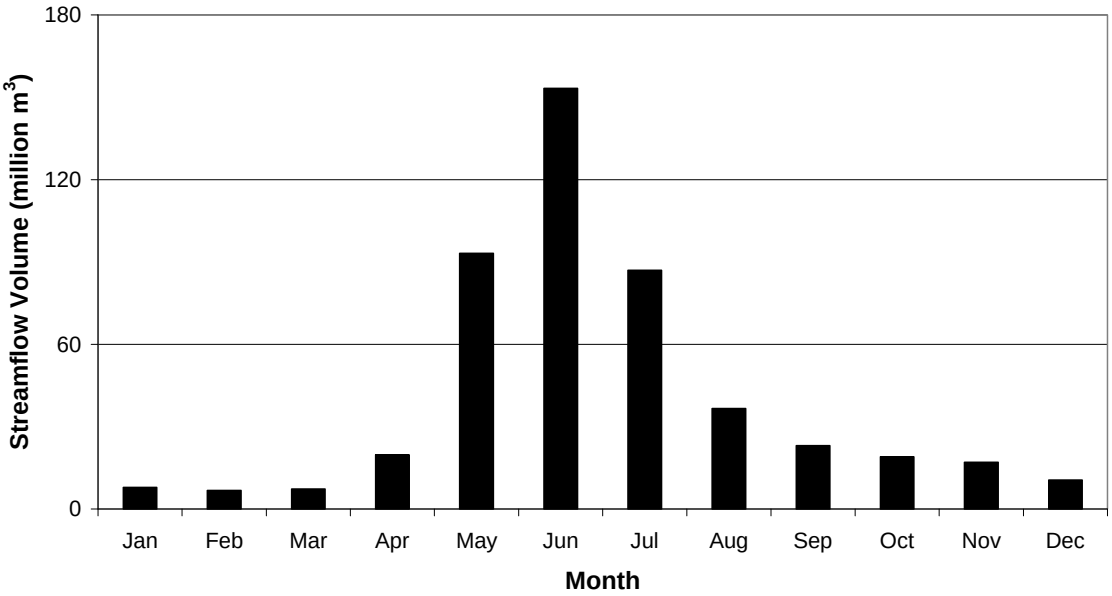

Figure 4.1. Study watershed average monthly naturalized streamflow volumes, 1961-2004.

Linear Regressions

The linear regression results for the 1961-2004 water years are shown in Table 4.1. The regressions show that S_{R3} is a superior measure to predict spring streamflow (models are bolded in Table 4.1), as it best reflected the variability in Q_S for all spring streamflow periods. In the best case, S_{R3} explained 64% of AMJJA streamflow variability. The S_{R3} volume measure was thus selected as the snowmelt runoff variable to predict spring streamflow. The results in Table 4.1 suggested, however, that two key improvements could be made to the statistical regression model.

Table 4.1. Linear regression results evaluating the three SWE volume measures (or S_R). Units are in million m^3.

Variables		Equation Terms Statistics						Model Statistics		
DV	IV	Constant			S_R					
Q_S	S_R	c	SE_c	p_c	a	SE_a	p_a	r^2	Adj. r^2	SE_y
MJJ	1	11.375	52.685	0.830	0.668	0.108	0.000	0.478	0.465	56.686
	2	2.019	53.254	0.970	0.683	0.108	0.000	0.486	0.474	56.214
	3	**-77.962**	**50.594**	**0.131**	**0.630**	**0.077**	**0.000**	**0.617**	**0.607**	**48.560**
AMJJ	1	34.539	51.539	0.506	0.661	0.105	0.000	0.483	0.471	55.454
	2	24.778	52.009	0.636	0.677	0.106	0.000	0.493	0.481	54.899
	3	**-54.462**	**49.165**	**0.274**	**0.624**	**0.074**	**0.000**	**0.626**	**0.617**	**47.188**
AMJJA	1	35.423	55.671	0.528	0.735	0.114	0.000	0.498	0.486	59.899
	2	24.278	56.098	0.667	0.753	0.114	0.000	0.509	0.497	59.215
	3	**-66.280**	**51.919**	**0.209**	**0.698**	**0.079**	**0.000**	**0.652**	**0.644**	**49.831**

SE is the term's standard error; p is the significance value; r^2 is the coefficient of determination; Adj. r^2 is the adjusted r^2 and accounts for changes in degrees of freedom associated with adding independent variables to the regression.

The first improvement involved addressing the limitation of using the exact same time period (e.g., AMJJA) to represent spring streamflow on any given year. For example, spring streamflow in some years occurred primarily during the earlier, AMJ period; whereas in other years, it occurred during later months, say JJA. Therefore, over the 30-year period, the peak streamflow volume resulting from snowmelt runoff was not captured most accurately. A time-sensitive means of determining the onset of spring snowmelt for each year would help remedy this issue.

The second improvement involved adding an effective rainfall runoff variable to the regression. This would help increase the variability already explained by the selected snowmelt runoff variable. A time-sensitive means of determining the watershed average day of snowpack depletion would make such a variable possible to use.

4.3.2 Spring Streamflow and Rainfall Runoff Variable Definition

Time-sensitive streamflow and rainfall runoff volumes were determined. To do this, the SWE Model output was used to determine the estimated onsets of both the spring snowmelt runoff period and the effective rainfall runoff period, for each water year. Estimations of two critical snowpack Julian dates for the watershed were used: the date of maximum snow accumulation (*Jmax*) and the date of snowpack depletion (*Jdep*).

4.3.2.1 Critical Snowpack Julian Dates

Spring Streamflow Volumes

The watershed *Jmax* was used as a proxy to estimate the onset of spring snowmelt, which coincides with the onset of spring streamflow. For each water year, the watershed *Jmax* was calculated as V_W in Equation 4.1. Using the watershed *Jmax*, spring streamflow periods (and associated volumes) were defined for each water year according to the number of days lapsed after *Jmax*. These end days were spaced on weekly time steps. The different spring streamflow periods were named according to their time duration in Julian days. Finally, the daily streamflow volumes for each defined spring streamflow period were summed. In any given water year for example, Q_{S121} represented the spring streamflow volume (Q_S) occurring in the period lasting 121 Julian days (four months) after the watershed *Jmax* determined for that year.

Rainfall Runoff Volumes

The watershed average day of snowpack depletion (*Jdep*) was used as a proxy to estimate the onset of the effective rainfall runoff period. Thus, the start of the effective rainfall

runoff period for the watershed was simulated to begin the day after the snowmelt runoff period ended (for the watershed). For each water year, the watershed *Jdep* was calculated as V_W in Equation 4.1, with the following minor adjustment: TCs corresponding to glaciated areas or permanent snowfields were assigned null values. These areas never experience snowpack depletion, and including their values would have skewed the *Jdep* value.

Once the watershed *Jdep* was determined for each year, the effective rainfall runoff volume (R_R) was calculated. For all TCs and for J > *Jdep*:

$$R_R = P \tag{4.1}$$

Where:

P is the total rain or snow in the period following snowpack depletion (million m^3)
R_R is the (potential effective) rainfall runoff volume (million m^3)

For each water year, a watershed value for R_R was calculated as *V* in Equation 4.1. Effective rainfall runoff periods (and associated volumes) were defined according to the number of days after *Jdep*. The periods increased by increments of 10 days. For example, for any given year, R_{R30} represented the effective rainfall runoff volume (R_R) occurring in the thirty-day period following *Jdep* for that year.

4.3.3 Multiple Linear Regression Model Selection

For the historical period, all the Q_S and R_R values were compiled according to year, along with the S_{R3} values selected earlier. Thus, S_R and R_R values represented watershed spring runoff (independent) variables, and were regressed with the spring streamflow (Q_S;

dependent) variables using multiple linear regression. Table 4.2 shows the set of regressions that yielded the best model results.

Compared to the results in Table 4.1, regressions are considerably improved. The best models occur for those using S_{R3} and R_{R40} (to predict various Q_S values), which show similar results to one another. For example, the adjusted R^2 ranges from 0.786 to 0.791 for these models. The selected model (bolded in Table 4.2) showed the best combination of variables with the lowest standard error, highest coefficient of determination, and lowest model standard error of the estimate. It was the model using S_{R3} and R_{R40} to predict Q_{S114}.

Table 4.2. Best model results from multiple linear regressions using S_{R3}, along with the various R_R and Q_S variables are shown. Results for the selected model are bolded.

Variables			Equation Terms Statistics									Model Statistics		
IV		DV	Constant			S_R			R_R					
S_R	R_R	Q_S	c	SE_c	p_c	a	SE_a	p_a	b	SE_b	p_b	R^2	Adj. R^2	SE_y
		107	-219.03	47.27	0.000	0.72	0.071	<0.005	1.03	0.304	0.002	0.769	0.758	43.95
3	30	114	-197.50	46.67	0.000	0.727	0.070	<0.005	1.03	0.301	0.000	0.770	0.759	43.42
		121	-183.51	47.00	0.000	0.714	0.071	<0.005	1.03	0.303	0.000	0.767	0.755	43.70
		107	-229.54	44.60	0.000	0.710	0.067	<0.005	1.06	0.245	0.000	0.796	0.786	41.30
3	**40**	**114**	**-208.83**	**43.64**	**0.000**	**0.701**	**0.065**	**<0.005**	**1.07**	**0.240**	**0.000**	**0.801**	**0.791**	**40.42**
		121	-195.46	43.72	0.000	0.698	0.066	<0.005	1.08	0.240	0.000	0.800	0.790	40.49
		107	-229.98	47.83	0.000	0.707	0.072	<0.005	0.924	0.266	0.000	0.772	0.760	43.71
3	50	114	-209.53	46.94	0.000	0.698	0.070	<0.005	0.944	0.261	0.000	0.776	0.765	42.90
		121	-195.87	47.14	0.000	0.695	0.071	<0.005	0.947	0.262	0.000	0.773	0.762	43.09

SE is the term's standard error; p is the significance value; R^2 is the coefficient of determination; Adj. R^2 is the adjusted R^2, which accounts for changes in degrees of freedom associated with adding IVs to the regression.

4.4 Results

Analyses were conducted on the selected multiple linear regression model. A step-wise linear regression revealed that S_{R3} accounted for 70% of the variability in Q_{S114}, while R_{R40} accounted for another 9%. (Hereafter, the variables are referred to simply as S_R, Q_S, and R_R, respectively). As expected, snowmelt runoff is a much more important factor in determining spring streamflow, but the spring rainfall runoff factor is not negligible. The independent, mass balance-based, variables (i.e., S_R and R_R) were not significantly correlated (Pearson's r = 0.228, p = 0.137).

The selected streamflow prediction model reproduced the historical streamflow very well. Figure 4.2 shows the scatter plot of observed versus modelled Q_{S114} (Q_S), for the period 1961-2004. The forced-origin trend line has a slope near to one (m = 0.987, SE = 0.017), indicating a close relationship. The student t-test statistic indicates that the slope of this line is not significantly different from the line with slope 1 (t = -0.779, p = 0.440). It is noted that low flow years were slightly over-predicted by the model.

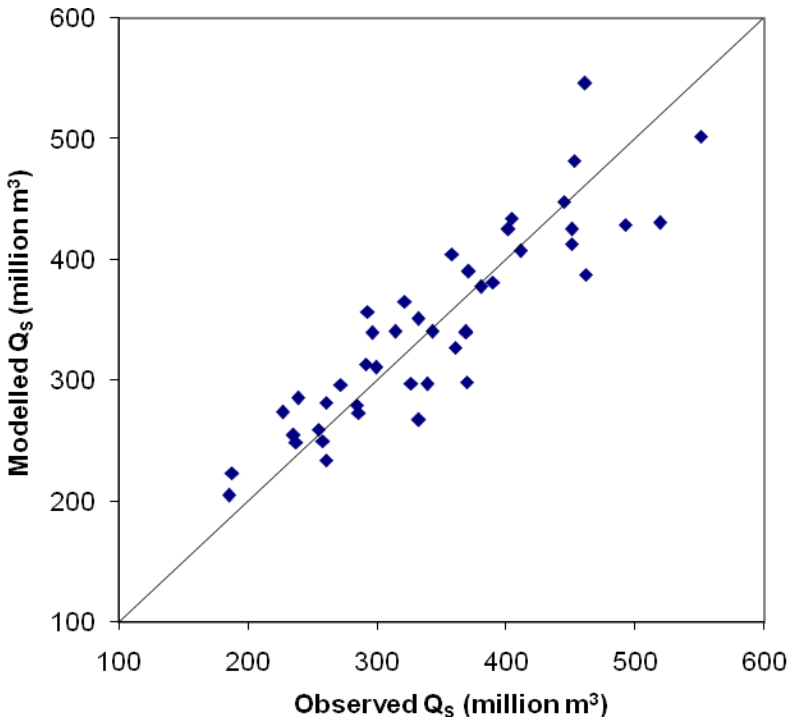

Figure 4.2. Prediction model results are shown by the observed versus modelled spring streamflow scatter plot, for the years 1961-2004. The 1:1 line is shown.

4.5 Summary

A statistical model to predict spring streamflow was developed for the study watershed. Refinements to the SWE Model were validated by evaluating three SWE volume measures. Once the best simulated snowmelt runoff variable was selected, multiple linear regressions were used to predict spring streamflow volumes. In addition to snowmelt runoff (S_R), effective rainfall runoff (R_R) volume was determined to round off the total maximum basin potential water available for spring runoff. Q_S represented 72% of the total annual streamflow volume over the historical period (1961-2004); the statistical streamflow model explained 79% of the annual variability in Q_S.

Together with the SWE Model, the statistical regression model completes the objective of developing a snow hydrology approach for the study watershed. It is deemed suitable for climate change impacts assessment, with the following words of caution. Since the statistical model has been developed over the historical period, its predictive abilities are limited. For example, simulated SWE volumes for many of the future years are likely to be smaller than those for the historical period. Consequently, as an independent variable, S_R values will be used for purposes for which the statistical model was not developed. The associated Q_S results, therefore, will carry this resultant inaccuracy. Despite the above, all the variables used in the statistical regression model are physical, mass balance-based outputs. Furthermore, the variables are time-sensitive on an annual basis.

CHAPTER 5: Climate Change Assessment of St. Mary Headwaters Snow Hydrology

5.1 Introduction

The need for climate change impacts assessment modelling increases as the effects of climate warming become more pervasive. Quantifying future changes in spring streamflow is valuable to both economic and environmental interests for the downstream regions supplied by the St. Mary River. Results provide an approximation of changes to be expected in the greater headwaters region of the Rocky Mountain Eastern slopes.

The objective of this chapter was to project the probable range of hydrologic change the St. Mary study watershed will experience due to climate warming. This was achieved in two steps. First, two climate change scenarios for the period 2010-2099 were developed. Second, the snow hydrology modelling approach, developed in Chapters 3 and 4, was applied.

5.2 Methods

Future climate scenarios form the basis for climate change impacts assessments. Projections on the expected changes to the system of interest, such as snow hydrology, are meaningful once GCM-derived future climate is linked with the regional-scale model. To achieve this, GCM scenarios were selected and used to construct the future climate for the study area.

5.2.1 Climate Change Scenarios Construction

5.2.1.1 Global Circulation Model Data

Climate change data for the study region was downloaded from the Pacific Climate Impacts Consortium (PCIC 2007). PCIC aims to develop regional impact assessments capacity, particularly in northwestern North America. The Consortium provides tools for organizations with which to collaborate and develop solutions to adapt to climate variability and change. Associated projects bridge the gap between research and application, working across sectors and disciplines.

Projected changes of monthly climate parameters (e.g., temperature, precipitation, wind, geopotential heights) output from a number of recognized Global Circulation Models (GCMs) may be obtained for any grid cell over the globe. The values represent average changes expected for three future time slices (i.e., 2020s, 2050s, and 2080s), relative to the base period (1961-1990). Each future time slice represents a thirty year period (i.e., 2010-2039, 2040-2059, and 2070-2099). A climate change scenario refers to the GCM output corresponding to the three future time slices under a particular emissions path. Data from six GCMs outputting minimum and maximum temperature change ($\Delta Tmax$, $\Delta Tmin$; °C), and precipitation change (ΔP; %) were downloaded. In total, there were 26 climate change scenarios.

Regional Averages

For the 26 scenarios, outputs from the four grid cells surrounding the St. Mary study area were averaged. The coarse resolution of GCMs does not capture mountain topography,

and the aim was to obtain more representative change values for the study area (Von Storch et al. 1993, Bonsal et al. 2003). Figure 5.1 shows the example grid cell extents of the CGCM2 surrounding the study site. Table 5.1 shows the coordinates of the upper left (northwestern; NW) and lower right (southeastern; SE) centre points for the grid cells along with the average grid resolutions of each GCM. Thus average monthly $\Delta Tmin$, $\Delta Tmax$, and ΔP, representing climate change over the study area, was compiled.

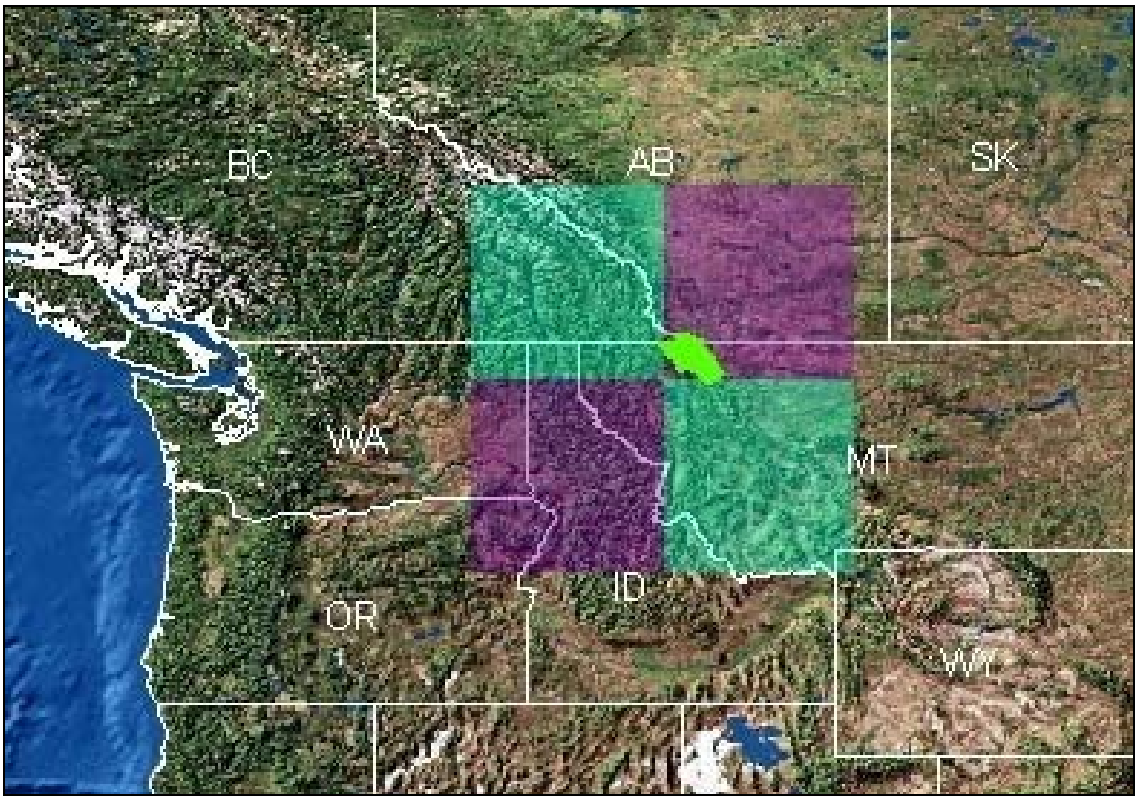

Figure 5.1. The four grid cells of the CGCM2 used to average the regional climate scenarios are shown, along with the area of Waterton-Glacier International Peace Park (within which lies the study watershed).

Table 5.1. The centre point coordinates of the upper left and lower right cells surrounding the St. Mary study area are shown to illustrate the extent of each model's spatial coverage, along with its resolution (defined as the average length of a grid cell side). (The bolded first letter(s) of the model acronym are those used for labeling model runs in Figure 5.2).

GCM	Centre coordinates (dec. deg.)		Avg. grid res. (km)
	NW	SE	
CGCM2	50.10N, 116.25W	46.39N, 112.50W	339
CCSRNIES	52.61N, 118.12W	47.07N, 112.50W	499
HadCM3	50.00N, 116.25W	47.50N, 112.50W	277
CSIROMk2b	49.38N, 118.12W	46.19N, 112.50W	386
NCARPCM	48.84N, 118.12W	46.05N, 115.31W	256
ECHAM4	48.84N, 118.12W	46.05N, 115.31W	256

5.2.1.2 Scenarios Selection

Ideally, data from the 26 climate change scenarios would be used in this study. As with most climate impacts studies, however, sufficient resources are not available to work with the large datasets this would entail. IPCC guidelines recommend that more than one scenario be used to capture the range of possible future climate in a particular region (IPCC-TGCIA 1999). Therefore, two scenarios were selected that would best represent the range of climate change scenarios.

The snow hydrology approach, developed in Chapter 3 and 4, focuses on the water balance inputs of winter and spring SWE, as well as spring and early summer rainfall. These inputs correspond approximately with the months from November to June. The model is thus most sensitive to the climatic changes occurring during this eight-month period of the water year. Therefore, the selection of scenarios was based on comparing their output changes for this eight-month period. Barrow and Yu (2005) used a similar method in their assessment of climate change for the province of Alberta.

Scenarios Analysis

Data for the 26 scenarios were plotted to compare projected climate changes (Figure 5.2). The uncertainty in model projections is important, and is shown by the variability in climate change scenarios. The primary source of variability results from uncertainties in future emissions and the associated effects of their radiative forcings on climate sensitivity (Cubasch et al. 2001, Wigley and Raper 2001). Uncertainties in GCM algorithms depicting the Earth's physical processes are secondary. Temporally, there is a greater degree of scatter observed during the 2080s owing to increased uncertainty in model projections (Cubasch et al. 2001).

The following points are noted from Figure 5.2:

- All model scenarios project increases in mean temperature through the future period, spanning 0.4°C during the 2020s (**CC**SRNIES **A1Fl**) to 8.2°C for the 2080s (**CC**SRNIES **A1T**).
- There is a clear cluster of **CC**SRNIES scenarios that lie beyond the 6.0°C warming line for the 2080s period. The associated scenarios were considered extreme, and not used in the selection process.
- Precipitation changes range from -5.06% (**CC**SRNIES A1F1) to +25.7% (**CS**IROMk2b **A21**) through the future time slice. The ranges within each time slice reflect much more uncertainty compared to temperature projections
- Expressed generally, climate change scenario projections differ in their warming *rate*, and their precipitation change.

Scenarios 1 and 2

Two scenarios were selected to best represent the range of precipitation variability, given the greater uncertainty in this parameter relative to temperature. Therefore, scenarios 1 and 2 were selected based on two criteria. First, each scenario had to show precipitation changes that were at the upper or lower ends of mean precipitation change. Second, the scenarios had to show similar projected rates of warming. This was a control of sorts, to help deduce the interaction of future temperature and precipitation changes. The **H**adCM3 **A1Fl** scenario was selected as "Scenario 1", and is denoted by the upper trend line in Figure 5.2. The **CS**IROMk2b **B11** scenario was chosen as "Scenario 2", and is denoted by the lower trend line in Figure 5.2. The dashed line between the two scenarios is calculated from the mean of all experiments, for each time slice, representing what a mean scenario projection would look like.

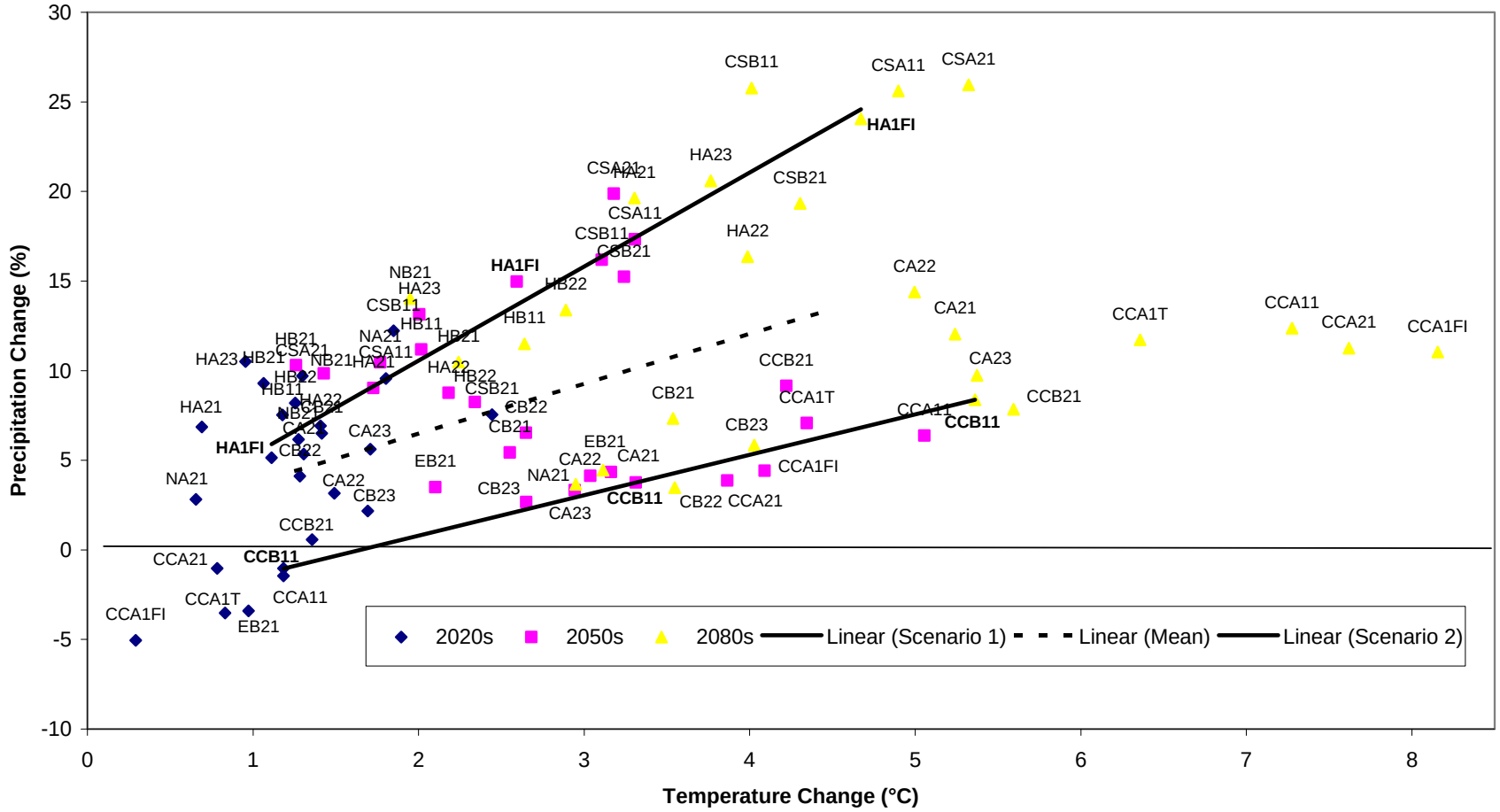

Figure 5.2. GCM climate change scenarios are shown through changes in precipitation and mean temperature relative to the base period. See Table 5.1 for GCM abbreviations. In addition to model acronym abbreviations, the emissions scenario identifier, along with the number of the model experiment appears as labels. For example, CB23 denotes the 3rd experiment of the CGCM2 forced by the B2 emissions scenario.

5.2.1.3 Downscaling

Scenarios 1 and 2 were each used to create data sets reflecting annual graduated St. Mary climate change spanning 2010-2099. The monthly $\Delta Tmax$, $\Delta Tmin$, and ΔP values for each time slice were averaged according to the following seasons: December through February (DJF), March through May (MAM), June through August (JJA), and September through November (SON).

The average seasonal changes for each time slice were "stretched", by assigning the values to each year within the represented 30-year period. To do this, the average seasonal change for each variable was plotted for each time slice. Trend lines were obtained for the points passing through the years 2020, 2050, and 2080, and extending from 2010 to 2099. The trend line equations were used to obtain annual values stretching through the three 30-year periods represented by each time slice (i.e., 2010-2039, 2040-2069, and 2070-2099). Thus $\Delta Tmax$, $\Delta Tmin$, and ΔP values were calculated, on a seasonal basis, for a continuous annual time series of incremental change, for each scenario.

Delta Change

The "delta technique" has been used in a number of impacts studies of this kind in the Mountain West (Morrison et al. 2002, Loukas et al. 2004, Merritt et al. 2006). For temperature and precipitation, the changes calculated above were used to perturb the St. Mary daily climate of the base period (1961-1990). Although common, the method does present limitations. For example, any large-scale patterns of variability present in the

base period climate are carried over in the future. However, patterns such as the Pacific Decadal Oscillation (PDO), Pacific North American Pattern (PNA), and El Niño Southern Oscillation (ENSO) are most likely to change in future (Hauer et al. 1997, Leung et al. 1999, Bond et al. 2003, Newman et al. 2003, Overland and Wang 2007). At present, no clear methods exist to remedy this.

The following examples show how the daily temperature and precipitation changes were applied to the St. Mary climate station daily data. The *Tmax* for a future time period, under a future scenario, and for a particular season was (all variables in °C):

$$Tmax_i(F) = Tmax_i(B) + \Delta Tmax_s(F) \quad (5.1)$$

Where:

$Tmax_i(F)$ is the maximum temperature at St. Mary station for the i^{th} day of the future time period

$Tmax_i(B)$ is the maximum temperature at St. Mary station for the i^{th} day of the base period daily climate record

$\Delta Tmax_s(F)$ is the change in maximum temperature, relative to the base period, for the appropriate season of the i^{th} day for the future time period

Equation 5.1 was also used to calculate *Tmin*, substituting appropriate values. For precipitation, future depths were obtained by using the percent change to calculate a depth change. This was then added to the St. Mary base period precipitation value. For a given future period, scenario, and season (as above, for example), the future precipitation was calculated using:

$$P_i(F) = P_i(B) + [P_i(B) \times (1 + \Delta P_s(F))] \quad (5.2)$$

Where:

$P_i(F)$ is the future precipitation at St. Mary station for the i^{th} day of the future time period (mm)
$P_i(B)$ is the precipitation at St. Mary station, for the i^{th} day of the base period daily climate record (mm)
$\Delta P_s(F)$ is the change in precipitation, relative to the base period, for the appropriate season of the i^{th} day of the future time period (%)

The scenarios were applied to the 1961-1990 historical data for the period extending to 2099. The resultant dataset combining historical 1961-2004 and future 2010-2099 data was a 140 year climate record reflecting graduated warming for scenarios 1 and 2. The record had a modest data gap for 2005-2009.

5.2.2 Snow Hydrology Model Runs

For all terrain categories (TCs), modelled snow hydrology for the future scenarios was developed as follows:

- The SWE Model was run for the 30-year periods to obtain the snow hydrology mass balance data, including daily snow water equivalent (SWE) and rainfall;
- The critical snowpack Julian dates of maximum snowpack accumulation (*Jmax*) and snowpack depletion (*Jdep*) were determined for the TCs and the watershed, for each year.
- *Jmax* and *Jdep* for each TC were used to determine the snowmelt runoff volume (S_R). The watershed *Jdep* was used to determine the timing and volume of the effective rainfall runoff volume (R_R). The watershed *Jmax* was used to determine the timing of spring streamflow volume (Q_S).
- The statistical spring streamflow prediction model, corresponding to the same multiple linear regression equation developed in Chapter 4 but for the years 1961-1990, was applied.

5.3 Analysis

Seasonal Climate Changes

Table 5.2 shows the seasonal $\Delta Tmax$, $\Delta Tmin$, and ΔP values for each time slice, and for each scenario. Figure 5.3 shows the actual seasonal climographs, having added the changes to the St. Mary base period climate. The following points are noted from Table 5.2 and Figure 5.3:

- The DJF period is the most critical in the snow hydrology model, since this is the period of greatest snow accumulation. Mean temperature is -4.0°C for the base period. It remains below zero for the 2020s, but passes the critical freezing temperature (dashed line in Figure 5.2) by the mid-2050s for Scenario 2. Both scenarios experience above-freezing temperatures for the 2080s.
- Both the MAM and SON seasons show relatively small changes in precipitation, for both scenarios.
- Scenario 1 shows substantial negative precipitation change during the JJA season. For Scenario 2, negative precipitation magnitudes are smaller, and spaced more evenly across seasons.
- Scenarios 1 and 2 were chosen because of their differing projected precipitations for the November-June periods. Based on this method, Scenario 1 was considered wetter, while Scenario 2 was drier. Interestingly, analysis of the *annual* hydroclimatic changes, under each scenario, reveals that each shows similar precipitation projections. This highlights the importance of keeping the impacts model's sensitivity in mind, when performing the GCM scenario selection (as was done for this study).

- Scenario 1 JJA *Tmax* changes by 10.9°C for the 2080s, while *Tmin* changes by 8.0°C (Table 5.2). These are large values, relative to the base period, and raises interesting questions regarding the certainty of such projections. Concurrently, precipitation decreases substantially during this season. If this projection were to occur, the resultant climate would be extremely drier than that observed for the base period, with severe consequences for ecosystems.

Table 5.2. Seasonal temperature and precipitation changes for each scenario, relative to the 1961-1990 base period. *Tmax* and *Tmin* changes are in °C, and precipitation changes are in %.

Season	Time Slice	Scenario 1			Scenario 2		
		ΔTmax	ΔTmin	ΔP	ΔTmax	ΔTmin	ΔP
DJF	2020s	0.9	1.5	9.5	1.2	1.2	-0.6
	2050s	2.3	3.7	26.2	3.6	3.7	6.1
	2080s	3.7	5.6	42.9	6.0	6.2	12.8
MAM	2020s	1.0	1.1	9.4	1.8	1.8	6.7
	2050s	2.5	2.5	15.2	3.7	3.5	11.2
	2080s	4.1	4.0	21.0	5.6	5.3	15.7
JJA	2020s	3.2	2.2	-17.1	1.8	1.6	-6.4
	2050s	7.1	5.3	-25.1	3.9	3.5	-4.7
	2080s	10.9	8.0	-33.0	5.9	5.5	-3.1
SON	2020s	2.0	1.6	-2.1	1.2	1.2	-3.8
	2050s	4.3	3.9	0.9	3.3	3.1	-5.5
	2080s	6.7	6.1	3.9	5.5	5.0	-7.1

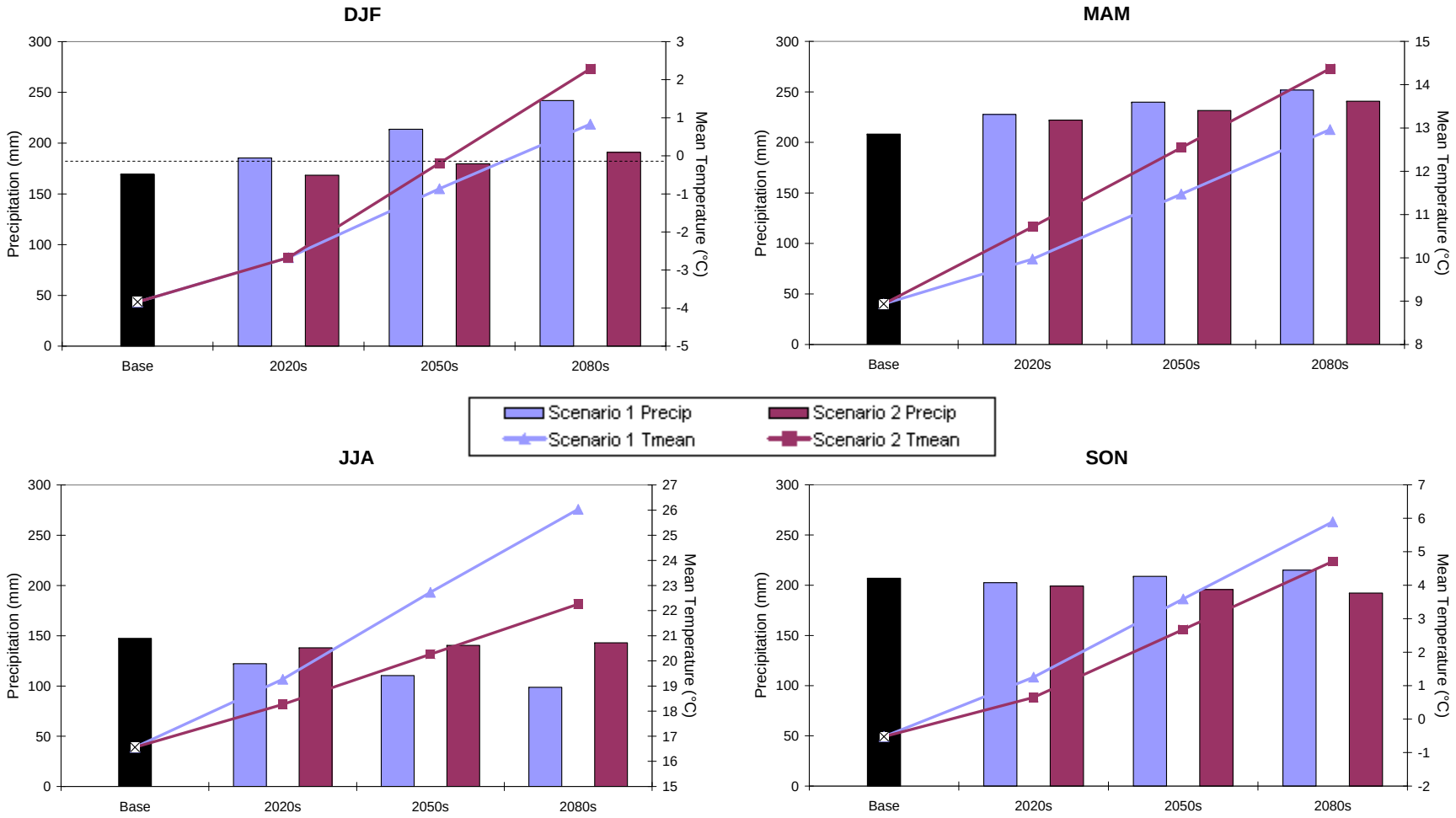

Figure 5.3. Changes in actual seasonal mean temperature (averaged from minima and maxima) and precipitation for the St. Mary station from one time slice to the next.

Representative Years

To provide a sense of the variability and compare future changes of the St. Mary headwaters snow hydrology, frequency analysis was applied. The Weibull function (Weibull 1951) was used to identify high, median, and low Q_S years for the base period. This function is capable of fitting a wide range of shapes and scales and is useful for representing Q_S for the analyses that follow in this section.

The frequency distribution plot for the years 1961-1990 is shown in Figure 5.4. Choosing high, medium, and low flow years from the base period frequency distribution enabled hydrologic change comparisons to be made with corresponding representative future years. The flow volumes and percentage probability are shown in Table 5.3. The corresponding future years within the transposed 30-year timeseries are also shown. For example, for the period 1961-1990, 1984 was a low flow year. This was year 14 within the base period. For the 2020s period, this equivalent low flow year (i.e., 9.7% probability) corresponded to the year 2033 (i.e., year 14 within 2010-2039). The corresponding years are thus representative years of high, medium, and low flow, based on the frequency distribution of the base period.

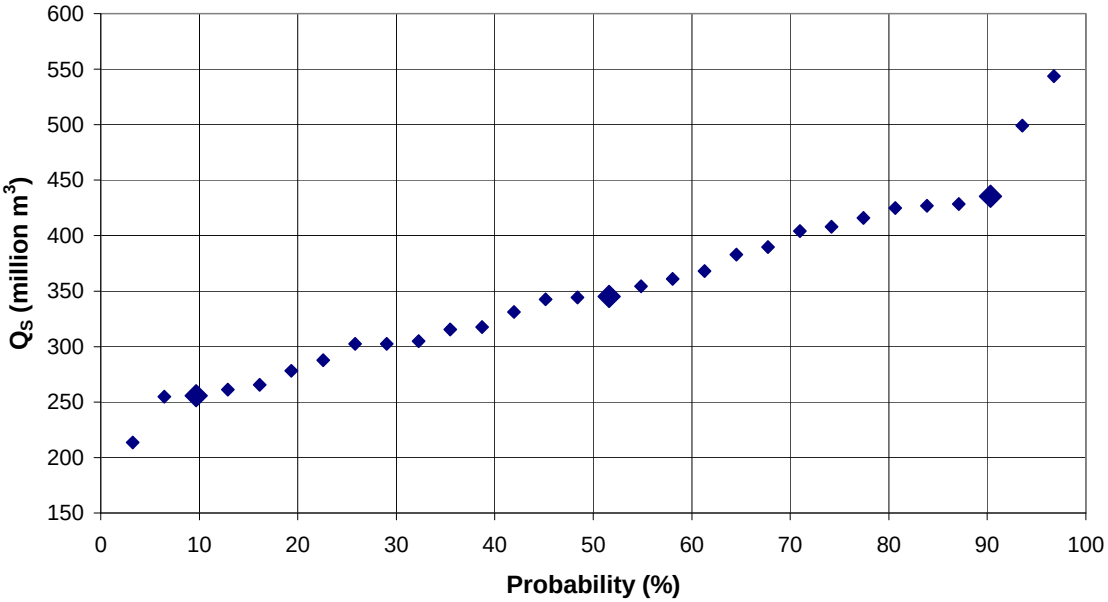

Figure 5.4. Weibull frequency distribution plot of the 1961-1990 modelled spring streamflow volumes. The high, median, and low Q_S years appear larger, for easy recognition.

Table 5.3. High, median, and low flow years used as representative years for snow hydrology comparisons. Percentage probabilities are those designated by the Weibull frequency distribution.

Modelled Q_S			Base Year	Corresponding Future Years		
Million m^3	% Prob.	Flow		2020s	2050s	2080s
435.4	90.3	High	1965	2014	2044	2074
345.1	51.6	Med.	1979	2028	2058	2088
255.8	9.7	Low	1984	2033	2063	2093

5.4 Results and Discussion

Hydrology

To compare future changes in snow hydrology on an annual basis, the statistical regression model variables for the representative years are shown in Table 5.4.

Observations include:

- S_R always decreases with time through the future, for each flow type, and for each scenario. This likely occurs because in all cases, the changes in precipitation

(even if positive during winter), do not compensate for increasing temperatures in the snow accumulation mass balance within the SWE Model.

- R_R varies from one scenario to the other, and through time periods. This reflects the greater variability in precipitation according to season, as shown in Figure 5.2.
- Similar to S_R, Q_S always decreases with time through the future, for each flow type, and for each scenario (with one exception, discussed next). This is logical given the importance S_R has in the statistical model predicting spring streamflow (Equation 5.3).
- For Scenario 1 median flow year, Q_S does not change from the 2020s to the 2050s, where an increase would be expected. This can be explained when looking at the SWE Model output of S_R and R_R. The DJF climograph of Figure 5.2 shows that average temperatures remain below the freezing line and average precipitation increases from the 2020s to the 2050s. This means that while S_R decreases from the 2020s to the 2050s, the decline is modest (644.2 versus 615.3 million m^3). The slightly earlier snowmelt means that effective rainfall runoff occurs earlier in the 2050s compared to the 2020s. This means that instead of occurring during JJA (when ΔP is negative, Table 5.3), it occurs during MAM (when ΔP is positive). Thus, R_R increases significantly from the 2020s to the 2050s (63.9 versus 84.5 million m^3, respectively). The above two factors result in the statistical regression model's projection of no change in Q_S value for the 2020s relative to the 2050s in the median flow year.
- Q_S is always higher for Scenario 1 than it is for Scenario 2, except for the 2020s time period. This trend is logical, given that the two scenarios show similar rates

of warming, and Scenario 1 has greater precipitation inputs for the critical November-June period. During the 2020s, Scenario 2 shows greater Q_S than Scenario 1 because of greater R_R for each flow year.

Table 5.4. Hydrologic variables under the two scenarios and three future periods, for the three flow type years. All units are in million m^3.

Period	Scenario	S_R			R_R			Q_S		
		High	**Med.**	**Low**	**High**	**Med.**	**Low**	**High**	**Med.**	**Low**
Base	–	787.9	696.7	538.3	84.8	56.8	75.5	435.4	345.1	255.8
2020s	1	766.4	644.2	471.1	89.9	63.9	62.1	425.8	316.3	196.5
	2	749.0	619.2	452.2	105.2	99.4	130.9	429.3	334.9	252.6
2050s	1	727.8	615.3	415.9	80.2	84.5	84.4	389.8	317.3	181.2
	2	681.7	574.2	367.6	102.9	82.4	87.5	381.1	287.1	151.4
2080s	1	676.1	579.8	345.9	94.2	85.6	94.3	368.5	294.2	143.5
	2	556.1	515.1	262.3	92.0	85.7	91.5	284.5	250.2	83.6

Figure 5.5 illustrates the streamflow trend through time. The solid black line represents the modelled historical Q_S. The period 1991-2004 is dashed, because its variability was not reproduced in the future climate. The historical period (1960-2004) shows a downward trend in spring streamflow, which is projected to continue for both scenarios. Despite their differences in November-June precipitation, both Q_S projections are very close to one another. This clearly demonstrates that the increased precipitation in Scenario 1 did not compensate for the temperature increases in the resultant spring streamflow volume, according to the model. The trend lines show that on average Q_S was 350 million m^3 during the base period. This declines to around 300 million m^3 for the 2020s, to between 250 and 270 million m^3 for the 2050s, and to between 190 to 220 million m^3 for the 2080s.

Also of interest is the frequency of low flow years. Using the base period low flow year (9.7% probability, Table 5.3) as a threshold, there were 3 years equal to or below 255.8 million m^3 during the base period. This number increases to 8 and 4 for Scenarios 1 and 2 during the 2020s. The number of low flow years represents half or more of the years during the 2050s (15 for Scenario 1, and 18 for Scenario 2). Finally, low flow years are very prevalent during the 2080s, as the Q_S for 21 and 24 years is equal to or below the threshold for Scenarios 1 and 2, respectively. Furthermore, Figure 5.5 shows that the driest year for Scenario 2 during the 2050s is very low (below 100 million m^3) and during the 2080s is extremely low (close to zero).

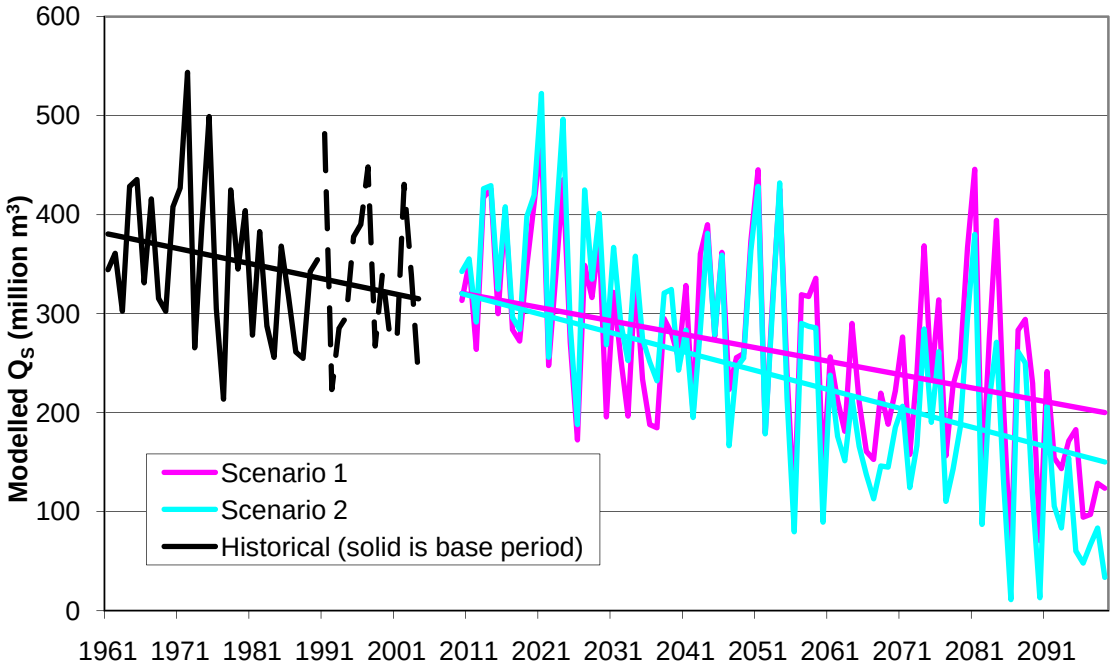

Figure 5.5. Modelled annual Q_S for the period 1961-2099. The variability of the three future periods (i.e., 2010-2039, 2040-2069, and 2070-2099) reflects that of the base period (1961-1990). The annual timeseries for the three future periods serve as examples of typical spring streamflow years in order to illustrate possible future ranges.

Timing

The projected streamflow decline is concurrent with the earlier dates of maximum snow accumulation (*Jmax*) and snow depletion (*Jdep*). The earlier dates of maximum snow accumulation are a proxy for the earlier onset of spring snowmelt. Table 5.5 shows the changes in these dates for the three flow type years. Figure 5.5 shows the trends for these dates, for Scenarios 1 and 2. For the base period, the average date of onset of snowmelt is 8-Apr (Julian day 98). It advances up to two weeks for the 2020s period. For the 2050s, the average snowmelt onset occurs between 5-Mar (Scenario 2) and 14-Mar (Scenario 1), fully one month before the same date for the base period. As well, the snowmelt season shortens through time as these dates approach each other. Figure 5.3 (b) shows that in some years for the 2080s, the date of maximum snow accumulation

actually occurs in December of the water year. During these years, there is nearly no snowmelt season, as *Jdep* occurs soon after *Jmax* has been reached.

Table 5.5. Julian dates of maximum snow accumulation (*Jmax*) and maximum snow depletion (*Jdep*) for the three flow type years.

Period	Scenario	Jmax			Jdep		
		High	**Med.**	**Low**	**High**	**Med.**	**Low**
Base	–	106	109	87	165	162	139
2020s	1	103	100	72	159	148	118
	2	99	94	65	155	142	111
2050s	1	90	88	54	141	134	96
	2	81	81	41	138	128	81
2080s	1	76	80	38	130	124	73
	2	62	71	24	108	113	51

a) Scenario 1

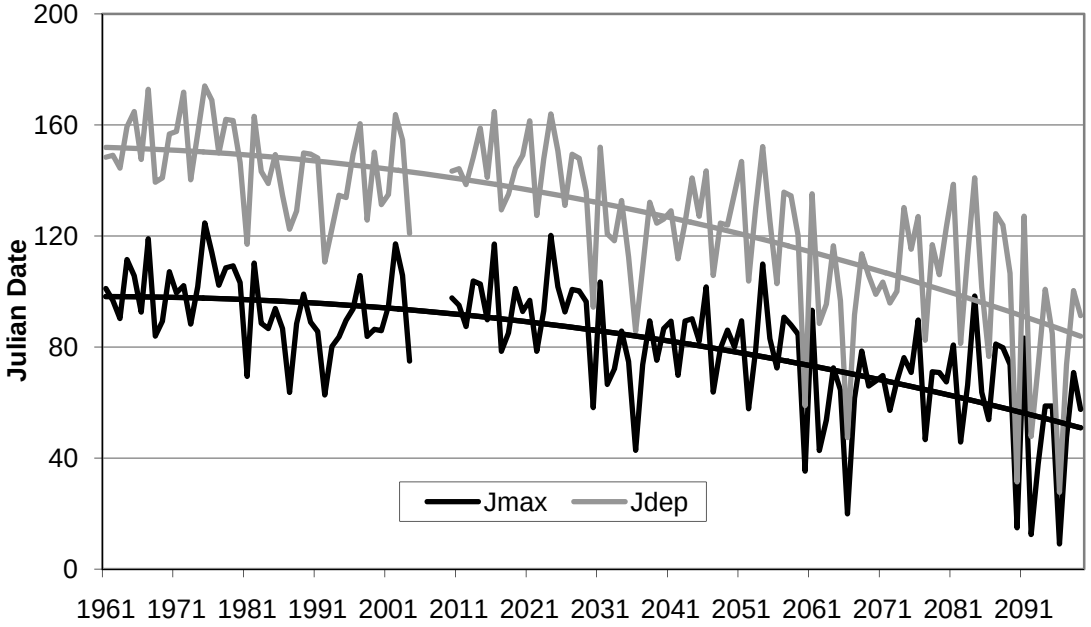

b) Scenario 2

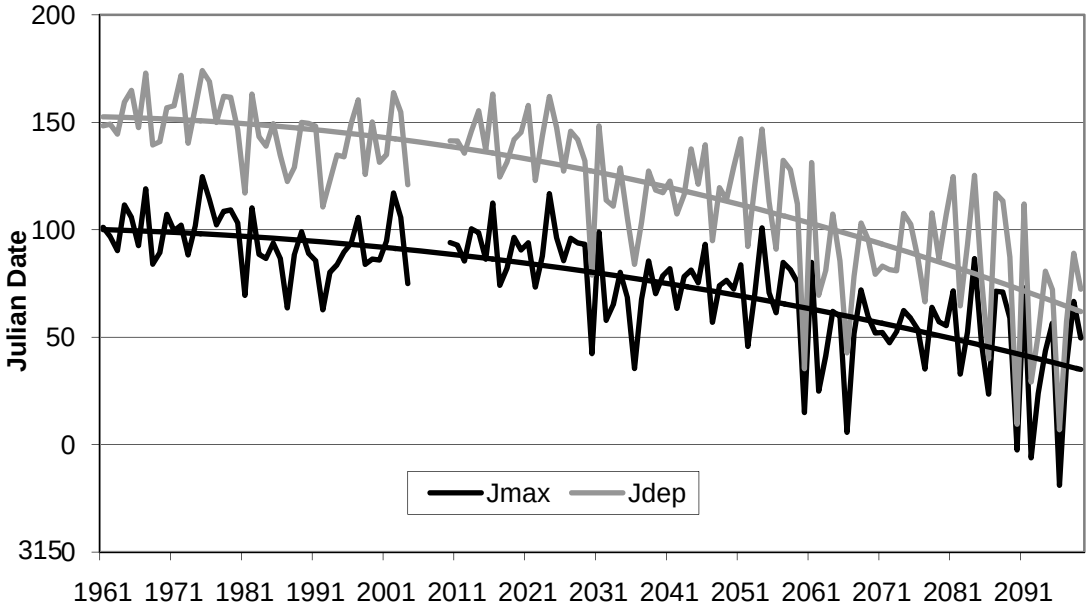

Figure 5.6. Changes in critical snowpack Julian dates indicating maximum snow accumulation (*Jmax*), and snowpack depletion (*Jdep*) for both scenarios. The difference between *Jdep* and *Jmax* is the length of the snowmelt season. The variability of the three future periods (i.e., 2010-2039, 2040-2069, and 2070-2099) reflects that of the base period (1961-1990). The annual timeseries for the three future periods serve as examples of typical Julian dates in order to illustrate possible future ranges.

5.5 Summary

Using GCM output, two scenarios were selected that would best test the sensitivity of the snow hydrology model for this climate change impacts assessment. Spring streamflow response was very similar between Scenario 1 and Scenario 2, despite their differences in winter precipitation input for the critical November-June period. Increasing temperatures contribute to snowpack decline through increasing rain-to-snow ratios and increasing the incidence of snowmelt. The decrease in SWE (and snowmelt runoff) results in decreased spring streamflow. The results show that projected increases in precipitation did not compensate for increases in temperature on spring streamflow. As expected with spring streamflow decline, low flow years occur more frequently. This is concurrent with an earlier onset of snowmelt, and shortening of the snowmelt season.

CHAPTER 6: Conclusions

6.1 Thesis Summary

In this thesis, a modelling approach was developed to assess the impacts of climate change on snow hydrology in the St. Mary River headwaters basin. This was achieved by first adopting and refining a SWE model for the study watershed. The SWE Model output was then used to develop a statistical streamflow prediction model, which was validated using observed streamflow data for the historical period (1961-2004). Changes to the following snow hydrology variables were assessed under two climate change scenarios, spanning the 2010-2099 period: snowmelt runoff volume (S_R); effective rainfall runoff volume (R_R); spring streamflow volume (Q_S); date of maximum snow accumulation (*Jmax*); and date of snow depletion (*Jdep*).

It was found that in the future, S_R would decline under both scenarios. Comparatively, R_R was found to vary from year to year. As expected, the projected Q_S trend is highly related to the S_R trend, and declines in the future for both scenarios. There was little difference between the Q_S results for Scenarios 1 and 2, despite their differences in precipitation for the months of interest (November-June). This finding suggests that increases in winter precipitation will not compensate for increases in winter temperature for spring runoff generation. Relative to the base period (1961-1990), Q_S was shown to decline between -3% and -12% for the 2020s, -25% to -32% for the 2050s, and -38 to -55% for the 2080s. In addition, whereas the spring snowmelt onset occurred on average on Apr 8 for the base period, it occurred as early as Mar 25 for the 2020s (Scenario 2). The earliest average snowmelt onset dates were Mar 5 during the 2050s (Scenario 2), and

Feb 17 for the 2080s (Scenario 2). Therefore, substantial decreases in water supply and earlier onset of snowmelt are expected in the future.

Implications

The findings of this project have implications for interests related to ecosystems, industry, and recreation. A decline in spring pulse volumes will affect river ecosystem management of minimum flows. Such flow requirements are needed to sustain floodplain cottonwood forests and aquatic species (Rood et al. 2005a). Additionally, lower flows and warmer air temperatures and longer warm seasons could increase water temperatures, affecting river ecosystems.

The allocation of minimum flows affects water volume supplied for irrigation purposes, and the two are generally considered as competing uses. A decline in spring volumes would enhance this conflict. The irrigation industry's increasing interest in using water transfers could further complicate matters. Additionally, transboundary allocation issues between Montana and Alberta, including First Nations rights, may become issues of greater contention in the future (Halliday and Faveri 2007).

With regards to recreation, the findings suggest that river based activities could be compromised. Reduced spring flows would decrease "whitewater" conditions and late season use due to low water levels. Recreational fishing could be affected depending on changes to aquatic ecosystems. Perhaps most significant will be the impacts of declining snowpack on skiing and other winter activities.

Annual Flow Volumes

This project focused on changes in spring streamflow volumes. Comparing these to changes in annual streamflow volumes would be beneficial to help answer important questions. For example, will annual flows decline to the same extent as spring flows? What will happen to winter flows, as both the incidence of mid-season melt and the rain-to-snow ratio increases in the watershed, especially at lower elevations? Quantifying changes in future annual flow volumes would require modelling more components of the water balance, and observing how these would respond to climate change. Many of the components that could be improved in the modelling process to achieve this objective, centered on the development of a fully distributed, physically-based, hydrologic model are discussed next.

6.2 Recommendations

The modelling approach used in this study proved adequate given the strong linkages between winter snowpack and spring streamflow. However, a number of improvements could be made to the modelling process to build on the findings of this thesis. Perhaps most important to any study related to hydrologic modelling is the need for better precipitation estimates. Gains will be made if the study scale is considered when improving datasets. For example, this study is most likely to be scaled-up to a larger geographic area, requiring precipitation interpolation surfaces; such estimates will need to incorporate mountain effects. This point and others may be addressed in the following three areas: physically-based hydrologic modelling; linking large-scale and regional climate variability; and data collection.

Physically-based Hydrologic Modelling

There are meaningful gains to be made in enhancing the SWE Model's capability by improving or linking the output to a fully distributed hydrologic model. Appropriate water storage routines (e.g., canopy interception, snowpack, soil, groundwater) could account for temporal lags in the system. This would allow annual hydrograph simulation, accounting for the following critical processes:

- Increased winter precipitation is likely to produce more runoff during this season. Simulating infiltration into frozen and unfrozen soils is thus critical.
- Related to the previous point, increased winter snowmelt water into (frozen) soils is likely to become more prevalent, resulting in increased winter soil water and runoff. This will affect shallow groundwater storage (Rock and Mayer 2007).
- Warmer winters will affect canopy albedo, and the resultant heat exchanges will change snowpack accumulation and ablation patterns, and SWE volumes;
- Evaporation changes could become considerable in spring and fall, affecting wind patterns. Simulating the effects of spring snow sublimation and soil water losses to the atmosphere would be significant to water supply volume and timing issues.

Linking Large-Scale and Regional Climate Variability

Incorporating explicit estimations of future climate variability is crucial, especially given that historically extreme conditions, such as intense precipitation events, are projected to become more frequent. Predicting the frequency of such events could be achieved by incorporating indices of large-scale climate variability into the regional model. The following are general ideas on how this may be achieved:

- Preliminary work for this project found that winter precipitation is linked to large-scale Pacific Ocean climate indices, such as the Pacific Decadal Oscillation (PDO) and Pacific North American Pattern (PNA). These indices track ocean temperatures over the Northern Pacific Ocean and geopotential height fields over northwestern North America, respectively. The winter synoptic climatology and resultant snow hydrology are linked to these indices (Romolo et al. 2006).
- As projections for these patterns are developed using GCMs, they could be incorporated into the regional-scale model, to help explain additional portions of year-to-year variability.
- Regional paleoclimate variability data, stemming from sources such as tree rings, can be useful in linking regional to large-scale climate variability. They can help us understand the long-term behaviour of the aforementioned indices (Sauchyn and Beaudoin 1998, D'Arrigo et al. 2001, Pederson et al. 2006).
- Regional Climate Models (RCMs) operate under GCM boundary conditions, and are resolved on an order of magnitude lower than GCMs (i.e., ~40 km versus ~400 km). This may help downscale large-scale variability. Also, RCMs are

likely to better reflect regional landscape effects, such as orographic precipitation (Kim and Kim 2002, Bronstert et al. 2007).

Integrated Monitoring

Increasing the number of high-quality data sets is always beneficial to derive or validate modelled surfaces of hydroclimate variables. Data in mountain locations is scarce; however, many improvements may be made by utilizing information from a variety of sources, fulfilling data needs at various temporal and spatial scales:

- Regional SWE databases, such as the one used in this study, could be further explored, but more extensive climate stations would be ideal. These need to be strategically located and would provide further insight into local topographical effects on precipitation.
- High-elevation glacier research data may possibly be linked with lower-elevation snow data to improve the understanding of snow mass balance, and precipitation-elevation relationships, at colder high altitudes.
- Low-cost temperature monitors, spaced in areas of varied topography and vegetation, could help in understanding heat energy transfers to and from snowpack (Hubbart et al. 2005, Walter et al. 2005). Knowledge of microclimate variability, such as of lapse rate changes, and associated melt and evapotranspiration could also be gained.
- Remotely-sensing data is promising (Bales et al. 2006). A number of satellites now deliver useful snow covered area surfaces which may be linked with ground-based data to produce watershed snow surfaces (Fassnacht et al. 2003).

REFERENCES

AAFRD. 2000. Irrigation in Alberta, Part 2. Alberta Agriculture, Food & Rural Development, Lethbridge, AB.

ACIA. 2004. Arctic Climate Impact Assessment (ACIA): Scientific Report. Cambridge University Press.

Aguado, E. 1990. Elevational and latitudinal patterns of snow accumulation departures from normal in the Sierra Nevada. *Theoretical Applications to Climatology* **42**:177-185.

Ahrens, C. D. 2007. Meteorology Today: An Introduction to Weather, Climate, and the Environment, Eighth edition. Thomson Brooks/Cole, Belmont, CA.

Allen, M. R., and W. J. Ingram. 2002. Constraints on future changes in climate and the hydrologic cycle. *Nature* **418**:224-232.

Anderson, E. A. 1973. National River Foreacast System - snow accumulation and ablation model. US Department of Commerce, Silver Spring, MD.

Anderson, E. A. 1976. A point energy mass balance model of a snowcover. US Department of Commerce, Silver Spring, MD.

Arnell, N. W. 1999. Climate change and global water resources. *Global Environmental Change* **9**:31-49.

Arnell, N. W. 2004. Climate change and global water resources: SRES scenarios and socio-economic scenarios. *Global Environmental Change* **14**:31-52.

ASCE. 1996. Hydrology Handbook. American Society of Civil Engineers.

Auer, A. H. 1974. The rain versus snow threshold temperatures. *Weatherwise* **27**:67.

Bales, R. C., and D. Cline. 2003. Chapter 25: Snow Hydrology and Water Resources (Western United States). Pages 443-457 *in* T. D. Potter and B. R. Colman, editors. Handbook of Weather, Climate, and Water: Atmospheric chemistry, hydrology, and society impacts. John Wiley and Sons, Hoboken, New Jersey.

Bales, R. C., N. P. Molotch, T. H. Painter, M. D. Dettinger, R. Rice, and J. Dozier. 2006. Mountain hydrology of the western United States. *Water Resources Research* **42**:13.

Barnett, T. P., J. C. Adam, and D. P. Lettenmaier. 2005. Potential impacts of a warming climate on water availability in snow-dominated regions. *Nature* **438**:1-7.

Barnett, T. P., R. Malone, W. Pennell, D. Stammler, B. Semtner, and W. Washington. 2004. The effects of climate change on water resources in the West: Introduction and overview. *Climatic Change* **62**:1-11.

Barrow, E., B. Maxwell, and P. Gachon. 2004. Climate Variability and Change in Canada: Past, Present and Future. Meteorological Service of Canada, Environment Canada, Toronto, Ontario.

Barrow, E., and G. Yu. 2005. Climate Scenarios for Alberta. Alberta Environment and PARC, Regina, Saskatchewan.

Barry, R. C. 1981. Mountain Weather and Climate. Methuen & Co. Ltd, London.

Barry, R. G., and R. J. Chorley. 1987. Atmosphere, Weather and Climate, 5th edition. Routledge.

Bayard, D., M. Stähli, A. Parriaux, and H. Fluhler. 2005. The influence of seasonally frozen soil on the snowmelt runoff at two Alpine sites in southern Switzerland. *Journal of Hydrology* **309**:66-84.

Bleha, J. A. 2004. Development and application of a MODIS driven snowmelt model in Northwestern Montana. M.Sc. Thesis. University of Michigan, Ann Arbor, Michigan.

Blennow, K. 1998. Modelling minimum air temperature in partially and clear felled forests. *Agricultural and Forest Meteorology* **91**:223-235.

Bond, N. A., J. E. Overland, M. Spillane, and P. Stabeno. 2003. Recent shifts in the state of the North Pacific. *Geophysical Research Letters* **30**:2183.

Bonsal, B., T. D. Prowse, and A. Pietroniro. 2003. An assessment of global climate model-simulated climate for the western cordillera of Canada (1961-90). *Hydrological Processes* **17**:3703-3716.

Bowling, L. C., J. W. Pomeroy, and D. P. Lettenmaier. 2004. Parameterization of blowing-snow sublimation in a macroscale hydrology model. *American Meteorological Society* **5**:745-761.

Braun, L. N. 1991. Modelling of the snow-water equivalent in the mountain environment. *20th General Assembly of the International Union of Geodesy and Geophysics, Vienna, Australia* **08/11-24/91**:3-17.

Bronstert, A., V. Kolokotronis, D. Schwandt, and H. Straub. 2007. Comparison and evaluation of regional climate scenarios for hydrological impact analysis: General scheme and application example. *International Journal of Climatology* **27**:1579-1594.

Brown, R. D. 2000. Northern hemisphere snow cover variability and change, 1915–97. *American Meteorological Society* **13**:2339-2355.

Brown, R. D., and R. O. Braaten. 1998. Spatial and temporal variability of Canadian monthly snow depths, 1946-1995. *Atmosphere-Ocean* **36**:37-54.

Brubaker, K., A. Rango, and W. Kustas. 1996. Incorporating radiation inputs into the Snowmelt Runoff Model. *Hydrological Processes* **10**:1329-1343.

Burn, D. H. 1994. Hydrologic effects of climatic change in west-central Canada. *Journal of Hydrology* **160**:53-70.

Byrne, J. M. 1989. Three phase runoff model for small Prairie rivers - 1. Frozen soil phase assessment. *Canadian Water Resources Journal* **14**:17-28.

Byrne, J. M., S. Kienzle, D. Johnson, G. Duke, V. Gannon, B. Selinger, and J. Thomas. 2006. Current and future water issues in the Oldman River Basin, Alberta, Canada. *Water Science and Technology* **53**:327-334.

Cayan, D. R. 1996. Interannual climate variability and snowpack in the western United States. *Journal of Climate* **9**:928-948.

Cayan, D. R., S. A. Kammerdiener, M. D. Dettinger, J. M. Caprio, and D. H. Peterson. 2001. Changes in the onset of spring in the western United States. *Bulletin of the American Meteorological Society* **82**:399-415.

CCCSN. 2007. A summary of the six main SRES Scenarios. http://www.cccsn.ca/Scenarios/SRESScenarios.html. Canadian Climate Change Scenarios Network, Accessed Apr 6, 2007.

Christensen, J. H., B. Hewitson, A. Busuioc, A. Chen, X. Gao, I. Held, R. Jones, R. K. Kolli, W.-T. Kwon, R. Laprise, V. M. Rueda, L. Mearns, C. G. Menéndez, J. Räisänen, A. Rinke, A. Sarr, and P. Whetton. 2007. Regional Climate Projections. Intergovernmental Panel on Climate Change, Cambridge, UK, and New York, USA.

Clark, M. P., M. C. Serreze, and D. A. Robinson. 1999. Atmospheric controls on Eurasian snow extent. *International Journal of Climatology* **19**:27-40.

Cohen, S., and K. Miller. 2001. North America; in Climate Change 2001: Impacts, Adaptation and Vulnerability. Cambridge University Press.

Coughlan, J., and S. W. Running. 1997. Regional ecosystem simulation: A general model for simulating snow accumulation and melt in mountainous terrain. *Landscape Ecology* **12**:119-136.

Crowley, T. J. 2000. Causes of climate change over the past 1000 years. *Science* **289**:270-277.

Cubasch, U., G. A. Meehl, and G. J. Boer. 2001. Projections of future climate change. Pages 525-582 *in* J. T. Houghton, editor. Climate Change 2001: The Scientific Basis. Contribution of Working Group I to the Third Assessment Report of the Intergovernmental Panel on Climate Change. Cambridge University Press.

D'Arrigo, R., R. Villalba, and G. Wiles. 2001. Tree-ring estimates of Pacific decadal climate variability. *Climate Dynamics* **18**:219-224.

Daly, C., R. P. Neilson, and D. L. Phillips. 1994. A statistical-topographic model for mapping climatological precipitation over mountainous terrain. *Journal of Applied Meteorology* **33**:140-158.

Del Genfo, A. D., A. A. Lacis, and R. A. Ruedy. 1991. Simulations of the effect of a warmer climate on atmospheric humidity. *Nature* **351**:382-385.

Déry, S. J., and M. K. Yau. 1999. A bulk blowing snow model. *Boundary-Layer Meteorology* **93**:237–251.

Diaz, H. F. 2005. Monitoring climate variability and change in the western united states. Pages 267-273 *in* U. M. Huber, H. K. M. Bugmann, and M. A. Reasoner, editors. Global Change and Mountain Regions. Springer, Dordrecht, The Netherlands.

Dickinson, R. E., and R. J. Cicerone. 1986. Future global warming from atmospheric trace gases. *Nature* **319**:109-115.

Dingman, S. 2002. Physical Hydrology, 2nd edition. Prentice-Hall, Upper Saddle River, NJ.

Dixon, K. W., T. L. Delworth, T. R. Knutson, M. J. Spelman, and R. J. Stouffer. 2003. A comparison of climate change simulations produced by two GFDL coupled climate models. *Global and Planetary Change* **37**:81-102.

Doesken, N. J., D. Chagnon, and T. B. McKee. 1989. Interannual variations in snowpack in the Rocky Mountain region. Pages 21-30 *in* Proceedings of the Western Snow Conference.

Döll, P., M. Flörke, M. Märker, and S. Vassolo. 2003. Einfluss des Klimawandels auf Wasserressourcen und Bewäasserungswasserbedarf: eine globale Analyse unter Berücksichtigung neuer Klimaszenarien (Impact of climate change on water resources and irrigation water requirements: a global analysis using new climate change scenarios). Pages 11-14 *in* H.-B. Keeberg, editor. Kilma - Wasser - Flussgebietsmanagement: im Lichte der Flut. Forum für Hydrologie und Wasserbewirtschaftung, Freiburg, Germany.

Donald, J. R., E. D. Soulis, and N. Kouwen. 1995. A land cover-based snow cover representation for distributed hydrologic models. *Water Resources Research* **31**:995-1009.

Dore, M. H. I. 2005. Climate change and changes in global precipitation patterns: What do we know? *Environment International* **31**:1167-1181.

Douville, H., F. Chauvin, S. Planton, J.-F. Royer, D. Salas-Melia, and S. Tyteca. 2002. Sensitivity of the hydrological cycle to increasing amounts of greenhouse gases and aerosols. *Climate Dynamics* **20**:45-68.

Dozier, J. 2004. Multispectral adn hyperspectral remote sensing of alpine snow properties. *Annual Review of Earth and Planetary Sciences* **32**:465-494.

Dye, D. G. 2002. Variability and trends in the annual snow-cover cycle in Northern Hemisphere land areas, 1972-2000. *Hydrological Processes* **16**:3065-3077.

Elder, K., and J. M. Dozier. 1991. Snow accumulation and distribution in an alpine watershed. *Water Resources Research* **27**:1541–1552.

Emori, S., T. Nozawa, A. Abe-Ouchi, A. Numaguti, M. Kimoto, and T. Nakajima. 1999. Coupled ocean-atmosphere model experiments of future climate change with an explicit representation of sulfate aerosol scattering. *Journal of Meteorological Society of Japan* **77**:1299-1307.

Essery, R., L. Li, and J. Pomeroy. 1999. A distributed model of blowing snow over complex terrain. *Hydrological Processes* **13**:2423-2438.

Fagre, D. 2006. Unpublished USGS data from the Climate Change in Mountain Ecosystems project at Glacier National Park. *in*. United States Geological Survey, West Glacier Field Station.

Fagre, D. B., D. L. Peterson, and A. E. Hessl. 2003. Taking the pulse of mountains: Ecosystem responses to climatic variability. *Climatic Change* **59**:263-282.

Fassnacht, S. R., K. A. Dressler, and R. C. Bales. 2003. Snow water equivalent interpolation for the Colorado River Basin from snow telemetry (SNOTEL) data. *Water Resources Research* **39**:1208.

Ferguson, R. I. 1999. Snowmelt runoff models. *Progress in Physical Geography* **23**:205-227.

Field, C. B., L. D. Mortsch, M. Brklacich, D. L. Forbes, P. Kovacs, J. A. Patz, S. W. Running, and M. J. Scott. 2007. North America. Cambridge University Press, Cambridge, UK.

Finklin, A. I. 1986. A climatic handbook of Glacier National Park —with data for Waterton Lakes National Park USDA Forest Service Ogden, UT.

Flato, G. M., and G. J. Boer. 2001. Warming assymetry in climate change simulations. *Geophysical Research Letters* **28**:195-198.

Frei, A., D. A. Robinson, and M. G. Hughes. 1999. North American snow extent: 1900-1994. *International Journal of Climatology* **19**:1517-1534.

Fyfe, J. C., and G. M. Flato. 1999. Enhanced climate change and its detection over the Rocky Mountains. *Journal of Climate* **12**:230-242.

Garen, D. C. 1992. Improved Techniques in Regression-Based Streamflow Volume Forecasting. *Journal of Water Resources Planning and Management* **118**:654-670.

Garen, D. C., and D. Marks. 2005. Spatially distributed energy balance snowmelt modelling in a mountainous river basin: Estimation of meteorological inputs and verification of model results. *Journal of Hydrology* **315**:126-153.

Gelfan, A. N., J. W. Pomeroy, and L. S. Kuchment. 2004. Modeling forest cover influences on snow accumulation, sublimation, and melt. *American Meteorological Society* **5**:785-803.

Giorgi, F., and J. W. Hurrell. 1997. Elevation dependency of the surface climate change signal: A model study. *Journal of Climate* **10**:288.

Glassy, J. M., and S. W. Running. 1994. Validating diurnal climatology logic of the MT-CLIM model across a climatic gradient in Oregon. *Ecological Applications* **4**:248-257.

Gordon, C., C. Cooper, C. A. Senior, H. Banks, J. M. Gregory, T. C. Johns, J. F. B. Mitchell, and R. A. Wood. 2000. The simulation of SST, sea ice extent and ocean heat transports in a version of the Hadley Centre coupled model without flux adjustments. *Climate Dynamics* **16**:147-168.

Gordon, H. B., and S. P. O'Farrell. 1997. Transient climate change in the CSIRO coupled model with dynamic sea ice. *Monthly Weather Review* **125**:875-907.

Grace, B. 1987. Chinooks. *Chinook* **9**:52-56.

Gray, D. M., and D. H. Male. 1981. Handbook of Snow: Principles, Processes, Management & Use.

Gray, D. M., and T. D. Prowse. 1993. Snow and Floating Ice. *in* D. R. Maidment, editor. Handbook of Hydrology. McGraw-Hill.

Groisman, P. Y., and D. R. Easterling. 1993. Variability and trends of total precipitation and snowfall over the United States and Canada. *Journal of Climate* **7**:184-204.

Groisman, P. Y., T. R. Karl, and R. W. Knight. 1994. Changes of snow cover, temperature, and radiative heat balance over the northern hemisphere. *Journal of Climate* **7**:1633-1655.

Groisman, P. Y., R. W. Knight, T. R. Karl, D. R. Easterling, B. Sun, and J. H. Lawrimore. 2004. Contemporary Changes of the Hydrological Cycle over the Contiguous United States: Trends Derived from In Situ Observations. *Journal of Hydrometeorology* **5**:64-84.

Groisman, P. Y., B. Sun, R. S. Vose, J. H. Lawrimore, P. H. Whitfield, E. Førland, I. Hanssen-Bauer, M. C. Serreze, V. N. Razuvaev, and G. V. Alekseev. 2003. Contemporary climate changes in high latitudes of the northern hemisphere. *in* 83rd Meteorological Society Meeting, Long Beach, CA.

Gurtz, J., A. Baltensweiler, and H. Lang. 1999. Spatially distributed hydrotope-based modelling of evapotranspiration and runoff in mountainous basins. *Hydrological Processes* **13**:2751-2768.

Halliday, R., and G. Faveri. 2007. The St. Mary and Milk Rivers: The 1921 Order revisited. *Canadian Water Resources Journal* **32**:75-92.

Hamlet, A. F., and D. P. Lettenmaier. 1999a. Columbia River streamflow forecasting based on ENSO and PDO climate signals. *ASCE Journal of Water Resources Planning and Management* **1215**:333-341.

Hamlet, A. F., and D. P. Lettenmaier. 1999b. Effects of climate change on hydrology and water resources in the Columbia River basin. *Journal of the American Water Resources Association* **35**:1597-1623.

Hamlet, A. F., P. W. Mote, M. P. Clark, and D. P. Lettenmaier. 2005. Effects of temperature and precipitation variability on snowpack trends in the western United States. *American Meteorological Society* **18**:4545-4561.

Hansen, J., and L. Nazarenko. 2004. Soot climate forcing via snow and ice albedos. *Proceedings of the National Academy of Sciences U.S.A.* **101**:423-428.

Hansen, J. E., M. Sato, P. Kharecha, G. Russell, D. W. Lea, and M. Siddall. 2007. Climate change and trace gases. *Philosophical Transactions of the Royal Society* **365**:1925-1954.

Harding, R. J., and J. W. Pomeroy. 1996. The energy balance of the winter boreal landscape. *Journal of Climate* **9**:2778–2787.

Hauer, F. R., J. S. Baron, D. H. Campbell, K. D. Fausch, S. W. Hostetler, G. H. Leavesley, P. R. Leavitt, D. M. Mcknight, and J. A. Stanford. 1997. Assessment of climate change and freshwater ecosystems of the Rocky Mountains, USA and Canada. *Hydrological Processes* **11**:903-924.

Hay, L., R. Viger, G. McCabe, K. Kovar, U. Tappeiner, N. E. Peters, and R. G. Craig. 1998. Precipitation interpolation in mountainous regions using multiple linear regression. *in* Hydrology, Water Resources and Ecology in Headwaters. IAHS Publication, Merano, Italy.

Hay, L. E., R. L. Wilby, and G. H. Leavesley. 2000. Comparison of delta change and downscaled GCM scenarios for three mountainous basins in the United States. *Journal of the American Water Resources Association* **36**:387-397.

Hedstrom, N. R., and J. W. Pomeroy. 1998. Measurements and modelling of snow interception in the boreal forest. *Hydrological Processes* **12**:1611-1625.

Hegerl, G. C., F. W. Zwiers, P. Braconnot, N. P. Gillett, Y. Luo, J. A. M. Orsini, N. Nicholls, J. E. Penner, and P. A. Stott. 2007. Understanding and Attributing Climate Change. *in* S. Solomon, D. Qin, M. Manning, Z. Chen, M. Marquis, K. B. Averyt, M. Tignor, and H. L. Miller, editors. Climate Change 2007: The Physical Science Basis. Contribution of Working Group I to the Fourth Assessment Report of the Intergovernmental Panel on Climate Change. Cambridge University Press, Cambridge UK, and New York, USA.

Hengeveld, H. G. 2000. Projections for Canada's climate future - a discussion of recent simulations with the Canadian Climate Model. *Meteorological Service of Canada. Minister of Public Works and Government Services Canada*.

Hirst, A. C., H. B. Gordon, and S. P. O'Farrell. 1997. Response of a coupled ocean-atmosphere model including oceanic eddy-induced advection to anthropogenic CO2 increase. *Geophysical Research Letters* **23**:3361-3364.

Hock, R. 2003. Temperature index melt modelling in mountain areas. *Journal of Hydrology* **282**:104-115.

Hood, E. W., M. W. Williams, and D. Cline. 1998. Sublimation from a seasonal snowpack at a continental, mid-latitude alpine site. *Hydrological Processes* **13**:1781-1797.

Houghton, J. T., Y. Ding, D. J. Griggs, M. Noguer, P. J. van der Linden, and D. Xiaosu. 2001. Climate Change 2001: The Scientific Basis. Contribution of Working Group I to the Third Assessment Report of the Intergovernmental Panel on Climate Change. Cambridge University Press, UK.

Howat, I. M., and S. Tulaczyk. 2005. Trends in spring snowpack over half a century of climate warming. *Annals of Glaciology* **40**:151-156.

Hubbart, J., T. Link, C. Campbell, and D. Cobos. 2005. Evaluation of a low-cost temperature measurement system for environmental applications. *Hydrological Processes* **19**:1517-1523.

Hungerford, R. D., R. R. Nemani, S. W. Running, and J. C. Coughlan. 1989. MTCLIM: Mountain Microclimate Simulation Model. Research Paper INT-414. U.S. Department of Agriculture, Forest Service, Intermountain Research Station, Ogden, UT.

Huntchinson, M. F. 1995. Interpolating mean rainfall using thin plate smoothing splines. *International Journal of Geographical Information Systems* **9**:385-403.

Huntington, T. G. 2006. Evidence for intensification of the global water cycle: Review and synthesis. *Journal of Hydrology* **319**:83-95.

IPCC-TGCIA. 1999. Guidelines on the Use of Scenario Data for Climate Impact and Adaptation Assessment. Version 1. Intergovernmental Panel on Climate Change, Task Group on Scenarios for Climate Impact Assessment.

IPCC. 2001. Summary for Policymakers. Cambridge University Press, Geneva, CH.

IPCC. 2007. Summary for Policymakers. Cambridge University Press, Cambridge, UK and New York, USA.

Jin, J., N. L. Miller, S. Sorooshian, and X. Gao. 2006. Relationship between atmospheric circulation and snowpack in the western USA. *Hydrological Processes* **20**:753-767.

Karl, T. R., P. Y. Groisman, R. W. Knight, and R. R. Heim. 1993. Recent variations of snow cover and snowfall in North America and their relation to precipitation and temperature variations. *Journal of Climate* **6**:1327-1344.

Karl, T. R., R. W. Knight, D. R. Easterling, and R. G. Quayle. 1995. Indices of climate change for the United States. *Bulletin of the American Meteorological Society* **77**:279-292.

Katz, R. W. 1999. Extreme value theory for precipitation: sensitivity analysis for climate change. *Advances in Water Resources* **23**:133-139.

Katz, R. W., and B. G. Brown. 1992. Extreme events in a changing climate: variability is more important than averages. *Climatic Change* **21**:289-302.

Kharin, V. V., and F. W. Zwiers. 2000. Changes in the extremes in an ensemble of transient climate simulations with a coupled atmosphere-ocean GCM. *Journal of Climate* **131**:3760-3788.

Kim, J., and T.-K. Kim. 2002. Impacts of increased atmospheric CO_2 on the hydroclimate of the western United States. *Journal of Climate* **15**:1926-1942.

Kimball, J. S., S. W. Running, and R. Nemani. 1997. An improved method for estimating surface humidity from daily minimum temperature. *Agricultural and Forest Meteorology* **85**:87-98.

Knowles, N., M. D. Dettinger, and D. R. Cayan. 2006. Trends in snowfall versus rainfall in the western United States. *Journal of Climate* **19**:4545-4559.

Kundzewicz, Z. W., L. J. Mata, N. W. Arnell, P. Döll, P. Kabat, J. Jiménez, K. A. Miller, T. Oki, Z. Sen, and I. A. Shiklomanov. 2007. Freshwater resources and their management. Cambridge University Press, Cambridge, UK.

Lapp, S., J. Byrne, S. Kienzle, and I. Townshend. 2002. Linking Global Circulation model synoptics and precipitation for western North America. *International Journal of Climatology* **22**:1807-1817.

Lapp, S., J. M. Byrne, S. W. Kienzle, and I. Townshend. 2005. Climate warming impacts on snowpack accumulation in an alpine watershed: A GIS based modeling approach. *International Journal of Climatology* **25**:521-526.

Larson, L., and E. Peck. 1974. Accuracy of precipitation measurements for hydrologic modeling. *Water Resources Research* **10**:853-857.

Lehning, M., I. Völksch, D. Gustafsson, T. A. Nguyen, M. Stähli, and M. Zappa. 2006. ALPINE3D: a detailed model of mountain surface processes and its application to snow hydrology. *Hydrological Processes* **20**:2111-2128.

Leith, R. M., and P. H. Whitfield. 1998. Evidence of climate change effects on the hydrology of stream in south-central B.C. *Canadian Water Resources Journal* **23**:219-230.

Lemke, P., J. Ren, R. B. Alley, I. Allison, J. Carrasco, G. Flato, Y. Fujii, G. Kaser, P. Mote, R. H. Thomas, and T. Zhang. 2007. Observations: Changes in Snow, Ice and Frozen Ground. Pages 338-383 *in* S. Solomon, D. Qin, M. Manning, Z. Chen, M. Marquis, K. B. Averyt, M. Tignor, and H. L. Miller, editors. Climate Change 2007: The Physical Basis. Contribution of Working Group I to the Fourth Assessment Report of the Intergovernmental Panel on Climate Change. Cambridge University Press, Cambridge, UK and New York, USA.

Lettenmaier, D. P., E. F. Wood, and J. R. Wallis. 1994. Hydro-climatological trends in the continental United States, 1948-88. *Journal of Climate* **7**:586-607.

Leung, L. R., A. F. Hamlet, D. P. Lettenmaier, and A. Kumar. 1999. Simulations of the ENSO hydroclimate signals in the Pacific Northwest Columbia River Basin. *Bulletin of the American Meteorological Society* **80**:2313-2329.

Leung, L. R., Y. Qian, X. Bian, W. M. Washington, J. Han, and J. O. Roads. 2004. Mid-century ensemble regional climate change scenarios for the western United States. *Climatic Change* **62**:75-113.

Leung, L. R., and M. S. Wigmosta. 1999. Potential climate change impacts on mountain watersheds in the Pacific Northwest. *Journal of the American Water Resources Association* **35**:1463-1471.

Link, T. E., and D. Marks. 1999. Point simulation of seasonal snow cover dynamics beneath boreal forest canopies. *Journal of Geophysical Research* **104**:27841–27858.

Liston, G. E., and K. Elder. 2006a. A distributed snow-evolution modeling system (SnowModel). *Journal of Hydrometeorology*:1259-1276.

Liston, G. E., and K. Elder. 2006b. A meteorological distribution system for high-resolution terrestrial modeling (MicroMet). *Journal of Hydrometeorology* **7**:217-234.

Loaiciga, H. A., J. B. Valdes, R. Vogel, J. Garvey, and H. Schwartz. 1996. Global warming and the hydrological cycle. *Journal of Hydrology* **174**:83-127.

Loukas, A., L. Vasiliades, and N. R. Dalezios. 2002a. Potential climate change impacts on flood producing mechanisms in southern British Columbia, Canada using hte CGCMA1 simulation results. *Journal of Hydrology* **259**:163-188.

Loukas, A., L. Vasiliades, and N. R. Dalezios. 2002b. Potential climate change impacts on flood producing mechanisms in southern British Columbia, Canada using the CGCMA1 simulation results. *Journal of Hydrology* **259**:163-188.

Loukas, A., L. Vasiliades, and N. R. Dalezios. 2004. Climate change implications on flood response of a mountainous watershed. *Water, Air and Soil Pollution: Focus* **4**:331-347.

Luce, C. H., D. G. Tarboton, and K. R. Cooley. 1998. The influence of the spatial distribution of snow on basin-averaged snowmelt. *Hydrological Processes* **12**:1671-1683.

Lundberg, A., and H. Koivusalo. 2003. Estimating winter evaporation in boreal forests with operational snow course data. *Hydrological Processes* **17**:1479-1493.

Manabe, S., and R. J. Stouffer. 1994. Multiple-century response of a coupled ocean-atmosphere model to an increase of atmospheric carbon dioxide. *Journal of Climate* **7**:5-23.

Manabe, S., and R. T. Wetherald. 1967. Thermal equilibrium of the atmosphere with a given distribution of relative humidity. *Journal of the Atmospheric Sciences* **24**:241-260.

Marks, D., J. Domingo, D. Susong, T. Link, and D. Garen. 1999. A spatially distributed energy-balance snowmelt model for application in mountain basins. *Hydrological Processes* **13**:2439-2452.

Marks, D., J. Kimball, D. Tingey, and T. Link. 1998. The sensitivity of snowmelt processes to climate conditions and forest cover during rain-on-snow: a case study of the 1996 Pacific Northwest flood. *Hydrological Processes* **12**:1569-1587.

Martinec, J. 1975. Snowmelt-Runoff Model for stream flow forecasts. *Nordic Hydrology* **6**:145-154.

McCabe, G. J., M. P. Clark, and L. E. Hay. 2007. Rain-on-snow events in the western United States. *Bulletin of the American Meteorological Society*:319-328.

McCabe, G. J., and D. M. Wolock. 1999. General-circulation-model simulations of future snowpack in the western United States. *Journal of the American Water Resources Association* **35**:1473-1483.

McCuen, R. H. 1985. Statistical Methods for Engineering. Prentice-Hall, Inc.

McGuffie, K., and A. Henderson-Sellers. 2001. Forty years of numerical climate modelling. *International Journal of Climatology* **21**:1067-1109.

McKechnie, N. 2005. Predicting Climate Change Impacts on Precipitation for Western North America. M.Sc. Thesis. University of Lethbridge, Lethbridge.

Meiman, J. R. 1970. Snow accumulation related to elevation, aspect and forest canopy. Pages 35-47 *in* Workshop Seminar on Snow Hydrology. Queen's Printer of Canada, Ottawa.

Merritt, W. S., Y. Alila, M. Barton, B. Taylor, S. Cohen, and D. Neilsen. 2006. Hydrologic response to scenarios of climate change in sub watersheds of the Okanagan basin, British Columbia. *Journal of Hydrology* **326**:79-107.

Milne, R., and J. Wallmann. 2007. Forecasting lee-side precipitation in the central and northern Sierra part II: Narrow cold frontal rainbands. National Oceanic and Atmopheric Administration, Reno, NV.

Mitchell, J. F. B., T. C. Johns, M. Eagles, W. J. Ingram, and R. A. Davis. 1999. Towards the construction of climate change scenarios. *Climatic Change* **41**:547-581.

Montesi, J., K. E. Elder, R. A. Schmidt, and R. E. Davis. 2004. Sublimation of intercepted snow within a subalpine forest canopy at two elevations. *Journal of Hydrometeorology* **5**:763–773.

Morrison, J., M. C. Quick, and M. G. G. Foreman. 2002. Climate change in the Fraser River watershed: flow and temperature projections. *Journal of Hydrology* **263**:230-244.

Mote, P. W. 2003. Trends in snow water equivalent in the Pacific Northwest and their climatic causes. *Geophysical Research Letters* **30**:1-4.

Mote, P. W., A. F. Hamlet, M. P. Clark, and D. P. Lettenmaier. 2005a. Declining mountain snowpack in western North America. *American Meteorological Society* **86**:39-49.

Mote, P. W., E. P. Salathe, and C. Peacock. 2005b. Scenarios of future climate for the Pacific northwest. *in* The future ain't what it used to be: Preparing for climate disruption. University of Washington, Seattle.

Nakićenović, N., J. Alcamo, G. Davis, B. d. Vries, J. Fenhann, S. Gaffin, K. Gregory, A. Grübler, T. Y. Jung, T. Kram, E. L. L. Rovere, L. Michaelis, S. Mori, T. Morita, W. Pepper, H. Pitcher, L. Price, K. Raihi, A. Roehrl, H.-H. Rogner, A. Sankovski, M. Schlesinger, P. Shukla, S. Smith, R. Swart, S. van Rooijen, N. Victor, and Z. Dadi. 2000. IPCC Special Report on Emissions Scenarios. Cambridge University Press, Cambridge, UK and New York, USA.

Nash, L. L., and P. H. Gleick. 1991. Sensitivity of streamflow in the Colorado Basin to climatic changes. *Journal of Hydrology (Amsterdam)* **125**:221-241.

NCDC. 2005. GHCN Global Daily. *in* National Climatic Data Centre. EarthInfo Inc.

Newman, M., G. P. Compo, and M. A. Alexander. 2003. ENSO-forced variability of the Pacific Decadal Oscillation. *Journal of Climate* **16**:3853-3857.

NOAA. 2006. Trends in Atmospheric Carbon Dioxide. National Ocean and Atmospheric Administration. Global Monitoring Division. Boulder, CO.

NOAA/NCDC. 2006. Web Climate Service. www.ncdc.noaa.gov/oa/climate/stationlocator.html. National Ocean and

Atmospheric Administration and National Climatic Data Center, Accessed Jun 15, 2006.

NRCS. 2007. SNOTEL Data & Products. http://www.wcc.nrcs.usda.gov/snow/. Natural Resources Conservation Service, Accessed Sep 2006.

Ohmura, A. 2001. Physical basis for the temperature-based melt-index method. *Journal of Applied Meteorology* **40**:753-761.

Overland, J. E., and M. Wang. 2007. Future climate of the North Pacific Ocean. *Eos* **88**:178-182.

Pagano, T. C., J. Erxleben, and T. Perkins. 2005. Operational simulation modeling at the NRCS National Water and Climate Center. *in* Western Snow Conference, Great Falls, Montana.

Payne, J. T., A. W. Wood, A. F. Hamlet, R. N. Palmer, and D. P. Lettenmaier. 2004. Mitigating the effects of climate change on the water resources of the Columbia River basin. *Climatic Change* **62**:233-256.

PCIC. 2007. Scenario Access Interface. http://www.pacificclimate.org/impacts/. Pacific Climate Consortium, Accessed Apr 4, 2007.

Pederson, G. T. 2004. Long-term Perspectives on Northern Rockies Climatic Variability from Tree Rings in Glacier National Park, Montana. M.Sc. Thesis. Montana State University, Bozeman, Montana.

Pederson, G. T., S. T. Gray, D. B. Fagre, and L. J. Graulich. 2006. Long-duration drought variability and impacts on ecosystem services: A case study from Glacier National Park, Montana. *Earth Interactions* **10**:1-27.

Pietroniro, A., M. N. Demuth, C. Hopkinson, P. Dornes, N. Kouwen, B. Brua, J. Toyra, and A. Bingeman. 2006. Streamflow shifts resulting from past and future glacier fluctuations in the eastern flowing basins of the Rocky Mountains. National Water Research Institute, Saskatoon, SK.

Pipes, A., and A. Quick. 1977. UBC Watershed Model Users Guide. Department of Civil Engineering, University of British Columbia, Vancouver, BC.

Pomeroy, J. W., and L. H. Essery. 1999. Turbulent fluxes during blowing snow: Field tests of model sublimation predictions. *Hydrological Processes* **13**:2963–2975.

Pomeroy, J. W., and D. M. Gray. 1995. Snowcover accumulation, relocation and management. Environment Canada, Saskatoon, SK.

Pomeroy, J. W., and L. Li. 2000. Prairie and Arctic areal snow cover mass balance using a blowing snow model. *Journal of Geophysical Research* **105**:26629–26634.

Pomeroy, J. W., J. Parviainen, N. Hedstrom, and D. M. Gray. 1998. Coupled modelling of forest snow interception and sublimation. *Hydrological Processes* **12**:2317-2337.

Prudhommes, C., D. Jakob, and C. Svensson. 2003. Uncertainty and climate change impact on the flood regime of small UK catchments. *Journal of Hydrology* **277**:1-23.

Quick, M. C. 1995. The UBC Watershed Model. Pages 233-280 *in* V. P. Singh, editor. Computer Models of Watershed Hydrology. Water Resources Publications, Highlands Ranch, Colorado.

Quick, M. C., and A. Pipes. 1977. UBC Watershed Model. *Hydrological Sciences Bulletin* **22**:153-162.

Rango, A., and J. Martinec. 1995. Revisiting the degree-day method for snowmelt computations. *Water Resources Bulletin* **31**:657-659.

Rango, A., and J. Martinec. 1999. Modeling snow cover/runoff response to global warming for varying hydrological years. *World Resources Review* **11**:76-91.

Redmond, K. T., and R. W. Koch. 1991. Surface climate and streamflow variability in the western United States and their relationship to large-scale circulation indices. *Water Resources Research* **27**:2381-2399.

Reece, B., and E. Aguado. 1992. Accumulation and melt characteristics of northeastern Sierra Nevada snowpacks. *in* AWRA 28th Annual Conference and Symposium: Managing Water Resources during Global Change. AWRA, Reno, NV.

Regonda, S. K., B. Rajagopalan, M. Clark, and J. Pitlick. 2005. Seasonal cycle shifts in hydroclimatology over the western United States. *Journal of Climate* **18**:372-384.

Reinelt, E. R. 1970. On the role of orography in the precipitation regime of Alberta. *Albertan Geographer* **6**:45-58.

Reuna, M. 1994. An operational grid method for estimation of the areal water equivalent of snow. *Geophysica* **30**:107-121.

Rind, D. 1996. Latitudinal temperature gradients and climate change. *Meteorology and Atmospheric Dynamics* **103**:5943.

Robinson, D. A., and A. Frei. 2000. Seasonal variability of northern hemisphere snow extent using visible satellite data. *Professional Geographer* **51**:307-314.

Rock, L., and B. Mayer. 2007. Isotope hydrology of the Oldman river basin, southern Alberta, Canada. *Hydrological Processes* **in press**.

Roeckner, E., and co-authors. 1996. The atmospheric general circulation model ECHAM-4: Model description and simulation of present-day climate. MPI für Meteorologie, Hamburg, Germany.

Rohrer, M. B. 1989. Determination of the transition air temperature from snow to rain and intensity of precipitation. Pages 475-482 *in* IAHS/WMO/ETH International Workshop on Precipitation Measurement, St. Moritz, Switzerland.

Romolo, L., T. D. Prowse, D. Blair, B. R. Bonsal, P. Marsh, and L. W. Martz. 2006. The synoptic climate controls on hydrology in the upper reaches of the Peace River Basin. Part II: Snow ablation. *Hydrological Processes* **20**:4113-4129.

Rood, S. B., J. M. Mahoney, D. E. Reid, and L. Zilm. 1995. Instream flows and the decline of riparian cottonwoods along the St. Mary River, Alberta. *Canadian Journal of Botany* **73**:1250-1260.

Rood, S. B., G. M. Samuelson, J. H. Braatne, C. R. Gourley, F. M. R. Hughes, and J. M. Mahoney. 2005a. Managing river flows to restore floodplain forests. *Frontiers in Ecology* **3**:193-201.

Rood, S. B., G. M. Samuelson, J. K. Weber, and K. A. Wywrot. 2005b. Twentieth-century decline in streamflows from the hydrographic apex of North America. *Journal of Hydrology* **306**:215-233.

Sauchyn, D. J., and A. B. Beaudoin. 1998. Recent environmental change in the southwestern Canadian plains. *Canadian Geographer* **42**:337.

Sauchyn, D. J., A. Pietroniro, and M. Demuth. 2006. Upland watershed management and global change - Canada's Rocky Mountains and the Western Plains. *in* Fifth Biennial Rosenberg Forum on Water Policy, Banff, Alberta.

Schindler, D. W., and W. F. Donahue. 2006. An Impending water crisis in Canada's western prairie provinces. *Princeton National Academy of Science* **103**:7210-7216.

Schweizer, J., K. Kronholm, J. B. Jamieson, and K. W. Birkeland. 2006. Spatial variability - so what? Pages 365-376 *in* J. A. Gleason, editor. International Snow Science Workshop, Telluride, CO.

Selkowitz, D. J., D. B. Fagre, and B. A. Reardon. 2002. Interannual variations in snowpack in the Crown of the Continent Ecosystem. *Hydrological Processes* **16**:3651-3665.

Serreze, M., M. P. Clark, R. L. Armstrong, D. A. McGinnis, and R. S. Purwaty. 1999. Characteristics of the western United States snow-pack telemetry (SNOTEL) data. *Water Resources Research* **35**:2145-2160.

Shabbar, A., and B. Bonsal. 2003. An assessment of changes in winter cold and warm spells over Canada. *Natural Hazards* **29**:173-188.

Shafer, S. L., P. J. Bartlein, and C. Whitlock. 2005. Understanding the spatial heterogeneity of global environmental change in mountain regions. Pages 21-29 *in* U. M. Huber, H. K. M. Bugmann, and M. A. Reasoner, editors. Global Change and Mountain Regions: An Overview of the Current State of Knowledge. Springer, Dordrecht, The Netherlands.

Shepperd, A. 1996. Modelling Hydrometeorology in the Upper Oldman River Basin. M.Sc. Thesis. University of Lethbridge, Lethbridge.

Smith, J. B., and M. Hulme. 1998. Climate Change Scenarios. *in* C. S. Feenstra, I. Burton, J. Smith, and R. S. J. Tol, editors. Handbook on Methods for Climate Change Impact Assessment and Adaptation Strategies. UNEP/Vrije Universiteit Institute for Environmental Studies, Amsterdam.

Stewart, I. T., D. R. Cayan, and M. D. Dettinger. 2004. Changes in snowmelt runoff timing in western North America under a 'business as usual' climate change scenario. *Climatic Change* **62**:217-232.

Stewart, I. T., D. R. Cayan, and M. D. Dettinger. 2005. Changes toward earlier streamflow timing across western North America. *Journal of Climate* **18**:1136-1115.

Thompson, A. M., R. A. Brown, N. J. Rosenberg, R. Srinivasan, and C. Izaurralde. 2005. Climate change impacts for the conterminous USA: An integrated assessment. *Climatic Change* **69**:67-88.

Thornton, P. E., H. Hasenauer, and M. A. White. 2000. Simultaneous estimation of daily solar radiation and humidity from observed temperature and precipitation: an application over complex terrain in Austria. *Agricultural and Forest Meteorology* **104**:255-271.

Thornton, P. E., S. W. Running, and M. A. White. 1997. Generating surfaces of daily meteorological variables over large regions of complex terrain. *Journal of Hydrology* **190**:214-251.

Trenberth, K. E., P. D. Jones, P. Ambenje, R. Bojariu, D. Easterling, A. K. Tank, and D. Parker. 2007. Observations: Surface and Atmospheric Climate Change. *in* S. Solomon, D. Qin, M. Manning, Z. Chen, M. Marquis, K. B. Averyt, M. Tignor, and H. L. Miller, editors. Climate Change 2007: The Physical Science Basis.

Contribution of Working Group I to the Fourth Assessment Report of the Intergovernmental Panel on Climate Change. Cambridge University Press, Cambridge and New York.

USACE. 1956. Snow Hydrology: Summary Report of the Snow Investigations. United States Army Corps of Engineers. North Pacific Division, Portland, Oregon.

USACE. 1991. User Manual, SSARR Model, Streamflow Synthesis and Reservoir. United States Army Corps of Engineers, North Pacific Division.

USACE. 1998. Engineering and Design Runoff from Snowmelt. United States Army Corps of Engineers, Washington, DC.

USGS. 2000. National Land Cover Data for Montana. http://nris.mt.gov/nsdi/nris/nlcdgrid.html United States Geological Survey, Accessed Feb 5, 2006.

USGS. 2007. National Water Information System: Web Interface. http://waterdata.usgs.gov/nwis. United States Geological Survey, Accessed Apr 15, 2007.

Vincent, L., and E. Mekis. 2006. Changes in daily and extreme temperature and precipitation indices for Canada over the twentieth century. *Atmosphere-Ocean* **44**:177-193.

Vincent, L. A., X. Zhang, and W. D. Hogg. 1999. Maximum and minimum temperature trends in Canada for 1895-1995 and 1945-1995. Pages 95-98 *in* 10th Symposium on Global Change Studies. American Meteorological Society, Dallas, TX.

Von Storch, H., E. Zorita, and U. Cubasch. 1993. Downscaling of global climate change estimates to regional scales: An application to Iberian rainfall in wintertime. *American Meteorological Society* **6**:1161-1171.

Walter, M. T., E. S. Brooks, D. K. McCool, L. G. King, M. Molnau, and J. Boll. 2005. Process-based snowmelt modeling: does it require more input data than temperature-index modeling? *Journal of Hydrology* **300**:65-75.

Walter, M. T., D. S. Wilkins, J. Y. Parlange, and B. L. Schneider. 2004. Increasing evapotranspiration from the conterminous United States. *Journal of Hydrometeorology* **5**:405-408.

Weibull, W. 1951. A statistical distribution function of wide applicability. *Journal of Applied Mechanics* **18**:293-297.

Whitfield, P. H., C. J. Reynolds, and A. Cannon. 2002. Modelling streamflow in present and future climates: example from the Georgia basin, British Columbia. *Canadian Water Resources Journal* **27**:427-456.

Wigley, T. M. L., and S. C. B. Raper. 2001. Interpretation of high projections for global-mean warming. *Science* **293**:451.

Winstral, A., and D. Marks. 2002. Simulating wind fields and snow redistribution using terrain-based parameters to model snow accumulation and melt over a semi-arid mountain catchment. *Hydrological Processes* **16**:3585-3603.

Wood, A. W., D. P. Lettenmaier, and R. N. Palmer. 1997. Assessing climate change implications for water resources planning. *Climatic Change* **37**:203-228.

Wyman, R. R. 1995. Modeling Snowpack Accumulation and Depletion. Pages 23-30 *in* B. T. Guy and J. Barnard, editors. Mountain hydrology: Peaks and valleys in research application. Canadian Water Resources Association, Vancouver, BC.

Xiuqing, Z., M. W. V. Liew, and G. N. Flerchinger. 2001. Experimental study of infiltration into a bean stubble field during seasonal freeze-that period. *Soil Science* **166**:3-10.

Zalikhanov, M. C. 1975. Hydrological role of avalanches in the Caucasus. Pages 390–394 *in* Snow and Ice. IAHS-AIHS International Association of Hydrological Sciences, Wallingford, U.K.

Zhang, X., L. A. Vincent, W. D. Hogg, and A. Niitsoo. 2000. Temperature and Precipitation Trends in Canada During the 20th Century. *Atmosphere-Ocean* **38**:395-429.

Zwiers, F. W., and V. V. Kharin. 1998. Changes in the extremes of the climate simulated by CCC GCM2 under CO2 doubling. *Journal of Climate* **11**:2200-2222.